Membrane reactors for separation and catalysis:
High integration and high efficiency

Von der Naturwissenschaftlichen Fakultät

der Gottfried Wilhelm Leibniz Universität Hannover

zur Erlangung des Grades

Doktor der Naturwissenschaften

Dr. rer. nat.

genehmigte Dissertation

von

M. Sc. Zhengwen Cao

geboren am 31.07.1984 in Shanghai, China

Hannover, 2014

Referent: Prof. Dr. Jürgen Caro

Korreferent: Prof. Dr. Heqing Jiang

Tag der Promotion: 13.02.2014

Preface

Under the supervision of Prof. Dr. Jürgen Caro, the results give in this thesis were achieved in the period of my Ph. D study at the Institute of Physical Chemistry and Electrochemistry at the Gottfried Wilhelm Leibniz Universität Hannover, from Nov. 2010 to Nov. 2013. In this time, I was a scientific co-worker and worked for the European projects NASA-OTM and NEXT-GTL.

Four research papers in which I am the first author are included within this thesis. I am co-author of further 4 papers not included in this thesis. The following statement will clarify my contribution to the four articles used for this thesis. For all these articles, I would like to thank the valuable discussions and suggestions from the co-authors and the referees, special thanks is to Prof. Dr. Jürgen Caro and Prof. Dr. Heqing Jiang for their kind help and instruction. I would like to thank Dr. Stefan Baumann, Dr. Wilhelm Albert Meulenberg from the Forschungszentrum Jülich GmbH providing high-quality asymmetric membranes used in my works.

An article studying the coupling of the two reactions, one reaction is generating oxygen and the other reaction is consuming oxygen, forms chapter 2 of this thesis. The two reactions are coupled through an oxygen transporting perovskite membrane. This article, *Simultaneous overcome of equilibrium limitations in BSCF oxygen-permeable membrane reactors: water splitting and methane coupling*, and published in **Catalysis Today,** was written by me. The measurements and the characterization works were done by Dr. Luo and me following an idea born in a discussion with Profs. J. Caro and H. Jiang. The membrane was prepared by Dr. S. Baumann and Dr. W. A. Meulenberg. I wrote the first draft. Prof Dr. J. Caro and Prof Dr. H. Jiang spent much time on correcting and improving the manuscript.

An article on the development of stable membrane for various applications is presented in Chapter 3. The paper, *An effective and simple method in the aim of improving the oxygen permeability of the dual-phase membrane based on $Ce_{0.9}Gd_{0.1}O_{2-\delta}$,* which will be submitted to **Journal of Membrane Science,** was written by me, I got support on the manuscript preparation from all the co-authors, especially from Prof. Dr. J. Caro, Prof. H. Jiang. The oxygen permeation measurements, the XRD and SEM characterizations were done by myself.

Two articles on improving a catalysis processes through the unique oxygen supply through the oxygen permeation membrane are shown in chapter 4. The first paper, *Nature gas to fuels and chemicals: Improved selectivity and catalyst durability for methane aromatization in an oxygen permeable membrane reactor*, and published in **Angewandte Chemie**, was written by me, and then revised by Prof. J. Caro and Prof. H. Jiang. The membrane employed in this work was prepared by Dr. S. Baumann. The measurements and characterizations were conducted by me following Prof. J. Caro's idea and Prof H. Jiang's instruction. I got great support from all co-authors. The second article is *Ostwald process: An efficient oxygen activation route for improved ammonia oxidation via an oxygen-permeable catalytic membrane*, which has been submitted to **Angewandte Chemie**. The draft was written by me, and then revised by Prof. J. Caro and Prof. H. Jiang. The membrane was supplied by Dr. S. Baumann. The experimental date was mainly done by me following instruction of Profs. J.Caro and H. Jiang. Prof. J. Caro and Prof. H. Jiang gave me great support on the preparation of this manuscript.

Acknowledgement

To those who have helped and encouraged me during my Ph.D. thesis research at the Institute of Physical Chemistry and Electrochemistry at the Gottfried Wilhelm Leibniz Universität Hannover, I would like to express my deepest gratitude.

First of all, I would like to give my appreciation to my supervisor, Prof. J. Caro, for giving me this opportunity to study and carry out my scientific work in his group. I am deeply thankful for his many support and patient guidance throughout my entire Ph.D. thesis. The work presented here cannot be finished without him. Furthermore, I sincerely thank him for his kind support not only for my whole work, but also for improving my working skill. I am deeply impressed by his hard-working, his wisdom and his patient. With the help from my dear Professor, I made a big progress during my Ph. D. study.

Additionally, I would also like to extend my gratitude to Prof. H. Jiang for his great help to my work, especially in the beginning of my Ph. D. study. His valuable suggestions and discussions are essential for all my works. Exceptional thanks to Dr. S. Baumann, Dr. W. A. Meulenberg, Dr. Hartwig Voss, and Prof. Armin Feldhoff for their kind and important support for my work, and for their help to revise my manuscripts. Exceptional thanks go to Prof. A. Feldhoff for his valuable cooperation on TEM measurements. Furthermore, I thank Dr. Oliver Czuprat, Dr. Konstantin Efimov, Dr. Huixia Luo, Dr. Fangyi Liang, Dr. Tobias Klande, Dr. Yi Liu and Dr. Yanying Wei for their help through my whole study.

I am thankful to Lisa Diestel, Nanyi Wang, Olga Ravkina, Alexaner Mundstock, Alexaner Schulz, Wei Fang, Jian Xue, Kaveh Partovi and Sebastian Friebe for their valuable cooperation in the last three years.

I am grateful to Yvonne Gabbey-Uebe, Kerstin Janze, Kerstin Battermann and Frank Steinbach for their great help in the past years. I enjoyed the good time with all the members in our group, and I would like to say thank you very much to all those kind people. I want to extend my gratitude to all other group members, especially Prof. Dr. Haihui Wang, Prof. Dr. Aisheng Huang, Prof. Dr. Yanshuo Li, Prof. Dr. Michael Wark, Dr Dirk Dorfs, Dr. Nadja Bigall, Dr. Juan Du, Dr. Monir Sharifi, Dr. Christian Dunkel, Olga Wittich, Dr. Jana Panke, Dr. Amira Ahmed, Dr. Florian Bittner, and Andreas Wolf. Especial thanks to the mechanical and electrical workshop to Miss Schlüter, Mr. Becker, Mr. Mühr, Mr. Köhler, Mr. Rogge and Mr. Ribbe.

Finally, last but not least, I would like to express my deepest thanks and regards to my dear parents who always love me without reason. My special thanks to my friends, for their help and their love.

Abstract

Following the concept of process intensification, the separation and catalysis processes were integrated in a membrane reactor based on oxygen transporting membrane. In order to achieve a high catalytic performance of the membrane reactors, the catalytic process was studied in a fixed bed reactor to learn the function of the catalyst: methane dehydroaromatization with Mo-based catalyst, NO production from ammonia on the perovskite catalyst, and Mn/Na_2WO_4 on SiO_2 catalyst in the oxidative coupling of methane. Whereas in most reactions the job of the perovskite membrane is to separate *in situ* oxygen from air and thus to provide a low oxygen partial pressure without major gradients over the reactor for a highly selective partial oxidation, in the case of NH_3 oxidation to NO the perovskite membrane plays a double role: It separates the oxygen from air and it serves itself as the catalyst providing highly selective lattice oxygen after the Mars and van Krevelen concept.

In chapter 2, main efforts were devoted to couple an oxygen producing reaction with another reaction which consumes oxygen. As a result, not only a high intensification of different processes was achieved, but also the equilibrium limitation of the particular reaction can be overcome. When the water splitting was combined with the oxidative coupling of methane, a hydrogen production rate of 3.3 $cm^3 \cdot min^{-1} \cdot cm^{-2}$ is achieved. At the same time, the methane conversion was enhanced from 3.7 % to 26 % while the C_2 yield increased from 3.1 % to 6.5 % when introducing the membrane concept at 950 ^{o}C.

A newly developed oxygen transporting membrane is presented in chapter 3, the introduction of 2 mol% cobalt improves the oxygen permeability of the dual-phase oxygen transporting membrane with the nominal composition of 25 wt. % $Gd_{0.4}Sr_{0.6}Fe_{1.0}O_{3-\delta}$ − 75 wt. % $Ce_{0.9}Gd_{0.1}O_{2-\delta}$.

The resulting membrane shows not only an elevated permeability, but also a good stability under CO_2 and reducing atmospheres.

Chapter 4 presents work on the efficient aromatization of methane and ammonia oxidation. When the membrane reactor concept was employed, a slower deactivation and an improved selectivity of methane dehydroaromatization can be achieved. In the ammonia oxidation, as high as 95 % selectivity and 81 % ammonia conversion were achieved at 850 ^{o}C in the membrane reactor which are decisively higher data than in the fixed bed reactor.

Zusammenfassung

Nach dem Konzept der Prozessintensivierung wurden Trenn- und Katalysefunktionen in einem Membranreaktor, der auf sauerstoffleitenden Membranen basiert, integriert. Um die Katalyse in Membranreaktoren zu verstehen und zu verbessern, wurden die Katalysatoren in Festbettreaktoren zuvor ausgeprüft: Methan-Dehydro-Aromatisierung mittels Mo-basierter Katalysatoren, die NO-Erzeugung aus Ammoniak an perowskitischen Katalysatoren und der Mn/Na_2WO_4 auf SiO_2–Katalysator in der oxidativen Kupplung von Methan. Während in den meisten Fällen die Funktion der Perowskitmembran passiv ist, nämlich Sauerstoff aus Luft abzutrennen und in den Reaktor zu dosieren, wodurch im Unterschied zur Co-Feed-Fahrweise keine größeren Gradienten des Sauerstoffpartialdruckes auftreten und die Partialoxidation selektiv erfolgen kann, besitzt die Perowskitmembran im Fall der NH_3-Oxidation zu NO eine Doppelfunktion: Sie trennt Sauerstoff aus Luft ab und ist zugleich der Katalysator, indem eine Oxidation mit Gittersauerstoff nach Mars und van Krevelen stattfindet.

In Kapitel 2 wurde die Kopplung einer sauerstoffproduzierenden und einer sauerstoffverbrauchenden Reaktion durch eine sauerstoffleitende Membran untersucht. Als Ergebnis wurde eine deutliche Verbesserung beider thermodynamisch limitierter Prozesse erhalten, und die Überwindung der üblicherweise vorliegenden Gleichgewichtsbeschränkung erreicht. Wenn die Spaltung von Wasser mit der oxidativen Kupplung von Methan kombiniert wurde, konnte eine Wasserstoff-Fluss von 3,3 cm^3 min^{-1} cm^{-2} erreicht werden. Bei einer Reaktortemperatur von 950 °C konnte der Methanumsatz von 3,7 auf 26 % und die Ausbeute an C_2-Kohlenwasserstoffen (Ethan + Ethen) von 3,1 auf 6,5 % erhöht werden.

Eine neuentwickelte sauerstofftransportierende Membran wird in Kapitel 3 vorgestellt. Durch die Zugabe von 2 mol % Kobalt wird die Sauerstoffpermeation der Membran mit der nominellen Zusammensetzung 25 Gew. % $Gd_{0.4}Sr_{0.6}Fe_{1.0}O_{3-\delta}$ - 75 Gew. % $Ce_{0.9}Gd_{0.1}O_{2-\delta}$ deutlich verbessert. Die verbesserte Membran zeigt nicht nur eine erhöhte Sauerstoffpermeabilität, sondern auch eine gute Stabilität unter CO_2 und reduzierenden Atmosphären.

Kapitel 4 behandelt die effiziente Aromatisierung von Methan und die Ammoniakoxidation nach Ostwald. Durch den Einsatz eines Membranreaktors konnte im Vergleich zum Festbett eine langsamere Deaktivierung und eine verbesserte Selektivität der Methan-Dehydro-Aromatisierung erreicht werden. Bei der Ammoniakoxidation konnte bei einer Temperatur von 850 °C eine Selektivität von 95 % und ein Ammoniakumsatz von 81 % erreicht werden.

Schlagwörter: Sauerstofftransportierende Membran, Membranreaktor, effiziente katalytische Verfahren.

Contents

Chapter 1

Introduction

Driven by the separation technology, different membrane forms have been developed since Nollet found the effect of osmotic pressure in 1748. According to the membrane construction, membranes can be simply divided into porous and dense membranes. Over the past decades, intensive efforts have been made to apply porous membranes for the sea water purification, bioproducts separation and recovering gas from mixtures.[1] Nowadays, the main interest is to develop effective pore membranes with a high separation factor and permeability. Extensive applications based on various types of porous membranes such as the micro- and ultrafiltration technology have been well established, and the membrane-based industry increases more than 10 % per year. Recent research indicates that the membrane process shows many unique advantages in some separation applications. For example, comparing with other conventional water treatment techniques, membrane processes are more simple and energy efficient, and provide a higher quality product, and therefore dominate the water purification industry.

In contrast to the porous membranes, the dense membranes frequently have a different separation mechanism and offer an infinite selectivity towards certain gases. In the early 1980s, dense membranes based on mixed proton and electronic conducting materials were applied for the hydrogen permeation, then dense oxygen transporting membranes based on mixed ionic and electronic conducting materials were also developed. The fact that these kinds of

inorganic membranes can withstand high temperatures has resulted in a wide range for the application of membranes in chemical reactors with increased conversions, better selectivity, and milder operating conditions. The effective integration of the two processes separation and reaction in a single unit using a membrane offers further advantages including simplifying the production plant and saving of the thermal energy. For example, Tokyo Gas built a membrane system to replace the conventional natural gas steam reformer system with hydrogen purification by pressure swing adsorption because of its integrated hydrogen production and purification.[2] Besides, to cover the coming shortage of the non-renewable energy sources, great attention has been given to utilize the remaining fossil resources more economic and develop an alternative clean energy concept. Various proposals for this aim employing mixed oxygen ions and electrons conducting membranes have been developed and evaluated on the laboratory scale.

In this work, the main effort is to demonstrate the implication of a membrane reactor using oxygen transporting membranes in the integration of the separation and catalysis processes.

1.1 Oxygen transporting membrane reactors

1.1.1 The development of oxygen transporting membranes

The typically studied material systems for oxygen permeation include perovskite-type structure (ABO_3)[3] and perovskite-related layered Ruddlesden-Popper structure $(A_2BO_{4+\delta})$[4], fluorite (AO_2)[5], Brownmillerite $(A_2B_2O_5)$[6] and pyrochlore $(A_2B_2O_7)$[7].

Among those systems, the material with the perovskite-type structure attracted most attention since Teraoka reported the oxygen permeation of $Sr_1Co_yFe_{1-y}O_{3-\delta}$ (SCF).[8] The SCF shows an excellent permeability towards oxygen because of its high oxygen vacancy concentration, owing to the total substitution of the A^{3+} metal ion by Sr^{2+} in the A-site of the perovskite. However, after intensive investigations,[3] the SCF was found to show a poor chemical and structural stability. The SCF perovskite phase tends to be transferred into the brownmillerite phase under a low oxygen partial pressure less than 0.1 atm and a temperature below 750 ^{o}C. However, such operation parameters are normally necessary for the membrane application in the pure oxygen production from air or in the partial oxidation of methane (POM).[9] Efforts have been made to replace some metal ion with others in the SCF in order to stabilize the perovskite phase. The substitution of Sr^{2+} with La^{3+} generally results in an enhancement of phase stability but a pronounced decrease of permeability caused by the suppression of the formation of oxygen vacancies. In order to make a tradeoff between the stability and permeability, Ba^{2+} was doped in the A-site of the SCF, and encouraging results were obtained. $Ba_{0.5}Sr_{0.5}Co_{0.8}Fe_{0.2}O_{3-\delta}$ (BSCF) shows superior phase stability and a comparable permeability like SCF owing to the effective suppression of the reduction from low valence state Co^{3+} and Fe^{3+} to high valence state Co^{4+} and Fe^{4+} so that the mechanical instability through the lattice expansion caused by the over uptake of lattice oxygen can be

avoided.[10] However, after intensive investigation of BSCF, many researchers recognized the deterioration of the permeability at the temperature below 850 ^{o}C. The phase transition from the cubic phase to the hexagonal phase or other phases at intermediate temperature range is in line with this decrease in the permeability, and it is assumed, therefore, as the reason for the instability.[11,12] Since the oxidation of Co^{4+} to Co^{3+} is still closely related to this transition and remains as the major factor for the decomposition of the cubic perovskite phase, efforts were also devoted to replace the Co with Fe or other elements in order to obtain a membrane with stable permeability at intermediate temperatures. Following this principle, a series of cobalt-free materials $Ba_{0.5}Sr_{0.5}Fe_{0.8}X_{0.2}O_{3-\delta}$ such as $Ba_{0.5}Sr_{0.5}Fe_{0.8}Zn_{0.2}O_{3-\delta}$ (BSFZ),[13] $Ba_{0.5}Sr_{0.5}Fe_{0.9}Al_{0.1}O_{3-\delta}$ (BSFA),[14] $Ba_{0.5}Sr_{0.5}Co_{0.8}Cu_{0.2}O_{3-\delta}$ (BSFC),[15] and many cobalt-reduced materials $BaCo_xFe_yX_{1-x-y}O_{3-\delta}$ such as $BaCo_{0.4}Fe_{0.4}Zr_{0.2}O_{3-\delta}$ (BCFZ), $BaCo_{0.7}Fe_{0.2}Ta_{0.1}O_{3-\delta}$ (BCFT),[16] $BaCo_{0.4}Fe_{0.4}Nb_{0.2}O_{3-\delta}$ (BCFN),[17] were developed. Those cobalt-free or cobalt- reduced materials show better stability than BSCF especially at lower temperature, and only slightly lower permeability.

Oxyfuel technology - which is based on an oxygen permeation membrane - is proposed as an effective method to capture the CO_2 and lower the CO_2 emission. The production of concentrated CO_2 through the combustion with pure oxygen is supposed to simplify the CO_2 capture and storage. Therefore, to satisfy such application, another aspect in addition to permeability and phase stability should also be considered, the stability of the oxygen transporting membrane in the presence of CO_2. Since the cobalt depletion is always accompanied with the carbonate formation, the Co substitution by other elements will improve the CO_2-resistance, however, to a limited degree only. The main reason remains the formation of carbonate on the surface of the alkaline earth-containing materials such as barium and strontium in the presence of CO_2,[18] which leads to a pronounced deterioration of the oxygen permeability.[19] Since the formation of barium carbonates is thermodynamically more favorable than that of strontium carbonate at intermediates

temperatures, it is proposed that the replacement of barium or even of strontium with other elements may lead to a sufficient CO_2-resistance of the membrane. As a consequence, $La_{0.5}Sr_{0.5}Co_{0.8}Fe_{0.2}O_{3-\delta}$ (LSCF) shows a considerable CO_2-resistance, however, its low permeability and degradation are identified.[20] $La_{0.6}Ca_{0.4}FeO_{3-\delta}$ (LCF) shows considerably improved CO_2-tolerance, although its stability needs to be further verified.[18]

A promising approach to obtain a stable membrane is to mix the two different phases and get so called dual-phase membrane. Generally speaking, through the combination of a phase (usually perovskite phase) with high electronic conductivity and another phase (usually fluorite phase) with high oxygen ionic conductivity, a mixed ionic-electronic conducting membrane can be obtained which provides a comparable permeability like single perovskite phase membranes. Since the phase with poor stability is covered by the phase possessing an excellent stability, the dual-phase membrane usually shows a superior CO_2-tolerance and also a higher stability in reducing atmospheres than single perovskite phase membranes. However, for the dual-phase membrane, the correlation of both phases remains an important factor for its performance. The homogeneity and the compatibility of the two phases are found to significantly affect the final permeability.[21] For example, the membrane obtained by one-pot method provides twice the permeability of the membrane obtained by hand mixing the powders, since a better homogeneous distribution is obtained through the one-pot method.[22] Recently, our group demonstrated a high performance oxygen permeation dual-phase cobalt-free membrane with considerable permeability and excellent CO_2-stablility and good reducing atmosphere stability.[23]

The K_2NiF_4-type oxide $La_2Ni_{0.9}Fe_{0.1}O_{4+d}$[24] also exhibits considerable CO_2 stability to meet such applications, but it tends to decompose easily in reducing atmospheres at low oxygen chemical potential.

Permeability and stability are the two most important major properties required for the industrialization of the oxygen transporting ceramic membranes. However, the two properties are frequently at odds with each other. Up to now, it is still hard to obtain an ideal membrane with high permeability, excellent phase and chemical stability either under CO_2 or reducing atmosphere. The best way may be to make a balance between those important issues and design special membranes for the various applications.

1.1.2 Oxygen transport through dense oxygen permeation membranes

Ionic conductivity and electronic conductivity

The ionic conductivity and electronic conductivity are two important factors determining the oxygen permeability of the different materials. Here the perovskite-type oxides will be taken as an example and discussed. Figure 1.1 illustrates the ideal structure of the perovskite-type oxide $ABO_{3-\delta}$.
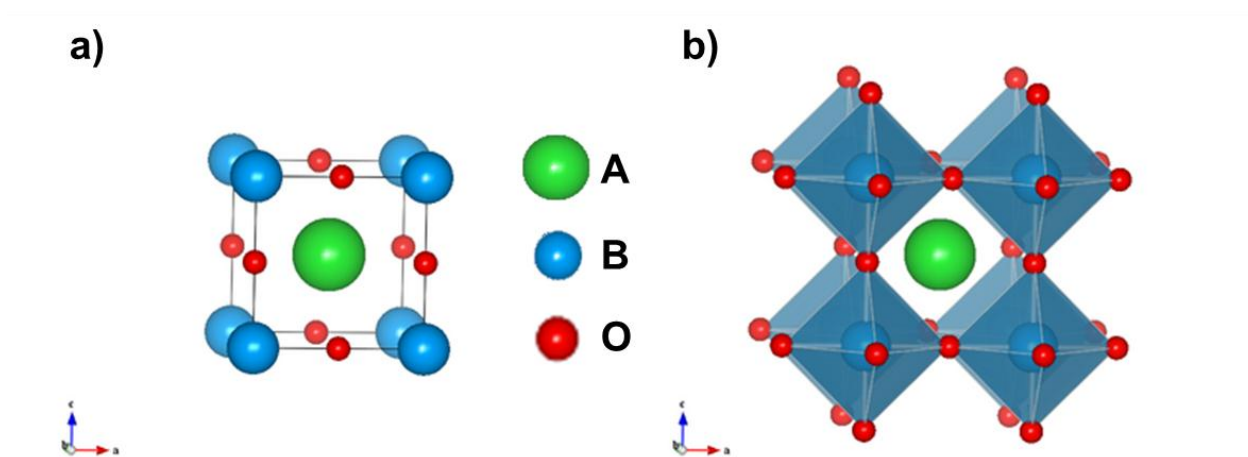

Figure 1.1. Ideal structure of perovskite-type oxides $ABO_{3-\delta}$.[25]

To understand how a perovskite allows electronic and ionic conductivity, it is necessary to know the structure of a typical perovskite. Generally, A is the large cation and 12-fold coordinated with oxygen anions, B is the small cation and 6-fold coordinated with oxygen anions. When A is placed in the center, a cubic structure is found, as shown in a), and for B is an octahedron, in b). Goldschmidt's tolerance factor t is an important parameter to describe the crystal structure of the perovskite oxides, as defined by the following formula:

$$t = \frac{r_A + r_O}{\sqrt{2}(r_B + r_O)}$$

where r_A, r_B and r_O are the radii of the cations A, B and of the oxygen ion, respectively. Since $\frac{r_A + r_O}{\sqrt{2}}$ is the distance of A-O, $(r_B + r_O)$ equals to the distance of B-O, as depicted in figure 1.1. If the radius of the A-site cation is small, the tolerance factor decreases. For the case that the B-site cation possesses a small radius, the tolerance factor increases to values > 1. $t < 0.8$ usually results in rhombohedra or orthorhombic distortion of the cubic structure, when $t > 1.05$ may lead to a hexagonal perovskite structure. However, this tolerance factor may only provide a rough approximation

The controlled formation of defects in the oxide lattice is the key issue to obtain an oxygen ion conducting perovskite, since the formation of oxygen vacancies is important for the oxygen ionic conductivity.
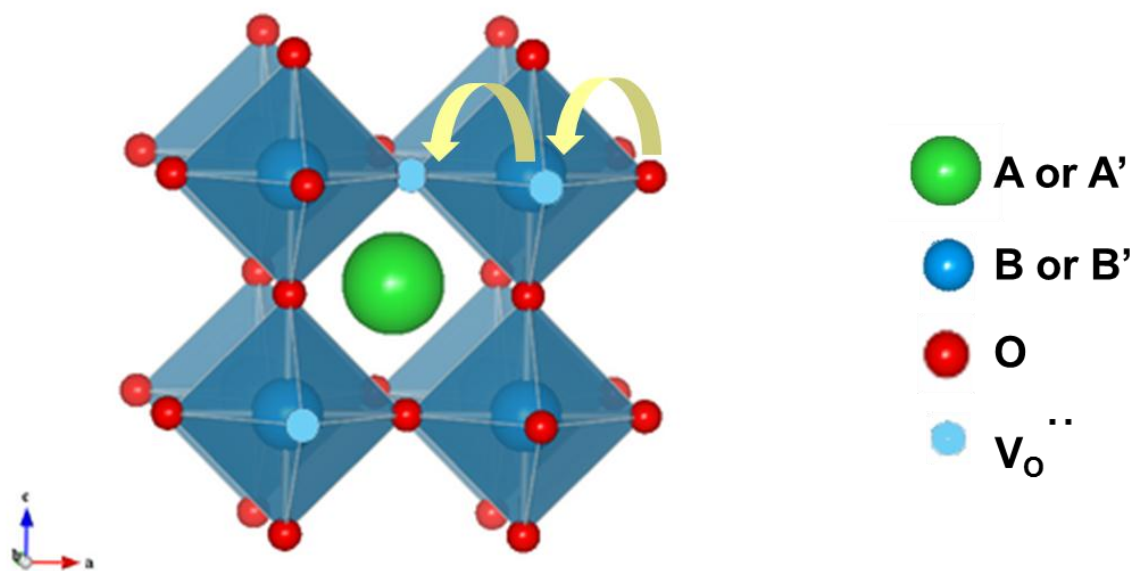
Figure 1.2. Molecular movement of oxygen ion in perovskite-type oxides $AA^{'}BB^{'}O_{3-\delta}$.[25]

The formation of the oxygen vacancies is closely related to the cations A and B. By doping appropriate cations $A^{'}$ or $B^{'}$ with lower valance state in comparison to A or B, oxygen vacancies are formed in order to keep the electrical neutrality. An increasing temperature also leads to the reduction of the B-site cation, accompanied by an additional loss of lattice oxygen which leads to more oxygen vacancies. As shown in figure 1.2, the oxygen vacancies allow the migration of the oxygen ion through the perovskite lattice. Generally, the concentration of the oxygen vacancies and the diffusion coefficients (discussed later) play an important role for the ionic conductivity of the material. An oxide exhibiting a large oxygen deficit - with retention of the perovskite crystal structure - usually shows a high ionic conductivity. For example, the excellent membrane material candidate BSCF is highly oxygen deficient with a maximum oxygen stoichiometry $(3 - \delta)$ of 2.339 at 873 K and a pO_2 of 1 atm and a minimum of $(3 - \delta)$ of 2.192 at 1173 K and a pO_2 of 10^{-3} atm. [26]

The electronic conductivity is realized through the small-polaron hopping with a mechanism similar to the Zener double exchange. With help of the 2p orbital of oxygen, the electron is allowed to transfer from one B-site cation to another, as shown in the following:[27]

$$B^{n+} - O^{2-} - B^{(n+1)+} \rightarrow B^{n+} - O^- - B^{n+} \rightarrow B^{(n+1)+} - O^{2-} - B^{n+}$$
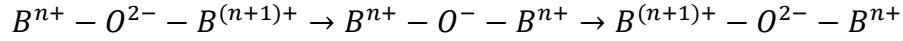
Clearly, a multivalent transition metal cation is important for the whole electronic conductivity of the material. For this reason, a fixed valence state doping element on the B-site causes a lower electronic conductivity while the cobalt and iron-containing perovskites normally exhibit a good electronic conductivity. Also, a small cation on either A or B site promotes the easy exchange of electrons and thus the overall electronic conductivity.

These properties of the perovskite ensure that oxygen can permeate from one side to the other through the membrane. However, to determine the permeability, the oxygen partial pressure difference as driving force and the diffusion rates through the membrane should also be considered.

Bulk diffusion and surface exchange

Figure 1.3 simply illustrates the bulk diffusion and the surface exchange of oxygen species through an oxygen transporting membrane: i) the gaseous molecular oxygen O_2 is first activated to atomic oxygen species O^* and then to an oxygen ion, the whole process is called surface exchange I at the oxygen feed side, ii) then the generated oxygen ion is transferred from the feed side to the permeate side of the membrane via bulk diffusion, iii) in the end, the recombination of two surface oxygen ions on the oxygen permeate side generates the gaseous oxygen and 4 electrons called as surface exchange II at the oxygen permeate side. At given oxygen partial

pressure gradient, varying the thickness of the membrane is a proper method to identify the rate limiting step of oxygen permeation.
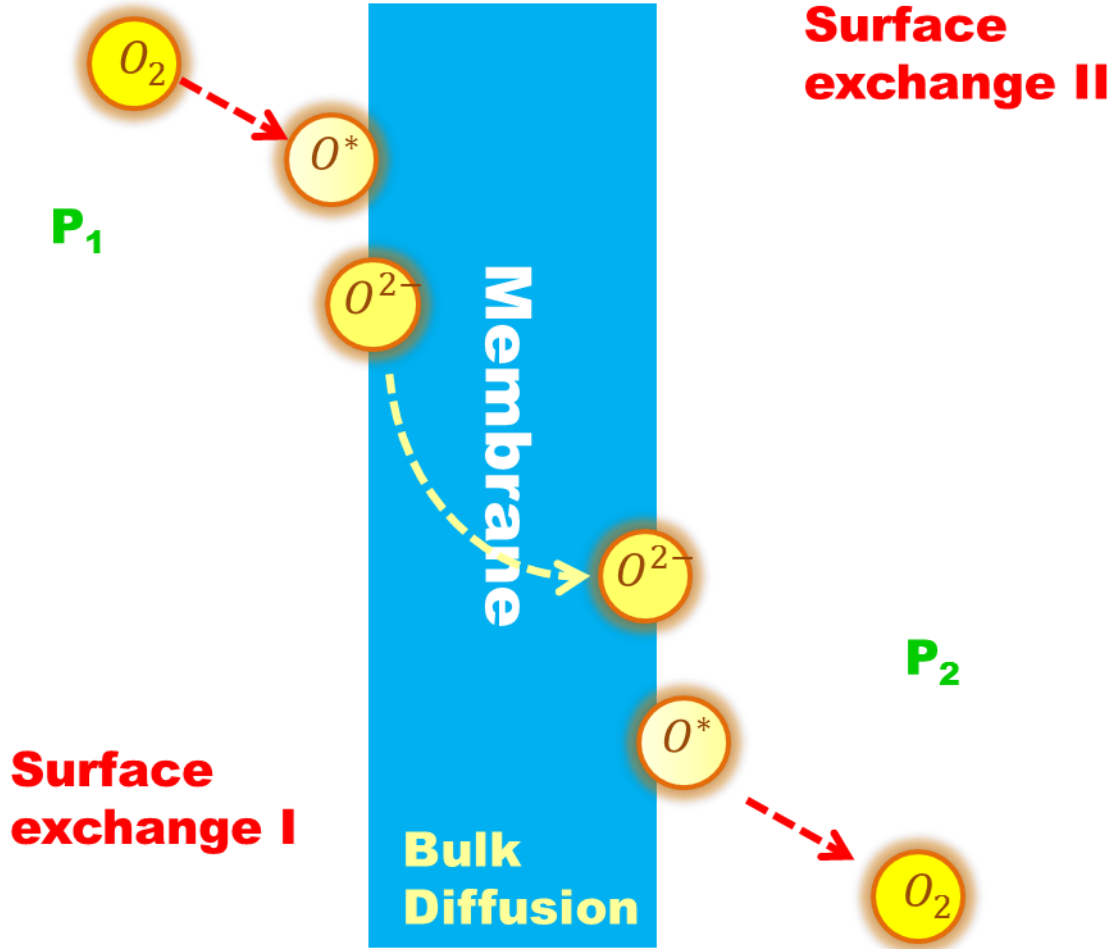

Figure 1.3. The surface exchange and bulk diffusion of oxygen through the membrane.

The overall migration of the oxygen through the membrane could be described by the Wagner equation, if the bulk diffusion is rate limiting for the membrane performance:

$$j(O_2) = \frac{RT}{(4F)^2 L} \cdot \int_{lnP_2}^{lnP_1} \frac{\sigma_{el}\sigma_{ion}}{\sigma_{el} + \sigma_{ion}} dlnP$$

where R, F and L are the gas constant, Faraday constant and temperature, respectively. σ_{el} and σ_{ion} denote the electronic and ionic conductivities. P_1 and P_2 represent the oxygen partial pressures on the feed side and the permeate side. As can be concluded from the equation, not only the intrinsic properties of the materials such as electronic and ionic conductivities play a role in the permeability, but also the thickness of the membrane, the temperature and the oxygen partial pressures are involved in the determination of the membrane performance. In the case of $\sigma_{el} \gg \sigma_{ion}$, the equation can be simplified as follows:

$$j(O_2) = \frac{RT\sigma_{ion}}{(4F)^2 L} \cdot ln\frac{P_1}{P_2}$$

Following this theory, it is clear that the oxygen permeability is a function of the thickness of the membrane L and the oxygen gradients along the thickness of the membrane, $ln\frac{P_1}{P_2}$. However, the Wagner theory can only be applied when the oxygen permeation flux is determined by the bulk diffusion rate, which is the case if the membrane thickness is greater than a critical value L_c.

The L_c is given by the ratio of the self-diffusion coefficient and surface exchange rate at given temperature.[28,29] If the membrane thickness is smaller than L_c, the surface exchange rate becomes dominating. In this case, the Wagner equation is no longer valid. Lee and Bouwmeester's work demonstrate that a liner relationship between the permeability and $(\frac{P_1}{P_0})^n - (\frac{P_2}{P_0})^n$ can be established if the surface exchange rate is the key step for the whole oxygen permeation process, shown as below:[30]

$$j(O_2) = K \left((\frac{P_1}{P_0})^n - (\frac{P_2}{P_0})^n \right)$$

where K is a coefficient effected by oxygen ion concentration, diffusion coefficient of the ion-electron hole pairs and oxygen concentrations of the interfaces of the membrane. The n is the

order of the chemical reaction at the gas-solid interface. Generally, the surface exchange rate can be the limiting step for the overall oxygen permeability when experimental is found that $n \geq 0.5$.

To increase the oxygen flux, the trend in actual R&D is to develop thinner permeation layers. However, upon decreasing thickness, the rate determining step changes from bulk diffusion rate to mixed bulk-surface rate and ultimately to the surface exchange rate. The determination of the decisive step of the overall permeation process is important for the analysis and development of the permeation membrane. In the case that the whole permeation is limited by the bulk diffusion rate, an effective way to improve the permeability is to reduce the thickness through various technologies such as thin film technology for the manufacture of ultrathin membranes[31] and phase inversion spinning followed by sintering for the production of thin-wall hollow fiber membrane.[32] If the performance is controlled by the surface exchange rate rather than by the bulk diffusion rate, coating of a porous layer with the same material as the membrane or other material with higher oxygen surface exchange coefficient can effectively enhance the surface exchange rate and thus the permeability.

1.1.3 Preparation of the oxygen transporting membranes

Various methods such as solid state reaction, hydrothermal synthesis, spray pyrolysis and sol-gel process can be applied in the preparation of the oxygen transporting materials. A modified ethylenediaminetetraacetic acid (EDTA) and citric acid (CA) sol-gel method are the conventional method applied in our group,[33] since this method is simple and offers high purity and highly homogeneous products. As depicted in figure 1.4, various metal nitrates according to the stoichiometric requirement were first mixed in a water based solution. Then, EDTA and CA were added into the solution, the molar ratio of EDTA : CA : total metal cations is 1:1.5:1. The

ammonia was then introduced into the solution until the pH is fixed to around 9. After stirring at around 400 K for 24 – 48 hours, the obtained gel was pre-calcined at ca. 900 K. Following by a calcination at 1223 K for 10 h, the resulting powder can be delivered.
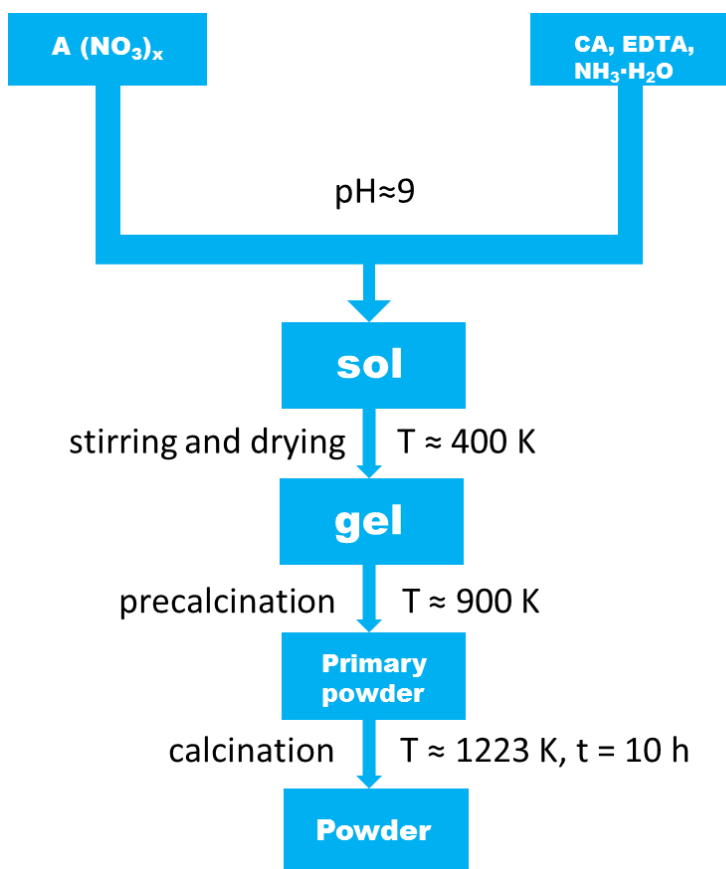

Figure 1.4. Processes involved in the preparation of the oxygen permeation material via sol-gel process.

The dual-phase oxygen transporting membrane material can be prepared through the mixture of two oxides in an ethanol-based solution. The calculated stoichiometric amounts of oxides were milled, mixed and stirred strongly in order to obtain a homogenous dispersion of the powders. After drying, the obtained sample was heated in the oven at 923 K for 1 h.

The membrane was prepared from the powder through pressing and sintering. The as-prepared powder was pressed to green disc membrane under a pressure of 5 MPa in a stainless steel

module with a diameter of 16 mm for the perovskite membrane, 18 mm for the dual phase membrane. The sintering temperature for the perovskite membrane is in the range of 1423-1523 K, while the for dual-phase membrane were sintered in the range of 1573-1673 K.

The tape casting is also known as doctor blading and knife coating as well. It is long-time used in the paint industry to test the covering power of paint formulations. The main advantage of this technology is that it is the easiest way to manufacture large-area, thin, flat ceramic or metallic parts.[34] This preparation method is applied for the preparation of the asymmetric BSCF membrane used in our work. BSCF powder (Treibacher Industie AG, Austria), with an average particle size of 1.7 μm, was used as the primary material, whereas the rice starch (Remy FG, BENEO-Remy), with a particle size of 2-8 μm and the corn starch (Cargill, Germany) with 2-30 μm were applied as the pore former in this work.[35] Two slurries were prepared for the membrane layer and support layer, respectively. The slurry for the membrane layer did not contain any corn starch, whereas the slurry for the support layer containing 15 - 30 wt % pore former.

A 50 μm casting gap was applied for the casting of the dense membrane layer first. After drying, the support layer was cast on top of the membrane layer with the casting gap of 1.9 mm. The obtained green tapes were co-fired at 1100 $^{\circ}$C for 3 h. After firing, the obtained membrane consists of a dense top layer of about 20 (70) μm and a 900 (830) μm thick porous support layer.

1.1.4 Membrane permeator and membrane reactor

The home-made oxygen permeator employed for this work is shown in figure 1.5. The disc membrane was sealed on top of an alumina tube by using gold paste (Heraeus, Germany) or ceramic sealant (Huitian, China). The heat treatment process of the sealing is: i) from room temperature to 950 $^{\circ}$C with a heating rate 2 $^{\circ}$C/min; ii) at 950 $^{\circ}$C, keep 2 h.
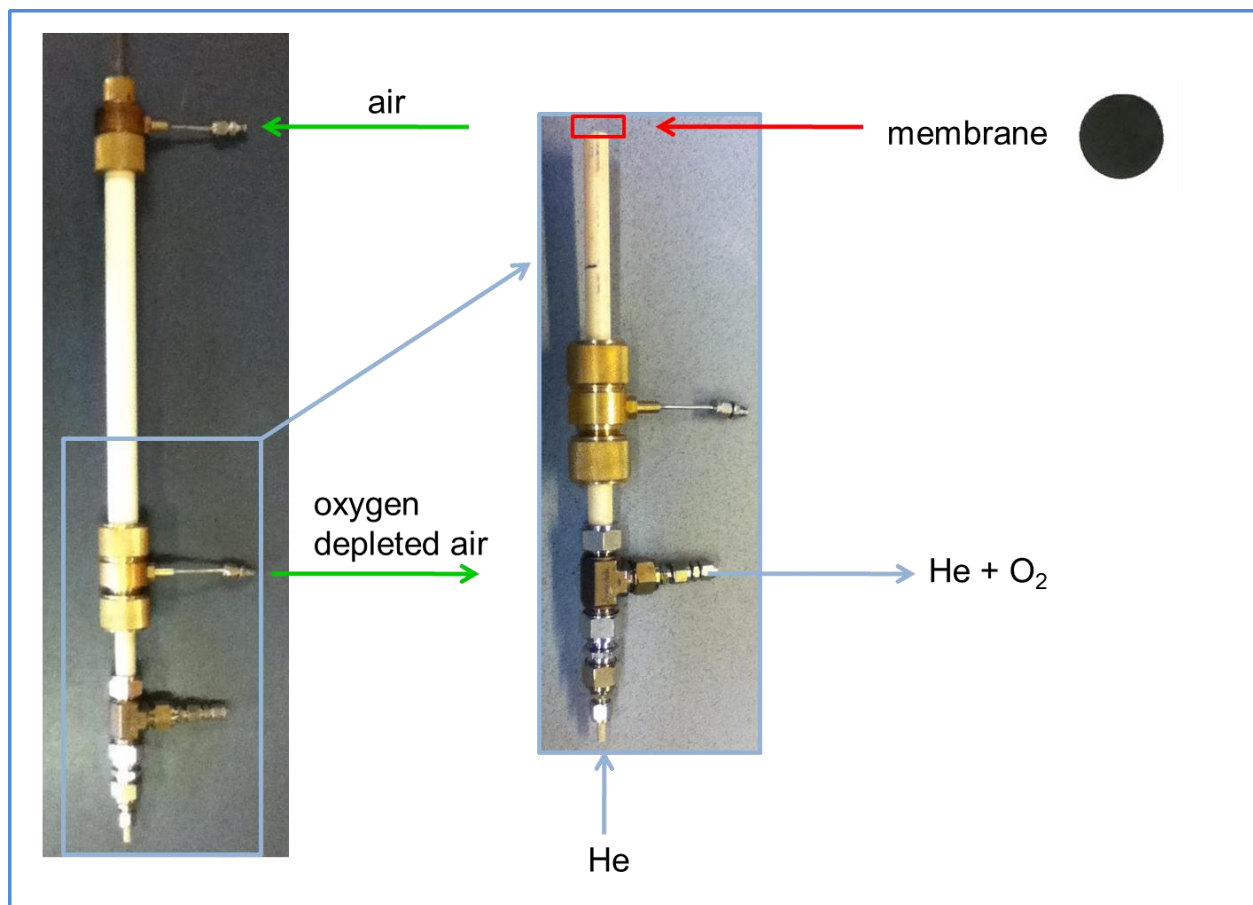
Figure 1.5. Illustration of the permeator.

After heat treatment, for a leakage test a mixture of 1 ml·min^{-1} neon and helium was fed to the permeate side of the membrane, whereas air was fed to the feed side. All gases were controlled by the gas mass flow controllers (Bronkhorst, Germany). Any leakage can be detected by the presence of nitrogen on the permeate side by gas chromatography (GC), since the oxygen transporting perovskite membrane is not permeable to nitrogen. The overall flow on the permeate side was measured by bubble flow meter and calculated from neon concentration, assuming no leakage,

$$F_{in}^{all} \times c_{in}^{Ne} = F_{out}^{all} \times c_{out}^{Ne}$$

After the determination of all gas concentrations, the gas permeation was calculated by the following equation:

$$j(O_2) = \left(c_{O2} - \frac{c_{N2}}{4.02}\right) \times \frac{F_{all}}{S}$$

where the c_{O2} and c_{N2} are the concentrations of oxygen and nitrogen at the outlet, S is the effective area of the membrane. Assuming the leakage of nitrogen and oxygen is in accordance with Knudsen diffusion, the fluxes of leaked N_2 and O_2 are related by 4.02.

The catalytic membrane reactor is based on the same oxygen permeator, the catalyst was packed in the same reactor, as shown in figure 1.6.
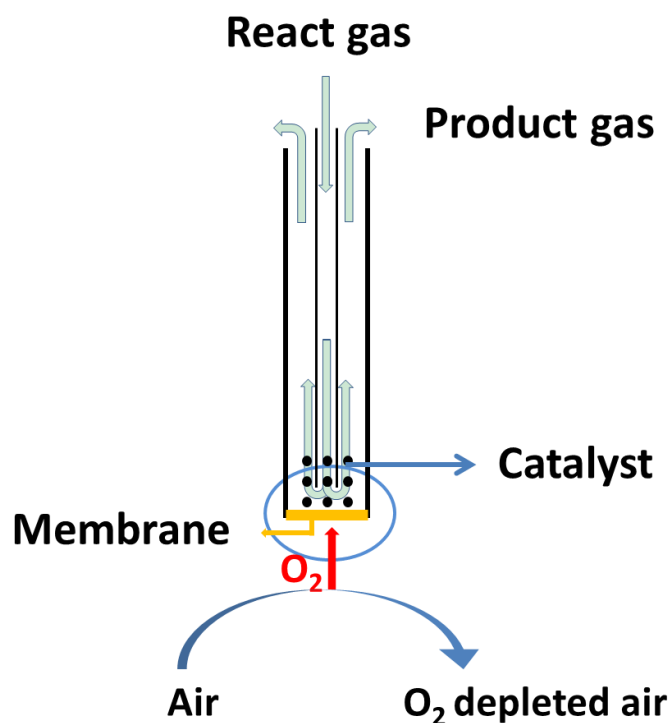

Figure 1.6. Illustration of the catalytic membrane reactor.

The catalyst was packed on top of the membrane; the reacting gas was fed through the small alumina tube into the reaction zone, where the catalyst was deposited. All flow rates were controlled by the gas MFC (Bronkhorst) and all connecting gas lines were heated to temperatures higher than 120 ^{o}C. The concentration of the particular gas was monitored by a gas chromatograph (Agilent 7890). The total gas flow rate at outlet (F_{out}) was calculated as described before. Therefore, the conversion X and the selectivity S were calculated as follows:

$$X = \left(1 - \frac{c_{gas,out} \times F_{all,out}}{F_{all,in}}\right) \times 100\%$$

$$S = \frac{c_{gas,out} \times F_{all,out}}{F_{gas,in} - c_{gas,out} \times F_{out}} \times 100\%$$

Here *gas* is the flow rate of species *i* on the reactant side of the disc membrane.

1.2 Catalysis in membrane reactors

Catalysis plays a key role in industry. Efforts have also been devoted to perform the catalysis process in a membrane rector, although the separation of oxygen from air is the typical application for oxygen transporting membranes.[36] A common implication of those permselective membranes for the reaction application is the selective removal of the product from the reaction zone. This way is an effective path to overcome the limited yields of equilibrium-restricted reactions. For example, the membrane reactor reached close to 100 % conversion for the cyclohexane conversion in comparison to the 18.7 % conversion according to the equilibrium restrictions without membrane concept.[37-42] Furthermore, the past decade has witnessed a huge increase of research interest in the study of highly efficient catalysis processes. The integration of

separation and catalysis in a membrane reactor is highly attractive in the concept of process intensification. The successful realization of the membrane reactor concept offers several advantages and may give a great potential of energy saving and elimination of the process steps.[43]

According to the different ways of catalyst deposition, the catalytic membrane reactors based on permselective membranes can be divided into packed-bed catalytic membrane reactors and membrane-catalyzed catalytic membrane reactor.[44]

1.2.1 Packed-bed catalytic membrane reactor

The principle of a permselective membrane reactor consists of a packed-bed of catalyst and a membrane and is illustrated in figure 1.7.
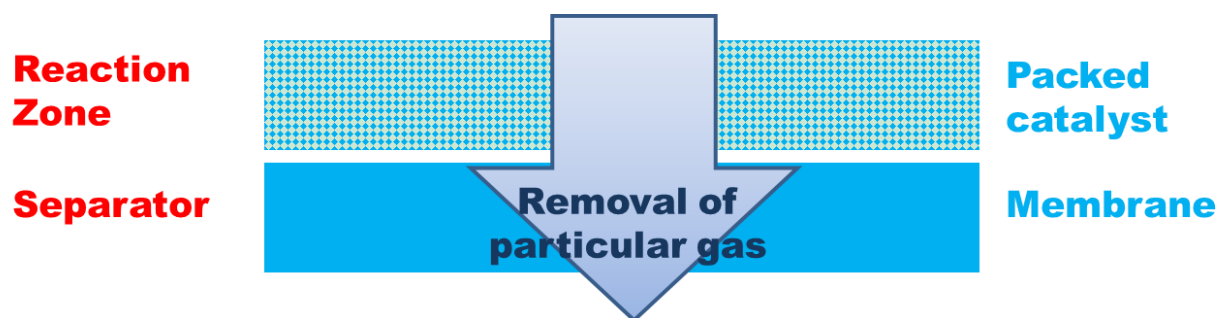

Figure 1.7. The packed-bed catalytic membrane reactor.

The reaction mainly occurs in the zone with packed catalyst, the product is then separated by the permselective membrane driven by the pressure gradient between two sides of the membrane. Conventional methods for the establishment of a sufficient driving force for permeation by reducing the partial pressure of the component to be permeated are the following three methods: a) using an inert sweep gas on the permeate side, b) establishing a pressure difference between the two sides of the membrane, and c) applying a reactive sweep gas to consume the permeated gas, in our case oxygen.[45] The extractor membrane reactor configuration is especially beneficial for

equilibrium limited reactions by extracting one of the product gas to increase the yield beyond the corresponding equilibrium constant.[46-52] However, an extra catalyst is essential since the membrane doesn't play any catalytic role. As a result, the interaction between the catalyst and the membrane should be considered. Following the concept of kinetic compatibility, the amount of products produced/educts consumed in a catalytic reaction must be equal to the amount of educts/products permeated through a membrane. On the other hand, it seems attractive to use the membrane both as separator and catalyst.

1.2.2 Membrane-catalyzed catalytic membrane reactor

If the membrane can play not only the role as a separator, but also as a catalyst, the processes can be further integrated, as depicted in figure 1.8. The membrane can play a role either in removing (a) or feeding (b) more or less selectively one or more components of a reaction mixture.
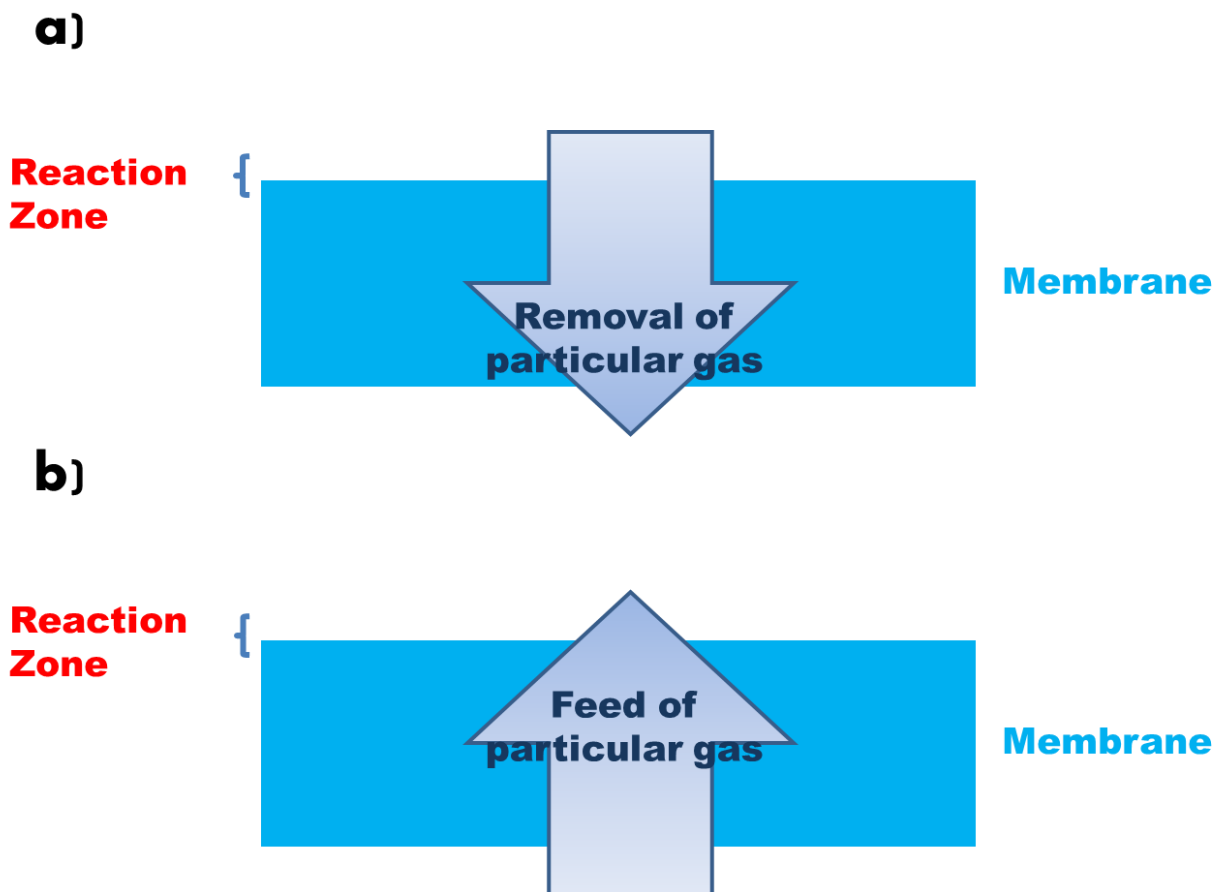
Figure 1.8. The membrane-catalyzed catalytic membrane reactor.

One big advantage of membrane catalysis can be the utilization of the different surface species which are present on the surface of a catalytic membrane. Such species like atomic hydrogen and lattice oxygen have the potential to improve the selectivity and productivity of a reaction.[53] Since oxygen is transformed into the ionic form through the permselective membrane, the presence of lattice oxygen and different forms of atomic surface oxygen species can be expected on the surface of the membrane. Gryaznov demonstrated this concept in numerous early works on catalytic membrane reactors based on hydrogen permeation through palladium membranes. They could proof the involvement of the atomic hydrogen species in the reaction and claimed that the participation of such atomic surface hydrogen (in contrast to the molecular hydrogen)

significantly improves the efficiency of some reactions.[54-59] Similar to the dehydrogenation and hydrogenation applications moderated by a hydrogen transporting membrane, the oxygen transporting membrane offers the possibility to steer partial oxidation and de-oxidation (reduction) reactions. Pioneering work was focused on the proper utilization of the lattice oxygen on the surface of oxygen transporting membranes. This oxygen species can improve the selectivity and the productivity of the oxidative dehydrogenation of the ethane.[60,61] The major reported operating temperature range for the oxygen permeation membrane is around 700 - 1000 ^{o}C. On the other side, the perovskite materials applied for the fabrication of oxygen transporting membranes are intrinsic catalysts for many industry applications.[62-74] Therefore, it becomes increasingly interesting to develop membrane reactors based on oxygen transporting membranes with intrinsic catalytic function to achieve the integration of the separation and catalytic process in the concept of process intensification.

1.3 Objects of this work

In this work it is impossible to illustrate the overall blueprint of the developments and the applications of the membrane reactor; rather than selected topics. The aim of this thesis is to: (a) demonstrate a common concept of combing different catalytic processes in one unit based on oxygen transporting membrane reactor and to propose some novel ideas for achieving a chemically stable membrane for those applications mentioned above, and to (b) achieve the integration of the air production and highly efficient catalytic process with a single oxygen transporting membrane. The membrane configuration is mainly applied for the clean energy generation and high efficient catalytic process.

1.3.1 Clean hydrogen generation

Hydrogen is regarded as a promising clean energy because the only product from its combustion is water. To explore the feasibility of hydrogen production in the membrane reactor, the hydrogen production from thermal water splitting as oxygen producing reaction in combination with oxygen consuming reactions using methane as feed in a membrane reactor will be studied in this work. Methane is regarded as a greatly under-utilized resource, which could serve as a feedstock for the production of future chemicals and liquid fuels.[75] The effective conversion of methane into more valuable chemicals thus remains a longstanding challenge. The work presented here demonstrates some potential alternative for the utilization of methane including oxidative coupling of methane to ethane and ethylene.

1.3.2 Highly efficient catalytic process

By using different catalysts, including extra catalyst or the membrane surface itself as catalyst, the highly efficient methane dehydroaromatization and ammonia oxidation were also studied in this work. The two catalytic processes were studied in this work to explore the feasibility of implicating the membrane configuration in industrial applications. One is the ammonia oxidation to NO, the fundamental process of the nitric acid production and occupies about 90 % of the whole production cost. The other is the methane dehydroaromatization (MDA), which attracts considerable interest from both academia and industry because of its potential in the conversion of methane to chemicals and liquid fuels.

1.4 Reference

1   Armor, J. N. Catalysis with permselective inorganic membranes. *Applied Catalysis* **49**, 1-25, doi:http://dx.doi.org/10.1016/S0166-9834(00)81418-9 (1989).

2   Graves, C., Ebbesen, S. D., Mogensen, M. & Lackner, K. S. Sustainable hydrocarbon fuels by recycling CO(2) and H(2)O with renewable or nuclear energy. *Renewable & Sustainable Energy Reviews* **15**, 1-23, doi:10.1016/j.rser.2010.07.014 (2011).

3   Kruidhof, H., Bouwmeester, H. J. M., v. Doorn, R. H. E. & Burggraaf, A. J. Influence of order-disorder transitions on oxygen permeability through selected nonstoichiometric perovskite-type oxides. *Solid State Ionics* **63–65**, 816-822, doi:http://dx.doi.org/10.1016/0167-2738(93)90202-E (1993).

4   Kharton, V. V., Viskup, A. P., Naumovich, E. N. & Tikhonovich, V. N. Oxygen permeability of LaFe1−xNixO3−δ solid solutions. *Materials Research Bulletin* **34**, 1311-1317, doi:http://dx.doi.org/10.1016/S0025-5408(99)00117-8 (1999).

5   Han, J., Zeng, Y. & Lin, Y. S. Oxygen permeation through fluorite-type bismuth-yttrium-copper oxide membranes. *J. Membr. Sci.* **132**, 235-243, doi:http://dx.doi.org/10.1016/S0376-7388(97)00064-1 (1997).

6   Kharton, V. V. *et al.* Oxygen ionic conduction in brownmillerite CaAl0.5Fe0.5O2.5+δ. *Materials Research Bulletin* **38**, 773-782, doi:http://dx.doi.org/10.1016/S0025-5408(03)00069-2 (2003).

7   Kharton, V. V. *et al.* Oxygen ionic and electronic transport in Gd2−xCaxTi2O7 −δ pyrochlores. *J Solid State Electrochem* **7**, 468-476, doi:10.1007/s10008-002-0348-6 (2003).

8   TERAOKA *et al. Oxygen permeation through Perovskite-type oxides*. (Chemical Society of Japan, 1985).

9   Pei, S. *et al.* Failure mechanisms of ceramic membrane reactors in partial oxidation of methane to synthesis gas. *Catal Lett* **30**, 201-212, doi:10.1007/bf00813686 (1994).

10   Švarcová, S., Wiik, K., Tolchard, J., Bouwmeester, H. J. M. & Grande, T. Structural instability of cubic perovskite BaxSr1 − xCo1 − yFeyO3 − δ. *Solid State Ionics* **178**, 1787-1791, doi:http://dx.doi.org/10.1016/j.ssi.2007.11.031 (2008).

11   Arnold, M., Gesing, T. M., Martynczuk, J. & Feldhoff, A. Correlation of the Formation and the Decomposition Process of the BSCF Perovskite at Intermediate Temperatures. *Chemistry of Materials* **20**, 5851-5858, doi:10.1021/cm801463h (2008).

12   Müller, P. *et al.* Secondary Phase Formation in Ba0.5Sr0.5Co0.8Fe0.2O3–d Studied by Electron Microscopy. *Chemistry of Materials* **25**, 564-573, doi:10.1021/cm303670m (2013).

13   Wang, H., Tablet, C., Feldhoff, A. & Caro, J. A Cobalt-Free Oxygen-Permeable Membrane Based on the Perovskite-Type Oxide Ba0.5Sr0.5Zn0.2Fe0.8O3–δ. *Advanced Materials* **17**, 1785-1788, doi:10.1002/adma.200401608 (2005).

14   Martynczuk, J., Liang, F., Arnold, M., Šepelák, V. & Feldhoff, A. Aluminum-Doped perovskites as high-performance oxygen permeation materials. *Chemistry of Materials* **21**, 1586-1594 (2009).

15   Efimov, K. *et al.* Novel cobalt-free oxygen-permeable perovskite-type membrane. *Chemistry of Materials* **22**, 1540-1544 (2010).

16   Luo, H. *et al.* Performance of a ceramic membrane reactor with high oxygen flux Ta-containing perovskite for the partial oxidation of methane to syngas. *J. Membr. Sci.* **350**, 154-160, doi:http://dx.doi.org/10.1016/j.memsci.2009.12.023 (2010).

17   Nagai, T., Ito, W. & Sakon, T. Relationship between cation substitution and stability of perovskite structure in SrCoO3-δ-based mixed conductors. *Solid State Ionics* **177**, 3433-3444 (2007).

18   Efimov, K., Klande, T., Juditzki, N. & Feldhoff, A. Ca-containing CO2-tolerant perovskite materials for oxygen separation. *J. Membr. Sci.* **389**, 205-215, doi:http://dx.doi.org/10.1016/j.memsci.2011.10.030 (2012).

19   Czuprat, O., Arnold, M., Schirrmeister, S., Schiestel, T. & Caro, J. Influence of CO2 on the oxygen permeation performance of perovskite-type BaCoxFeyZrzO3-δ hollow fiber membranes. *J. Membr. Sci.* **364**, 132-137,

20   Benson, S. J., Waller, D. & Kilner, J. A. Degradation of La0.6Sr0.4Fe0.8Co0.2O3-δ in carbon dioxide and water atmospheres. *J. Electrochem. Soc.* **146**, 1305-1309 (1999).

21   Zhu, X., Wang, H. & Yang, W. Relationship between homogeneity and oxygen permeability of composite membranes. *J. Membr. Sci.* **309**, 120-127, doi:http://dx.doi.org/10.1016/j.memsci.2007.10.011 (2008).

22   Luo, H. *et al.* CO2-Stable and Cobalt-Free Dual-Phase Membrane for Oxygen Separation. *Angewandte Chemie International Edition* **50**, 759-763, doi:10.1002/anie.201003723 (2011).

23   Luo, H. *et al.* Novel Cobalt-Free, Noble Metal-Free Oxygen-Permeable 40Pr0.6Sr0.4FeO3-δ– 60Ce0.9Pr0.1O2−δ Dual-Phase Membrane. *Chemistry of Materials* **24**, 2148-2154, doi:10.1021/cm300710p (2012).

24   Kharton, V. V. *et al.* Mixed conductivity, oxygen permeability and redox behavior of K2NiF4-type La2Ni0.9Fe0.1O4+δ. *J. Solid State Chem.* **181**, 1425-1433, doi:http://dx.doi.org/10.1016/j.jssc.2008.03.019 (2008).

25   http://www.mrl.ucsb.edu/~dshoe/218/.

26   McIntosh, S., Vente, J. F., Haije, W. G., Blank, D. H. A. & Bouwmeester, H. J. M. Oxygen Stoichiometry and Chemical Expansion of Ba0.5Sr0.5Co0.8Fe0.2O3-δ Measured by in Situ Neutron Diffraction. *Chemistry of Materials* **18**, 2187-2193, doi:10.1021/cm052763x (2006).

27   AN, B., ZHOU, W., GUO, Y., RAN, R. & SHAO, Z. *A composite oxygen-reduction electrode composed of SrSC[0.2]CO[0.8]O[3-δ]perovskite and Sm[0.2]Ce[0.8]O[1.9] for an intermediate-temperature solid-oxide fuel cell*. Vol. 35 (Elsevier, 2010).

28   Steele, B. C. H. Interfacial reactions associated with ceramic ion transport membranes. *Solid State Ionics* **75**, 157-165 (1995).

29   Bouwmeester, H. J. M., Kruidhof, H. & Burggraaf, A. J. Importance of the surface exchange kinetics as rate limiting step in oxygen permeation through mixed-conducting oxides. *Solid State Ionics* **72**, 185-194 (1994).

30   Lee, T. H., Yang, Y. L., Jacobson, A. J., Abeles, B. & Zhou, M. Oxygen permeation in dense SrCo0.8Fe0.2O3-δ membranes: Surface exchange kinetics versus bulk diffusion. *Solid State Ionics* **100**, 77-85 (1997).

31   Baumann, S. *et al.* Ultrahigh oxygen permeation flux through supported Ba0.5Sr0.5Co0.8Fe0.2O3−δ membranes. *J. Membr. Sci.* **377**, 198-205, doi:10.1016/j.memsci.2011.04.050 (2011).

32   Wang, H., Werth, S., Schiestel, T. & Caro, J. Perovskite Hollow-Fiber Membranes for the Production of Oxygen-Enriched Air. *Angewandte Chemie International Edition* **44**, 6906-6909, doi:10.1002/anie.200501914 (2005).

33   Martynczuk, J., Arnold, M., Wang, H., Caro, J. & Feldhoff, A. How (Ba0.5Sr0.5)(Fe0.8Zn 0.2)O3-δ and (Ba0.5Sr0.5) (Co0.8Fe0.2)O3-δ perovskites form via an EDTA/citric acid complexing method. *Advanced Materials* **19**, 2134-2140 (2007).

34   Twiname, T. c. t. a. p. R. E. M. a. E. R.

35   Schulze-Küppers, F., Baumann, S., Meulenberg, W. A., Stöver, D. & Buchkremer, H. P. Manufacturing and performance of advanced supported Ba0.5Sr0.5Co0.8Fe0.2O3−δ (BSCF) oxygen transport membranes. *J. Membr. Sci.* **433**, 121-125, doi:http://dx.doi.org/10.1016/j.memsci.2013.01.028 (2013).

36   Dyer, P. N., Richards, R. E., Russek, S. L. & Taylor, D. M. Ion transport membrane technology for oxygen separation and syngas production. *Solid State Ionics* **134**, 21-33, doi:http://dx.doi.org/10.1016/S0167-2738(00)00710-4 (2000).

37   Itoh, N. Limiting conversions of dehydrogenation in palladium membrane reactors. *Catalysis Today* **25**, 351-356 (1995).

38   Itoh, N. & Sathe, A. M. Hydrogen transport from gas to liquid phase through a palladium membrane. *J. Membr. Sci.* **137**, 251-259 (1997).

39   Itoh, N. & Wu, T. H. An adiabatic type of palladium membrane reactor for coupling endothermic and exothermic reactions. *J. Membr. Sci.* **124**, 213-222 (1997).

40   Itoh, N., Xu, W. C., Hara, S., Kimura, H. M. & Masumoto, T. Solubility of hydrogen in amorphous Pd(1-χ)Si(χ) alloys as hydrogen permeable membranes. *J. Membr. Sci.* **126**, 41-51 (1997).

41   Itoh, N., Xu, W. C., Hara, S., Kimura, H. M. & Masumoto, T. Permeability of hydrogen in amorphous Pd((1-χ))Si(χ) alloys at elevated temperatures. *J. Membr. Sci.* **139**, 29-35 (1998).

42   Wu, T. & Itoh, N. The dehydrogenation and separation of hydrogen occurring in tubular palladium membrane reactors. *Huaxue Gongcheng/Chemical Engineering* **25**, 22-26+33 (1997).

43   Agar, D. W. & Ruppel, W. Multifunktionale Reaktoren für die heterogene Katalyse. *Chemie Ingenieur Technik* **60**, 731-741, doi:10.1002/cite.330601003 (1988).

44   Dittmeyer, R., Höllein, V. & Daub, K. Membrane reactors for hydrogenation and dehydrogenation processes based on supported palladium. *J. Mol. Catal. A: Chem.* **173**, 135-184 (2001).

45   Tsotsis, T. T., Champagnie, A. M., Vasileiadis, S. P., Ziaka, Z. D. & Minet, R. G. Packed bed catalytic membrane reactors. *Chem. Eng. Sci.* **47**, 2903-2908, doi:http://dx.doi.org/10.1016/0009-2509(92)87149-K (1992).

46   Coronas, J. & Santamaría, J. Catalytic reactors based on porous ceramic membranes. *Catalysis Today* **51**, 377-389 (1999).

47   Saracco, G., Neomagus, H. W. J. P., Versteeg, G. F. & Van Swaaij, W. P. M. High-temperature membrane reactors: Potential and problems. *Chem. Eng. Sci.* **54**, 1997-2017 (1999).

48   Zaman, J. & Chakma, A. Inorganic membrane reactors. *J. Membr. Sci.* **92**, 1-28 (1994).

49   Saracco, G., Vesteeg, G. F. & Van Swaaij, W. P. M. Current hurdles to the success of high-temperature membrane reactors. *J. Membr. Sci.* **95**, 105-123 (1994).

50   Armor, J. N. Membrane catalysis: Where is it now, what needs to be done? *Catalysis Today* **25**, 199-207 (1995).

51   Armor, J. N. Applications of catalytic inorganic membrane reactors to refinery products. *J. Membr. Sci.* **147**, 217-233 (1998).

52   Sirkar, K. K., Shanbhag, P. V. & Kovvali, A. S. Membrane in a reactor: A functional perspective. *Ind. Eng. Chem. Res.* **38**, 3715-3737 (1999).

53   Callahan, J. L., Grasselli, R. K., Milberger, E. C. & Strecker, H. A. Oxidation and ammoxidation of propylene over bismuth molybdate catalyst. *Industrial and Engineering Chemistry Product Research and Development* **9**, 134-142 (1970).

54   Tereschenko, G. F. *et al.* New Ti-Ni dense membranes with low palladium content. *International Journal of Hydrogen Energy* **32**, 4016-4022 (2007).

55   Gryaznov, V. M., Ermilova, M. M. & Orekhova, N. V. Membrane-catalyst systems for selectivity improvement in dehydrogenation and hydrogenation reactions. *Catalysis Today* **67**, 185-188 (2001).

56   Gryaznov, V. Metal containing membranes for the production of ultrapure hydrogen and the recovery of hydrogen isotopes. *Sep. Purif. Methods* **29**, 171-187 (2000).

57   Gryaznov, V. Membrane catalysis. *Catalysis Today* **51**, 391-395 (1999).

58   Gryaznov, V. M. *et al.* Preparation and catalysis over palladium composite membranes. *Applied Catalysis A, General* **96**, 15-23 (1993).

59   Gryaznov, V. M. HYDROGEN PERMEABLE PALLADIUM MEMBRANE CATALYSTS. *Platinum Met. Rev.* **30**, 68-72 (1986).

60   Wang, H. H., Cong, Y. & Yang, W. S. Continuous oxygen ion transfer medium as a catalyst for high selective oxidative dehydrogenation of ethane. *Catal Lett* **84**, 101-106 (2002).

61   Wang, H. H., Cong, Y. & Yang, W. S. High selectivity of oxidative dehydrogenation of ethane to ethylene in an oxygen permeable membrane reactor. *Chemical Communications*, 1468-1469, doi:10.1039/b203168j (2002).

62   Arai, H., Yamada, T., Eguchi, K. & Seiyama, T. Catalytic combustion of methane over various perovskite-type oxides. *Applied Catalysis* **26**, 265-276 (1986).

63   Bu, Y., Zhong, Q., Xu, D. & Tan, W. Redox stability and sulfur resistance of Sm0.9Sr0.1CrxFe1-xO3-δ perovskite materials. *J. Alloys Compd.* **578**, 60-66 (2013).

64   Centi, G. & Perathoner, S. Catalysis by layered materials: A review. *Microporous Mesoporous Mater.* **107**, 3-15 (2008).

65   Choudhary, T. V., Banerjee, S. & Choudhary, V. R. Catalysts for combustion of methane and lower alkanes. *Applied Catalysis A: General* **234**, 1-23 (2002).

66   Kato, H., Kobayashi, H. & Kudo, A. Role of Ag+ in the band structures and photocatalytic properties of AgMO3 (M: Ta and Nb) with the perovskite structure. *J. Phys. Chem. B* **106**, 12441-12447 (2002).

67   Machida, M., Yabunaka, J. I. & Kijima, T. Synthesis and photocatalytic property of layered perovskite tantalates, RbLnTa2O7 (Ln = La, Pr, Nd, and Sm). *Chemistry of Materials* **12**, 812-817 (2000).

68   McCarty, J. G. & Wise, H. Perovskite catalysts for methane combustion. *Catalysis Today* **8**, 231-248 (1990).

69   Nishihata, Y. *et al.* Self-regeneration of a Pd-perovskite catalyst for automotive emissions control. *Nature* **418**, 164-167 (2002).

70   Peña, M. A. & Fierro, J. L. G. Chemical structures and performance of perovskite oxides. *Chem. Rev.* **101**, 1981-2017 (2001).

71   Ponce, S., Peña, M. A. & Fierro, J. L. G. Surface properties and catalytic performance in methane combustion of SR-substituted lanthanum manganites. *Applied Catalysis B: Environmental* **24**, 193-205 (2000).

72   Teraoka, Y., Nakano, K., Shangguan, W. & Kagawa, S. Simultaneous catalytic removal of nitrogen oxides and diesel soot particulate over perovskite-related oxides. *Catalysis Today* **27**, 107-113 (1996).

73   Tu, H. Y., Takeda, Y., Imanishi, N. & Yamamoto, O. Ln0.4Sr0.6Co0.8Fe0.2O 3-δ (Ln=La, Pr, Nd, Sm, Gd) for the electrode in solid oxide fuel cells. *Solid State Ionics* **117**, 277-281 (1999).

74   Yoshimura, J., Ebina, Y., Kondo, J., Domen, K. & Tanaka, A. Visible light induced photocalytic behavior of a layered perovskite type niobate, RbPb2Nb3O10. *J. Phys. Chem.* **97**, 1970-1973 (1993).

75   Lunsford, J. H. Catalytic conversion of methane to more useful chemicals and fuels: a challenge for the 21st century. *Catalysis Today* **63**, 165-174 (2000).

Chapter 2

Coupling of two reactions in a membrane reactor

2.1 Summary

The oxygen transporting membrane offers a possibility to directly remove oxygen from an oxygen containing gas mixture without further operation. This advantage provides the potential to integrate the oxygen separation and the catalytic process in a single unit. The main efforts in this chapter were devoted to couple two reactions, one of them producing oxygen and the second one consuming oxygen. Therefore, a high intensification and the overcome of the equilibrium limitation of the particular reaction can also be achieved.

In this chapter, when the water splitting was performed with the coupling of methane in the membrane reactor, the equilibrium limitations of both the non-oxidative methane coupling and the thermal waters splitting are overcome. High processes intensification is achieved. As a result, the methane conversion was increased from 3.7 % to 26 % while the C_2 yield increased from 3.1% to 6.5 %, and a hydrogen production rate of 3.3 cm^3 min^{-1} cm^{-2} is achieved.

2.2 Simultaneous overcome of the equilibrium-limitations in BSCF oxygen-permeable membrane reactors: water splitting and methane coupling

Zhengwen Cao [a], Heqing Jiang [b,*], Huixia Luo [a], Stefan Baumann [c], Wilhelm A. Meulenberg [c], Hartwig Voss [d] and Jürgen Caro [a,*]

[a] *Institute of Physical Chemistry and Electrochemistry, Leibniz University of Hannover, Callinstr.3A, D-30167 Hannover, Germany*

[b] *Max-Planck-Institut für Kohlenforschung, Kaiser-Wilhelm-Platz 1, D-45470 Mülheim an der Ruhr, Germany*

[c] *Forschungszentrum Jülich GmbH, Institute of Energy and Climate Research, Leo-Brandt-Str., D-52425 Jülich, Germany*

[d] *BASF SE, D-67056 Ludwigshafen, Germany*

[*] Corresponding authors. Tel.: +49 511 7623175; Fax: +49 511 76219121.

E-mail addresses: hq.jiang@yahoo.com(H. Jiang), juergen.caro@pci.uni-hannover.de (J. Caro).

Abstract

The equilibrium-limitations of water splitting and the coupling of methane to C_2 hydrocarbons (ethane + ethylene) were simultaneously overcome by using a perovskite $Ba_{0.5}Sr_{0.5}Co_{0.8}Fe_{0.2}O_{3-\delta}$ (BSCF) oxygen-permeable membrane reactor. Oxygen produced from thermal water splitting was transported through the BSCF membrane and consumed in the coupling of methane. The BSCF membrane consists of an about 70 μm thick dense BSCF layer on an about 0.8 mm thick porous BSCF layer as support. By applying the membrane reactor concept instead of a fixed bed reactor without oxygen supply, the methane conversion and C_2 yield increased from 3.7 % to 26 % and 3.1 % to 6.5 % at 950 ^{o}C, respectively. In both experiments, the supported 2 wt. % Mn - 5 wt. % Na_2WO_4 catalyst was used at 950 ^{o}C. Simultaneously, about 9 % of the H_2O injected was converted to hydrogen with a production rate of about 3.3 cm^3 min^{-1} cm^{-2} at 950 °C which is higher than 1 m^3 (STP) H_2 m^{-2} h^{-1}.


Keywords: water splitting, methane coupling, equilibrium limitation, oxygen permeable membrane, perovskite

1.   Introduction

Increasing R&D activities can be observed to convert methane into useful chemicals [1-5]. The direct coupling of methane to C_2 hydrocarbons (ethane + ethylene) is considered as a promising process for the reasonable utilization of natural gas resources because no intermediate step is required [6-8]. However, the production of C_2 through the non-oxidative coupling of methane (reaction 1) is suffering from the relatively low methane conversion as well as C_2 yield [9-11].

$$2CH_4 \leftrightarrows C_2H_6 + H_2 \qquad (1)$$
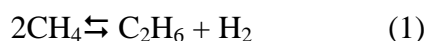
The low equilibrium constant of reaction (1) is due to the positive Gibbs Enthalpy ($\triangle_R G$ (1000 K) = + 71 kJ·mol^{-1}) [12]. However, the C_2 production can be improved when the produced hydrogen is selectively combusted to water. In the so-called oxidative coupling of methane (2), the equilibrium is completely on the side of the products ($\triangle_R G$ (1000 K) = - 159.7 kJ·mol^{-1}). Oxidative coupling of methane to C_2 in oxygen transporting membrane reactors has found, therefore, also industrial interest [13].

$$2 CH_4 + \frac{1}{2} O_2 \rightarrow C_2H_6 + H_2O \quad (2)$$

$$H_2O \leftrightarrows H_2 + \frac{1}{2} O_2 \qquad (3)$$
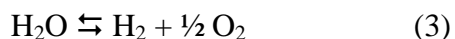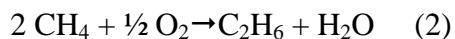
On the other hand, water splitting (3) at high temperatures is also a thermodynamically controlled reaction. Only small amounts of hydrogen can be generated at equilibrium due to the very low equilibrium constant of $K \approx 2 \times 10^{-8}$ even at 950 $^\circ$C [14]. One technique to enhance the hydrogen production rate from the equilibrium-limited water splitting is the in situ removal of the simultaneously produced oxygen using a mixed oxygen ion and electron conducting membrane [15-17], which has been thoroughly studied for oxygen separation from air [18], methane conversion [19] and oxidative dehydrogenation of hydrocarbons [20].

Recently, we have reported several successful couplings of oxygen-producing with oxygen-consuming reactions in membrane reactors [21, 22] using oxygen transporting perovskite membranes. Jiang et al. [23] reported the simultaneous production of synthesis gas and hydrogen by coupling the partial oxidation of methane with water splitting, which was also reported by Evdou et al. [24]. In addition, the effective decomposition of NO [25] and N_2O [26] was achieved by coupling them respectively with the partial oxidation of methane to synthesis gas. In this paper, the combination of thermal water splitting with the oxidative coupling of methane (OCM) to ethane and ethylene is for the first time reported. A novel asymmetric BSCF disc membrane [27, 28] with high oxygen permeation flux (J_{o2}) is used in our membrane reactor.

2. Experimental Section

2.1. Preparation and characterization of membrane

The asymmetric $Ba_{0.5}Sr_{0.5}Co_{0.8}Fe_{0.2}O_{3-\delta}$ (BSCF) perovskite oxygen transporting membranes consist of a dense oxygen separation layer and a porous support layer. Both layers were manufactured by tape casting using a commercial BSCF powder (Treibacher Industrie AG, Austria), which provides perfect chemical compatibility and the same thermal expansion of the two layers. Two different slurries were prepared for the membrane layer and support layer. The slurry for the support layer contained 20 wt. % corn starch (Cargill, Germany) in relation to the total solid content, whereas the slurry used for the membrane layer did not contain any corn starch as pore former. After sintering at 1100 ^{o}C for 3 hours in air, the dsic membrane consists of a dense top layer of about 70 μm and an 830 μm thick porous support layer with 34 % open porosity [29], as shown in Fig. 2.

The crystallinity of the BSCF perovskite membrane before (unused) and after (used) reactions was characterized by X-ray diffraction using a Bruker D8 instrument with Cu_{Ka} radiation. A JEOL JSM-6700F field-emission scanning electron microscope was used to the surface morphology study of the BSCF membrane.

2.2. Preparation of the catalyst

The catalyst applied for OCM consists of 2 wt. % Mn and 5 wt. % Na_2WO_4 supported on SiO_2 [30, 31]. For catalyst preparation, SiO_2 (Davisil, Grade 636, Sigma-Aldrich) was impregnated with aqueous $Mn(NO_3)_2$ $4H_2O$ (Sigma-Aldrich) solution and the mixture was dried at 110 ^{o}C for 4 h. This sample was then impregnated with an aqueous solution of Na_2WO_4 $2H_2O$ (Sigma-Aldrich) to get a catalyst containing 2 wt. % Mn and 5 wt. % Na_2WO_4 (grain size area 0.07 μm^2). Finally, the impregnated sample was heated at 800 ^{o}C for 8 h. Further information can be found in [12].

2.3.   Disc membrane reactor and permeator

For membrane evaluation, the oxygen permeation of the BSCF membrane was studied in a self-made high-temperature oxygen permeator (see Fig. 1) as described previously [32]. The disc membrane was sealed by using gold paste (Heraeus, Germany) onto the alumina tube at 950 ^{o}C for 5 h. The oxygen permeation was first studied under the air/He oxygen partial pressure gradient. Air was fed at a rate of 100 cm^3 min^{-1} to the feed side; a mixture of He (49 cm^3 min^{-1}) and Ne (1 cm^3 min^{-1}) as the internal standard gas was fed to the sweep side. The porous side of the BSCF membrane was exposed to the air, the dense one to the helium side.

In addition, the same permeator was used as membrane reactor for the combination of water splitting and coupling of methane, with an OCM catalyst on the methane side (see Fig. 1). A mixture of steam and He was fed to the water splitting side and a mixture of CH_4 and He with traces of Ne as internal standard was fed to the methane coupling side. The porous side of the BSCF membrane was exposed to the water splitting side; the catalyst containing 2 wt. % Mn and 5 wt. % Na_2WO_4 was packed on top of the dense side of the BSCF membrane, i.e. on the methane coupling side. The study of the methane coupling without membrane support was performed in a fixed-bed reactor which consists of a dense alumina tube with an inside diameter of 4 mm containing 0.5 g 2 wt. % Mn and 5 wt. % Na_2WO_4 catalyst.

All gas flows (CH_4, Ne, He) were controlled by gas mass-flow controllers (Bronkhorst). The concentrations of the outlet gases were measured online by a gas chromatograph (Agilent 6890). The relative leakage of O_2 was found to be less than 5% of the total amount of O_2 detected. The H_2O flow was controlled by liquid mass-flow controllers (Bronkhorst), all pipes connecting reactor and gas chromatograph were heated to 180 ^{o}C.

Hydrogen production rate on the water splitting side was calculated from the total outlet flow rate F_{ws} (water splitting, cm^3 min^{-1}), hydrogen concentration c (H_2), and membrane area S (cm^2) by using the equation below:

$$J(H_2) = \frac{F_{ws} \times c(H_2)}{S}$$

The ethane and ethylene production rates were calculated from the total flow rate on the methane side F_{out}(cm^3 min^{-1}), the ethane or ethylene concentration, $c(C_2H_6)$ or $c(C_2H_4)$. The CH_4 conversion $X(CH_4)$, the C_2 hydrocarbons selectivity, also $S(C_2H_4) + S(C_2H_6)$, $S(C_2)$ and the C_2 yield $Y(C_2)$ were calculated as:

$$X(CH_4) = \left[\frac{F(out, C_2) \times 2 + F(out, CO) + F(out, CO_2)}{F(out, C_2) \times 2 + F(out, CO) + F(out, CO_2) + F(out, CH_4)} \right] \times 100\%$$

$$S(C_2) = \left[\frac{F(out, C_2) \times 2}{F(out, C_2) \times 2 + F(out, CO) + F(out, CO_2)} \right] \times 100\%$$

$$Y(C_2) = X(CH_4) \times S(C_2)$$

where F(i) is the flow rate of species i on the methane coupling side of the disc membrane. By using gas chromatography, if Ne is present in the water splitting side, the leakage can be detected. Both the leakage detection and the catalytic measurements were conducted at the same time.

3. Results and discussion

3.1. Asymmetric BSCF membrane

The BSCF disc membrane (Fig. 2) consists of a 70 μm dense layer and an 830 μm porous support layer. Fig. 2b indicates that the two layers are well attached to each other and no interface

delamination or crack formation was observed. Some small closed pores can be seen in the membrane layer, whose density is about 97 % (Fig. 2b) [29] assuring sufficient gas-tightness. SEM (Fig. 2c) of the BSCF membrane shows that the dense BSCF layer is well sintered and no cracks could be detected. The support (Fig. 2d) is a fine-grained porous layer with about 34 % open porosity enabling gas transport through the support. Further details can be found in [29] and references therein.

3.2.   Oxygen permeation

The oxygen permeation under an air/He oxygen concentration gradient was studied in the temperature range from 850 to 950 ℃. Fig. 3 depicts the effect of temperature on the oxygen permeation flux of the BSCF disc membrane. The permeation flux increased with increasing temperature and an oxygen permeation flux of 3.3 cm^3 min^{-1} cm^{-2} was obtained at 950 ^{o}C. A previous study [33] pointed out that both bulk diffusion of oxygen ions and the surface exchange processes determine the permeation flux. Due to the ultra thin dense BSCF layer of 70 μm, the contribution of the bulk oxygen ions diffusion to the overall oxygen transport resistance is relatively low. Meanwhile the surface reaction is enhanced, since more sites for the dissociation of molecular oxygen to oxygen ions are provided by the porous support layer. Therefore, relatively high oxygen fluxes were obtained at 950 ^{o}C when using He as sweep gases, which are higher than those reported in previous work [32].

Fig. 4 demonstrates the influence of the sweep gas flow rate on the oxygen permeation. An almost doubling of the oxygen permeation rate can be observed when the sweep gas rate is raised from 10 to 50 cm^3 min^{-1}. A further increase of the sweep gas flow rate only slightly improves the oxygen permeation flux and J_{O2} reaches 3.7 cm^{3}min^{-1}cm^{-2} at a sweep rate of 150 cm^3 min^{-1}. According to the well-known Wagner theory, the driving force for the oxygen permeation is the

oxygen partial pressure gradient between the two sides of the membrane [34]. J_{O2} can be enhanced by increasing the oxygen partial pressure gradient via increasing the sweep gas flow rate.

3.3.   Coupling of methane: oxidative and non-oxidative

The coupling of methane to C_2 was studied in both (i) fixed bed reactor and (ii) membrane reactor. using 2 wt. % Mn and 5 wt. % Na_2WO_4 on SiO_2 as catalyst at 950 ^{o}C (Fig. 5). A methane conversion of 26 % and a C_2 product yield of 6.5 % can be realized at 950 ^{o}C in the membrane reactor (ii), while the methane conversion and C_2 yield obtained in case (i) is only 3.7 % and 3.1 %, respectively. This experimental finding can be explained as follows. With increasing temperature, the equilibrium constant of the thermal water splitting increases, and higher oxygen partial pressures are found on the water side. Rising temperature also increases the oxygen transport performance of the BSCF membrane. On the methane coupling side, with increasing temperature more ·CH_3 radicals are formed over the catalyst which recombine in a homogeneous gas phase reaction to C_2H_6, which can undergo a subsequent dehydrogenation to C_2H_4. Since the oxygen permeated through the membrane is consumed quickly by the hydrogen combustion, the oxygen partial pressure on the methane coupling side is very low and a continuous flow of oxygen from the water side to the methane side starts. As a result, the methane conversion increases by a factor of 6 when the catalytic membrane reactor concept is applied.

Fig. 6 shows the temperature dependence of the conversion of methane, the selectivity and yield of C_2 formation when feeding 20 vol% CH_4. The methane conversion as well as the C_2 yield increase with increasing temperature. It is noteworthy that the C_2 selectivity increases with increasing temperature in the temperature range < 925 ^{o}C and decreases for temperature > 925 ^{o}C. Compatibility of the two reactions means that the amount of oxygen transported through the

BSCF membrane is the stoichiometric amount of oxygen for the selective hydrogen combustion. Obviously, best compatibility between the two reactions was achieved under our experimental conditions at 925 ℃.

3.4.   Hydrogen production from water splitting

In a previous paper we reported that if only helium is used as sweep gas to remove the oxygen generated from water splitting in the case of a hollow fiber membrane, the hydrogen production rate is very low even at 950 ^{o}C [23]. Higher oxygen partial pressure gradients, and thus higher driving forces, can be reached if the oxygen partial pressure on the permeate side is decreased by consuming the oxygen in a chemical reaction, here in the selective hydrogen combustion. Fig. 7 presents the hydrogen production rate on the water dissociation side at various temperatures with methane coupling on the opposite side of the membrane. By feeding 100 cm^3 min^{-1} of a He/CH$_4$ mixture with 20 % CH$_4$, the hydrogen production rate increases from 0.4 to 3.3 cm^3 min^{-1} cm^{-2} when rising the temperature from 850 to 950 ^{o}C. Thus, a hydrogen production rate of over 1 m^3 (STP) H$_2$ m^{-2} h^{-1} can be achieved at 950 ^{o}C. Since no oxygen was detected on the steam side, oxygen produced from water splitting was transported to the methane side, and has been consumed there by OCM. The oxygen production rate is around 1.65 cm^3 min^{-1} cm^{-2} (50% of the hydrogen production rate), which is lower than that in the case of oxygen permeation under an air/He oxygen partial pressure gradient. Several factors are responsible for this experimental finding: a) the equilibrium constant of the endothermic water splitting is increased leading to higher oxygen-equilibrium concentrations at high temperatures, b) the oxygen transport through the BSCF membrane is enhanced with increasing temperature according to Wagner Theory [35], and c) oxygen is consumed faster in the OCM at higher temperatures.

Fig. 8 presents the room temperature X-ray diffraction patterns of the unused and used BSCF disc membranes. The starting BSCF membrane is mainly composed of cubic BSCF perovskite, but also small amounts of a foreign phase identified as hexagonal perovskite can be found [36]. After 20 h use in the OCM reaction, a decrease of the perovskite reflections is observed while the reflections of different cobalt-containing phases increased. In previous works, the extraction of cobalt species from perovskite in high-temperature reactions was reported [37, 38]. Obviously, cobalt escapes from the BSCF bulk phase and form different cobalt oxides of low oxidation state and even metallic cobalt, when BSCF is operated under reducing atmospheres. We have to state, therefore, that the cobalt-containing perovkite BSCF is not long-time stable under the reaction conditions of OCM. Thus, further search for perovskite materials that are more stable under reducing atmospheres is required.

4.   Conclusion

Methane coupling and water dissociation were for the first time successfully combined in a catalytic membrane reactor. The achievable conversions of the two equilibrium-limited reactions, the water splitting and the methane coupling, were significant improved. The methane conversion was enlarged from 3.7 % to 26 % while the C_2 yield increased from 3.1% to 6.5 % using a 2 wt. % Mn - 5 wt. % Na_2WO_4 on SiO_2 as catalyst at 950 ^{o}C. On the other hand, although the equilibrium constant of water splitting is only about 2×10^{-8} at this temperature, about 9 % H_2O were converted to hydrogen and oxygen due to the in situ removal of oxygen through the BSCF membrane. As a result, a hydrogen production rate of 3.3 cm^3 min^{-1} cm^{-2} is achieved on the water splitting side of the membrane. The catalytic membrane reactor provides not only a possibility to overcome equilibrium limitations; it also separates the different products inherently. However, the BSCF membrane turned out to be not long-time stable in the reducing atmosphere of the methane coupling.
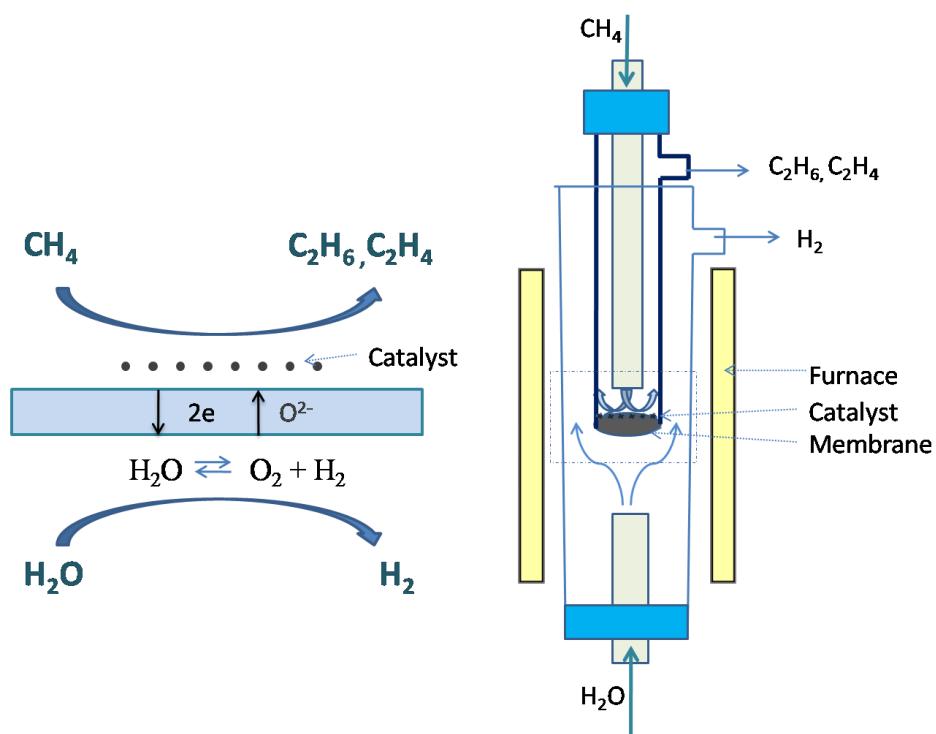
Fig. 1. Schematic diagram of performing oxidative methane coupling and water splitting in an oxygen-transporting perovskite disc membrane reactor.
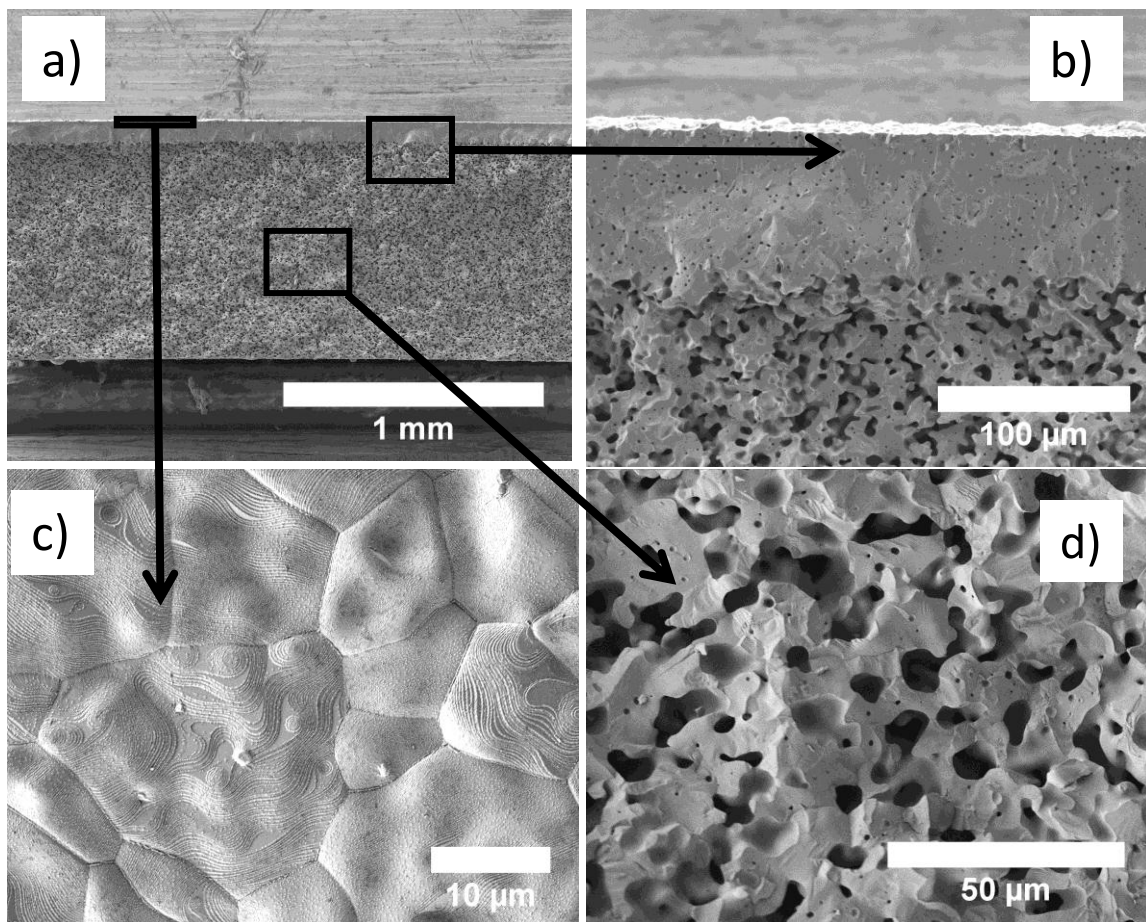
Fig. 2. SEM micrographs of the unused BSCF membrane: a) overview of the membrane, b) cross section of the dense BSCF part, c) surface of the dense BSCF side, d) cross section of the porous BSCF part which acts as support for the dense part.
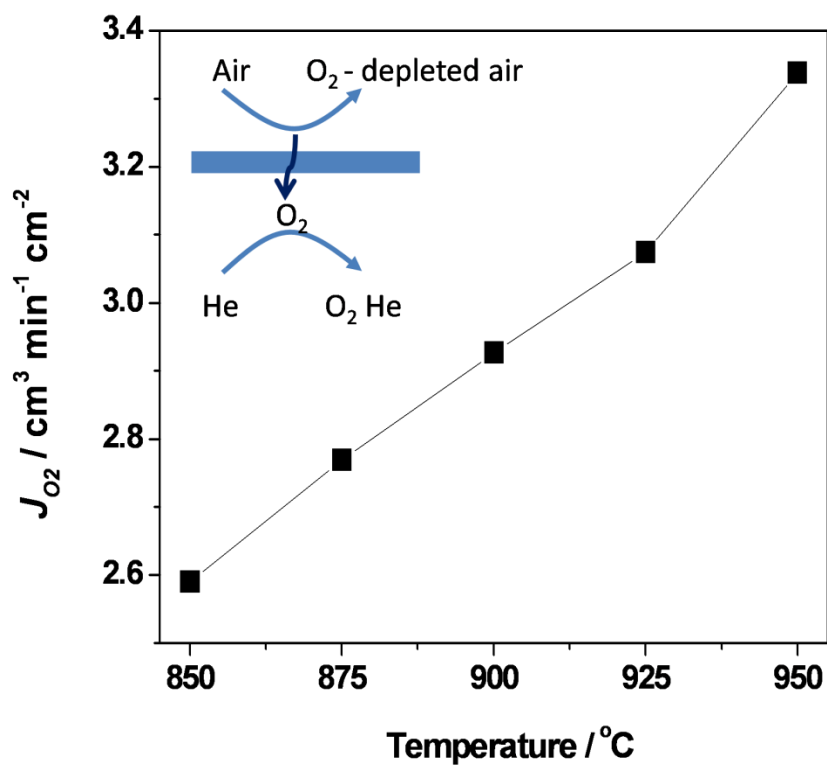
Fig. 3. Oxygen-permeation flux as a function of temperature through a BSCF membrane. Feed side: $F_{Air} = 100$ cm^3 min^{-1}; Sweep side: $F_{He} = 49$ cm^3 min^{-1} and $F_{Ne} = 1$ cm^3 min^{-1}.
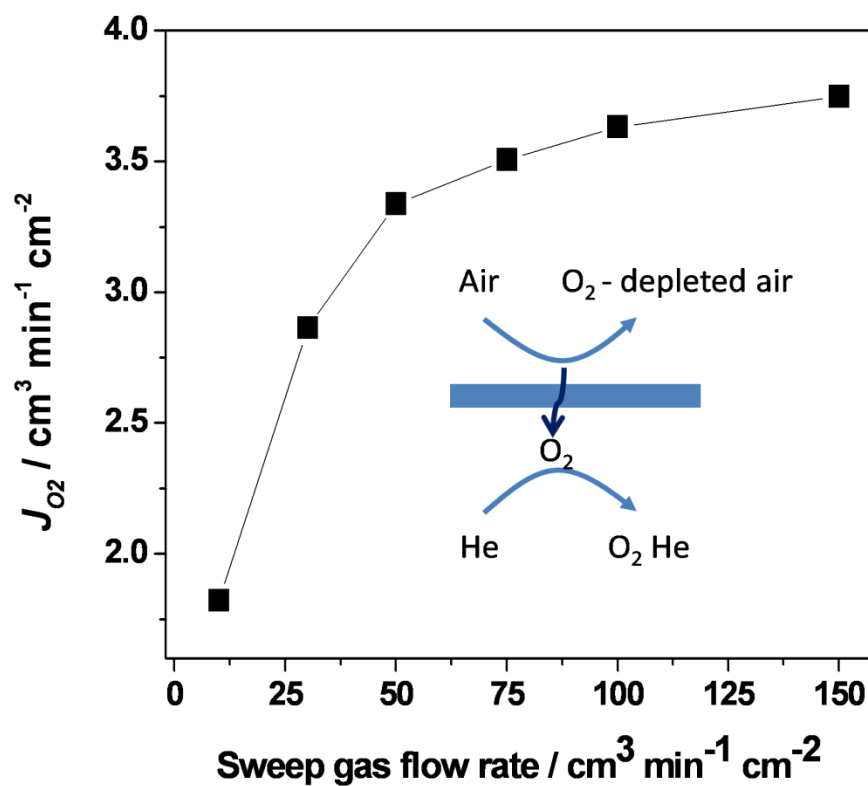
Fig. 4. Oxygen-permeation flux through a BSCF membrane at 950 ^{o}C as a function of the sweep gas flow rate. Feed side: F_{Air} = 100 cm^3 min^{-1}; Sweep side: F_{Ne} = 1 cm^3 min^{-1} and F_{He} = F_{sum} - F_{Ne}.
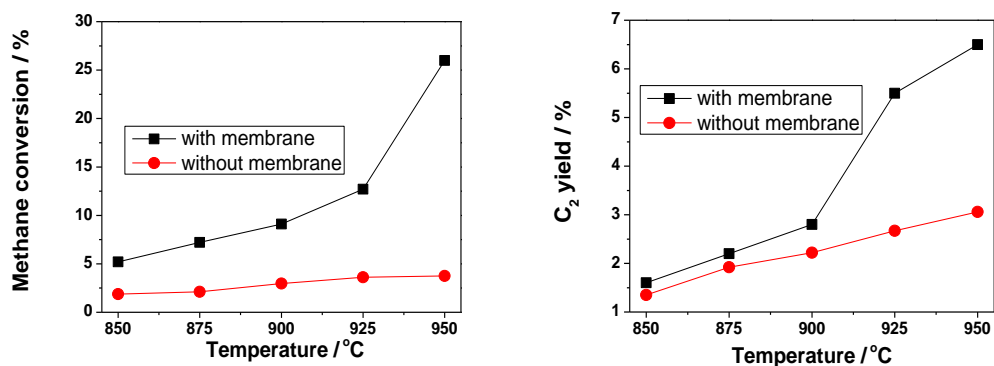
Fig. 5. Methane conversion (left) and C_2 yield (right) with and without membrane as a function of temperature with diluted methane as feed. The flow rates for the membrane reactor are on the water splitting side: $F_{H2O} = 30$ cm^3 min^{-1} and $F_{He} = 10$ cm^3 min^{-1}, on the methane coupling side: $F_{Ne} = 1$ cm^3 min^{-1}, $F_{CH4} = 20$ cm^3 min^{-1} and $F_{He} = 79$ cm^3 min^{-1}. Without membrane: $F_{Ne} = 1$ cm^3 min^{-1}, $F_{CH4} = 20$ cm^3 min^{-1} and $F_{He} = 79$ cm^3 min^{-1}. 0.5 g catalyst.
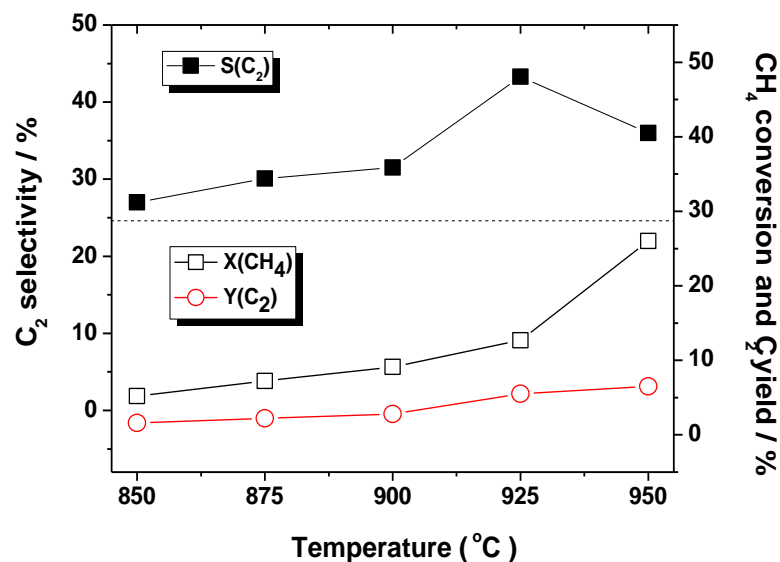
Fig. 6. Methane conversion X(CH$_4$), ethane + ethylene selectivity S (C$_2$) and yield Y (C$_2$) as a function of temperature. Water splitting side: F$_{H2O}$ = 30 cm^3 min^{-1} and F$_{He}$ = 10 cm^3 min^{-1}, methane coupling side: F$_{Ne}$ = 1 cm^3 min^{-1}, F$_{CH4}$ = 20 cm^3 min^{-1} and F$_{He}$ = 79 cm^3 min^{-1}. 0.5 g catalyst.
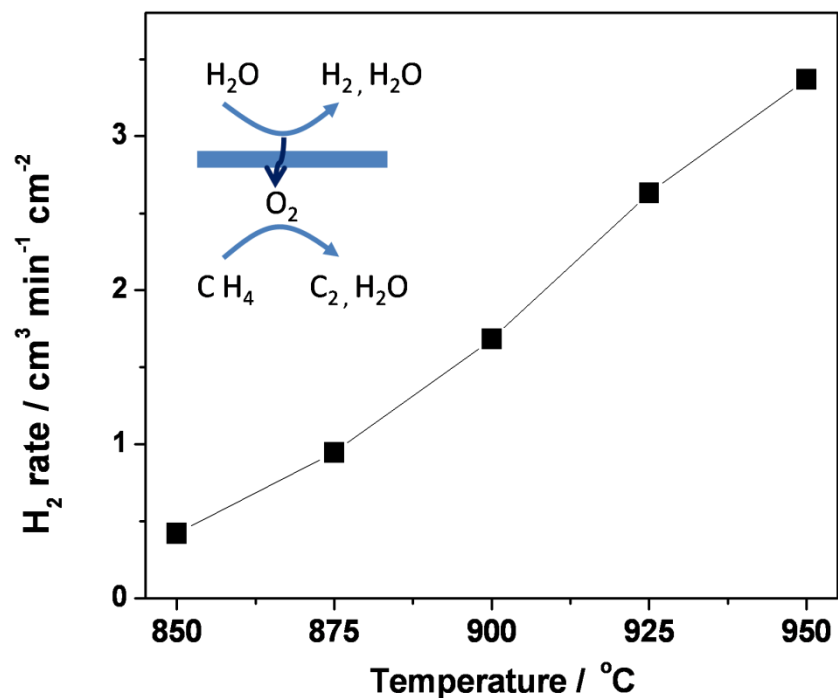
Fig. 7. H_2 production rates as a function of temperature for the BSCF membrane reactor. Water splitting side: $F_{H2O} = 30$ cm^3 min^{-1} and $F_{He} = 10$ cm^3 min^{-1}, methane coupling side: $F_{Ne} = 1$ cm^3 min^{-1}, $F_{CH4} = 20$ cm^3 min^{-1} and $F_{He} = 79$ cm^3 min^{-1}, 0.5 g of catalyst.
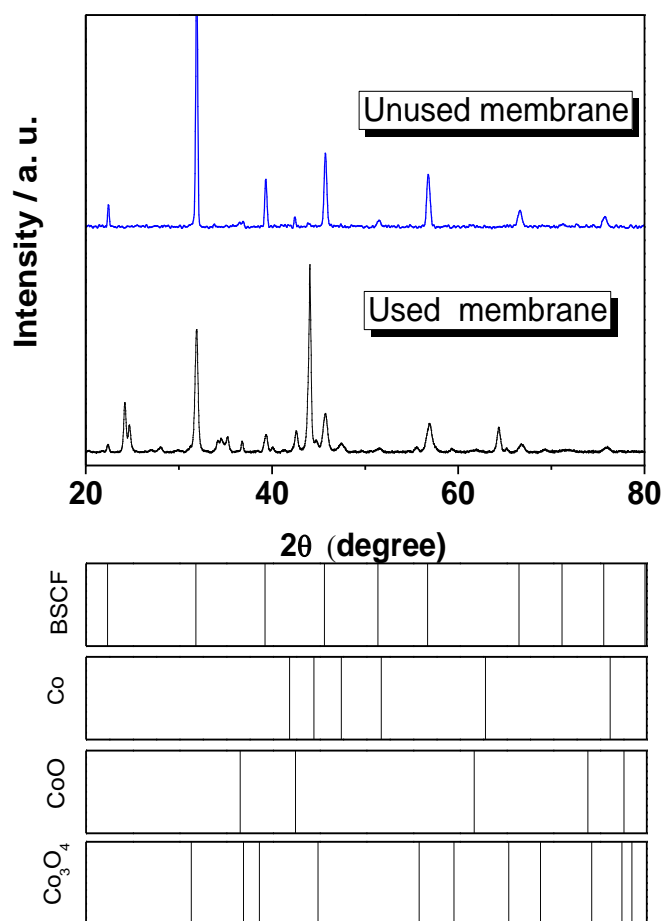
Fig. 8. XRD patterns of unused and used (after 20 h in the membrane reactor, applying for OCM/water splitting at the temperature range between 850 and 950 ^{o}C) BSCF membranes. Shown is the dense BSCF layer exposed to the methane coupling side.

Reference

[1]   H.J.M. Bouwmeester, Catal. Today 82 (2003) 141-150.
[2]   D.A. Hickman, L.D. Schmidt, Science 259 (1993) 343-346.
[3]   J.H. Lunsford, Catal. Today 63 (2000) 165-174.
[4]   J.R. Rostrupnielsen, Catal. Today 18 (1993) 305-324.
[5]   C.S. Chen, S.J. Feng, S. Ran, D.C. Zhu, W. Liu, H.J.M. Bouwmeester, Angew. Chem. Int. Ed. 42 (2003) 5196-5198.
[6]   S.M. Liu, X.Y. Tan, K. Li, R. Hughes, CATAL. REV-SCI. ENG. 43 (2001) 147-198.
[7]   Y.P. Lu, A.G. Dixon, W.R. Moser, Y.H. Ma, U. Balachandran, J. Membr. Sci. 170 (2000) 27-34.
[8]   S.J. Xu, W.J. Thomson, AIChE J. 43 (1997) 2731-2740.
[9]   Y.T. Liu, X.Y. Tan, K. Li, Ind. Eng. Chem. Res. 45 (2006) 3782-3790.
[10]   M. Belgued, P. Pareja, A. Amariglio, H. Amariglio, Nature 352 (1991) 789-790.
[11]   Z.P. Shao, H. Dong, G.X. Xiong, Y. Gong, W.S. Yang, J. Membr. Sci. 183 (2001) 181-192.
[12]   O. Czuprat, T. Schiestel, H. Voss, J. Caro, Ind. Eng. Chem. Res. 49 (2010) 10230-10236.
[13]   E. Schwab, H. Voss, F. Kiesslich, O. Machhammer, A. Dittmar, M. Noack, U. Dingerdissen, G. Georgi, WO Pat. Appl. 2009/071463 from June 11, 2009, asigned to BASF. (2009).
[14]   S. Ihara, Bull. Electrotech. Lab. 41 (1977) 259-280.
[15]   H. Fjellvag, B.C. Hauback, R. Bredesen, J. Mater. Chem. 7 (1997) 2415-2419.
[16]   H.X. Luo, K. Efimov, H.Q. Jiang, A. Feldhoff, H.H. Wang, J. Caro, Angew. Chem. Int. Ed. 50 (2011) 759-763.
[17]   J. Sunarso, S. Baumann, J.M. Serra, W.A. Meulenberg, S. Liu, Y.S. Lin, J.C.D. da Costa, J. Membr. Sci. 320 (2008) 13-41.
[18]   F.Y. Liang, H.Q. Jiang, T. Schiestel, J. Caro, Ind. Eng. Chem. Res. 49 (2010) 9377-9384.
[19]   H.Q. Jiang, H.H. Wang, S. Werth, T. Schiestel, J. Caro, Angew. Chem. Int. Ed. 47 (2008) 9341-9344.
[20]   H.H. Wang, Y. Cong, W.S. Yang, Catal. Lett. 84 (2002) 101-106.
[21]   R. Dittmeyer, V. Hollein, K. Daub, J. Mol. Catal. A. Chem. 173 (2001) 135-184.
[22]   J.M. van de Graaf, M. Zwiep, F. Kapteijn, J.A. Moulijn, Chem. Eng. Sci. 54 (1999) 1441-1445.
[23]   H.Q. Jiang, H.H. Wang, F.Y. Liang, S. Werth, S. Schirrmeister, T. Schiestel, J. Caro, Catal. Today 156 (2010) 187-190.
[24]   A. Evdou, V. Zaspalis, L. Nalbandian, Fuel 89 (2010) 1265-1273.
[25]   H.Q. Jiang, L. Xing, O. Czuprat, H.H. Wang, S. Schirrmeister, T. Schiestel, J. Caro, Chem. Commun. (2009) 6738-6740.
[26]   H.Q. Jiang, H.H. Wang, F.Y. Liang, S. Werth, T. Schiestel, J. Caro, Angew. Chem. Int. Ed. 48 (2009) 2983-2986.
[27]   W.Q. Jin, S.G. Li, P. Huang, N.P. Xu, J. Shi, J. Membr. Sci. 185 (2001) 237-243.
[28]   L. Tan, X.H. Gu, L. Yang, L.X. Zhang, C.Q. Wang, N.P. Xu, Sep. Purif. Technol. 32 (2003) 307-312.
[29]   S. Baumann, J.M. Serra, M.P. Lobera, S. Escolástico, F. Schulze-Küppers, W.A. Meulenberg, J. Membr. Sci. (2011) doi: 10.1016.
[30]   Z.C. Jiang, C.J. Yu, X.P. Fang, S.B. Li, H.L. Wang, J. Phys. Chem. 97 (1993) 12870-12875.
[31]   J.G. Wu, S.B. Li, J. Phys. Chem. 99 (1995) 4566-4568.
[32]   H.H. Wang, C. Tablet, A. Feldhoff, H. Caro, J. Membr. Sci. 262 (2005) 20-26.
[33]   C. Tablet, G. Grubert, H.H. Wang, T. Schiestel, M. Schroeder, B. Langanke, J. Caro, Catal. Today 104 (2005) 126-130.
[34]   S. Kim, Y.L. Yang, A.J. Jacobson, B. Abeles, Solid State Ionics 106 (1998) 189-195.
[35]   M. Schroeder, Phys. Chem. Chem. Phys. 7 (2005) 166-172.
[36]   S. Svarcova, K. Wiik, J. Tolchard, H.J.M. Bouwmeester, T. Grande, Solid State Ionics 178 (2008) 1787-1791.

[37]   H.Q. Jiang, Z.W. Cao, S. Schirrmeister, T. Schiestel, J. Caro, Angew. Chem. Int. Ed. 49 (2010) 5656-5660.

[38]   L. Bedel, A.C. Roger, C. Estournes, A. Kiennemann, Catal. Today 85 (2003) 207-218.

Chapter 3

The development of high-performance oxygen transporting membrane

3.1 Summary

The dual-phase oxygen transporting membrane is regarded as a potential candidate for various applications because it consists of two different phases for ionic and electronic conductivity, respectively. Compared to the single perovskite oxygen transport membrane, it is easier to vary and fine-tune the property of a dual-phase membrane by adjusting the composition and the chemical composition of the constituents.

This chapter demonstrates the development of a new oxygen transporting membrane for the membrane reactor with the aim of various applications such as hydrogen production.

The paper shows that the introduction of 2 mol % cobalt into the cerium-gadolinium mixed oxide (CGO) improves the oxygen permeability of the dual-phase oxygen transporting membrane with the composition of 25 wt. % $Gd_{0.4}Sr_{0.6}Fe_{1.0}O_{3-\delta}$ − 75 wt. % $Ce_{0.9}Gd_{0.1}O_{2-\delta}$. The membrane shows an elevated permeability in comparison with the un-doped membrane, and a good stability under CO_2 and reducing atmospheres.

Note: This paper will be submitted to **Journal of Membrane Science**.

3.2 An effective and simple method in the aim of improving the oxygen permeability of the dual-phase membrane based on $Ce_{0.9}Gd_{0.1}O_{2-\delta}$

Zhengwen Cao [a], Heqing Jiang [b], Huixia Luo [a], and Jürgen Caro [a,]

[a] *Institute of Physical Chemistry and Electrochemistry, Leibniz University of Hannover, Callinstr.3A, D-30167 Hannover, Germany*

[b] *Key Laboratory of Biobased Materials, Qingdao Institute of Bioenergy and Bioprocess Technology, Chinese Academy of Sciences, 189 Songling Road, 266101 Qingdao, China*

Abstract

The introduction of 2 wt % cobalt significantly improves the oxygen permeability of the dual-phase oxygen transporting membrane with the composition of 25 wt.% $Gd_{0.4}Sr_{0.6}Fe_{1.0}O_{3-\delta}$ − 75 wt % $Ce_{0.9}Gd_{0.1}O_{2-\delta}$. The resulted membrane shows not only an elevated permeability, but also a good stability under CO_2 and reducing atmospheres.

1. Introduction

Oxygen permeation membranes have particular properties that meet various special applications such as catalytic oxidation of alkanes, decomposition of NO or N_2O, overcoming the equilibrium-limited of different reactions, pure oxygen production and CO_2-capture oxyfuel process. With a continued growth in the worldwide demand of clean energy generation, there is increasing interest in the development of oxygen permeation membranes possessing high permeability and good stability to meet these different applications. Fundamental challenge facing the commercialization of the oxygen transport membrane based on the widely investigated single perovskite phase materials is their poor stability under CO_2 or reducing atmosphere because of the containing of alkaline earth metal (carbonates formation) or the reducible metals such as cobalt, respectively. A cobalt-free membrane based on the dual-phase concept is positioned to play an increasingly significant role in industry and academia, specifically in the development of the CO_2 and reducing atmospheres–stable oxygen permeation membranes. The shortage of such membranes is their low oxygen permeability compared to perovskite-type oxide membranes. The oxygen permeability can be increased by coating porous layer on the both surfaces of the membrane thus increasing the oxygen surface exchange rates, however, to a certain extent.

For a dual-phase mixed ionic and electronic conducting membrane, both the oxygen ionic conductivity of one phase (e.g. fluorite) and the electronic conductivity of the other (e.g. perovskite) are important for the oxygen permeability. Furthermore, the dual phase continuity ensuring the ambipolar transport of the electrons and oxygen ions is a major factor determining the permeation performance. For example, Lin et. al. found a non-percolative dual-phase sample exhibited a much low electronic conductivity than a percolative sample.[1] Zhu et. al. proposed many different powder preparation methods in order to gain uniformly mixed powders.[2] The

experimental finding of our group demonstrated that the oxygen permeation flux of the membrane can be significantly improved by achieving a continuous electrons and ions transport network in the bulk with a narrow grain size and a homogeneous dispersion.[3] Therefore, if a better continuity of both electronic and ionic transfers can be achieved, an increased permeability can be thus expected.

Doping cobalt is an attractive option for the membrane development. It offers the advantages of elevated electronic conductivity as well as high permeability, whereas its easy reducibility usually causes the crash of the membrane. However, if the cobalt was not doped into the perovskite structure, the decomposition of the perovskite structure might be avoided. Cobalt dissolved in $Ce_xGd_{1-x}O_{2-\delta}$ can also enhance the grain boundary conductivity of the material and lower the sintering temperature.[4] The improved electronic transport through the ionic conducting phase contributes to the continual transport of electrons in the dual-phase membrane; meanwhile the relativity lower sintering temperature is beneficial for narrowing grain size as well as homogeneous dispersion. Therefore, a promoted dual-phase membrane with elevated permeability can be expected.

For the first time, we propose a novel method to add cobalt in the dual phase membrane in the aim of high permeability while maintaining its attractive features. To verify this concept, dual-phase membranes, based on $Ce_xGd_{1-x}O_{2-\delta}$ fluorite, 25 wt. % $Gd_{0.4}Sr_{0.6}FeO_{3-\delta} - 75$ wt. % (2 mol % Co) $Ce_{0.9}Gd_{0.1}O_{2-\delta}$ with (GSF-CoCGO) or without cobalt-adding (GSF-CGO) are prepared and evaluated.

2. Experimental Section

The perovskite structure oxide $Gd_{0.4}Sr_{0.6}FeO_{3-\delta}$ (GSF), fluorite structure oxides $Ce_{0.9}Gd_{0.1}O_{2-\delta}$ (CGO) and 2 mol % $Co-Ce_{0.9}Gd_{0.1}O_{2-\delta}$ (CoCGO) were prepared via the conventional process described in somewhere else.[5] The obtained powders were weighted according to the given weight ratio and milled, following mixed in an ethanol-based solution, stirred overnight, then dried at 650 ^{o}C for 1 h. After pressed under ~ 5 MPa in a stainless steel module, the green disc was sintered at 1400 ^{o}C (GSF-CGO) or 1325 ^{o}C (GSF-CoCGO) for 5 h with heating and cooling rates of 2 $^{o}C/min$. The permeation tests were conducted in a home-made permeator, applying different sweep gases, helium or carbon dioxide.[6] The structure and the morphology of the samples were analyzed by X-ray diffraction (XRD, D8 Advance, Bruker-AXS, with Cu_{ka} radiation) and studied by the scanning electron microscopy (SEM) and energy dispersive X-ray spectroscopy (EDXS) using a JEOL JSM-6700F, respectively.

3. Results and discussion

The characterization results, as presented in figure 1 and 2, clearly demonstrate that the dual-phase membranes GSF-CGO and GSF-CoCGO were successfully synthesized and the doping of minor cobalt doesn't not result any phase transfer in the fluorite oxide CoCGO as well as in the dual-phase GSF-CoCGO membrane. The XRD patterns (Fig.1) of CGO and CoCGO show that both oxides are fluorite structure oxides, no other phase was formed because of the minor amount doping cobalt. After mixed with GSF, the resulted GSF-CGO and GSF-CoCGO membranes consist of only the perovskite GSF phase and the fluorite CGO or CoCGO phase, and do not reveal any other phase. The conclusion was further endorsed by the SEM analysis, as shown in figure 2, the SEM images and corresponding EDXS micrographs clearly illustrate that the as-prepared GSF-CGO (Fig.2 a,b) and GSC-CoCGO (Fig.2 c,d) membranes consist of two different phases, each can be easily distinguished from the other. The sintering temperatures (T_s) of GSF-

CoCGO membrane differs from the GSF-CGO. The experimental finding indicates the T_s of GSF-CGO and GSF-CoCGO membranes are 1400 ^{o}C and 1325 ^{o}C, respectively. The as-synthesized GSF-CoCGO membrane tend to melt when sintering at the 1400 ^{o}C, indicating that the minor cobalt doping lowers the ideal sintering temperature of the membrane. The ideal T_s of the dual phase membrane is usually determined by the T_ss of involved oxides and somewhere between them. In terms of that the cobalt-doping is an effective way to accelerate the densification of CGO at lower temperature,[7] a pronounced decrease can be expected in the sintering temperature of CoCGO, therefore the GSC-CoCGO. However, this decrement doesn't show any negative influence on the densification of our dual-phase membranes, as illustrated in figure 2c, a well sintered surface is observed, also agreeing with the gas-tight measurement.

The use of minor cobalt permits a significant improvement of the permeability of our dual-phase, as presented in figure 3. Applying helium as sweep gas, the oxygen permeation flux of GSF-CGO membrane is only 0.03 cm^3 cm^{-2} min^{-1}, whereas the permeation flux of GSF-CoCGO membrane is 0.28 cm^3 cm^{-2} min^{-1} at 950 ^{o}C. The permeability of the minor cobalt doped membrane is about one order of magnitude higher than the undoped. This remarkable enhancement can be attributed to the ensuring of the continual transport of electrons in our GSF-CoCGO dual-phase membrane owing to the fact that the electronic conductivity of the can be significantly improved by doping cobalt.

When the pure carbon oxide was applied as the sweep gas instead of helium, a pronounced decrease of the permeability is observed over the whole measured temperature range. The different surface exchange rate caused by the adsorption of CO_2 may be the main reason for this drop. Since some surface active sites are occupied by the CO_2, a lower recombination rate of the lattices rate is expected and therefore reduces the oxygen permeation flux. As shown in figure 4,

comparing the activation energies obtained using He and CO_2 as sweep gases, one can see a distinct reduction of the apparent activation energy with increasing temperature using CO_2 as sweep gas. This variation can be related to the different adsorption behavior of CO_2 at different temperatures, since the adsorption degree of CO_2 is lower at higher temperature. As a result, in comparison to using helium, the oxygen permeation flux decreases when applying CO_2 as sweep gas.

A long-term stable permeability is a key factor to evaluate the oxygen permeation membrane, our oxygen permeation tests (figure 5) clearly demonstrate that the GSF-CoCGO membrane exhibit a stable oxygen permeability for at least 300 hours under CO_2 or He atmosphere. After an initialization time of about 10 h, a permeability of 0.28 cm^3 cm^{-2} min^{-1} is obtained and lasted for 90 h at 950°C. When CO_2 was applied, a permeability of 0.21 cm^3 cm^{-2} min^{-1} is obtained and lasted for at least 160 h. The new-developed GSF-CoCGO membrane also shows an excellent stability in the oxygen permeability when switching the sweep gas between CO_2 and He, as illustrated in figure 6. The permeability of the membrane remains unchangeable towards same atmosphere, indicating the good structure stability of the membrane. The studies of the spent membrane using XRD is also in agreement of this experimental result. As presented in figure 7, no addition peak indicating foreign phase was observed in the XRD patterns of the spent membrane.

4. Conclusions

In conclusions, this work illustrates a new method to improve the oxygen permeation flux of the dual-phase membrane. By doping 2 mol % cobalt in the ionic conduct phase, the oxygen permeation flux of the membrane was improved from 0.03 to 0.28 cm^3 cm^{-2} min^{-1} at 950 ^{o}C. Furthermore, it was identified that the doping minor cobalt has no negative effect on the stability

of the membrane. The resulting membrane shows a superior oxygen permeation flux and an excellent stability towards CO_2-atomsphere.
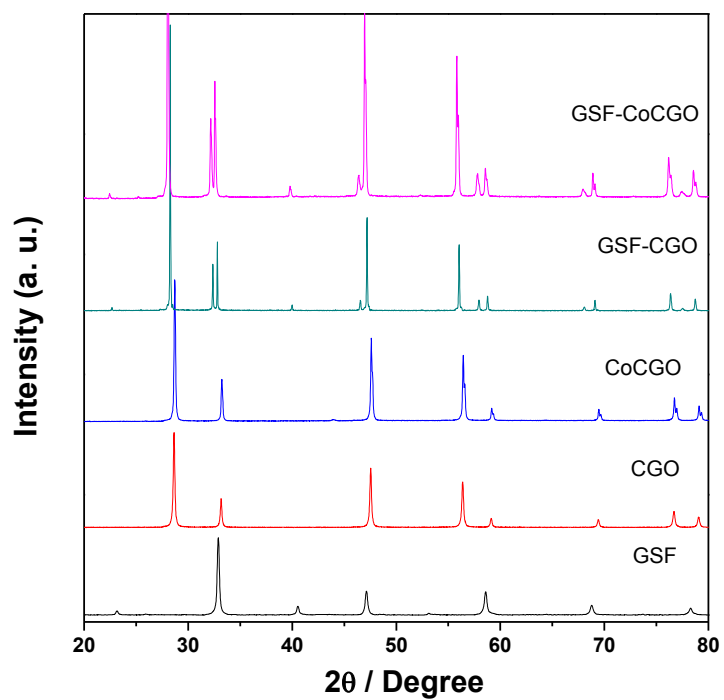
Figure 1. XRD patterns of calcined GSF, CGO and CoCGO powders at 950 ^{o}C plus sintered GSF-CGO and GSF-CoCGO, at 1400 ^{o}C and 1325 ^{o}C, respectively,
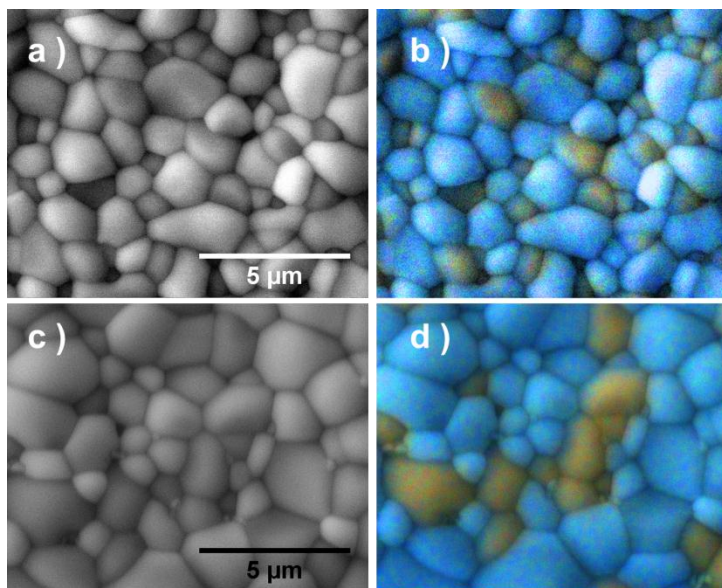
Figure 2. SEM images and corresponding EDXS results of the GSF-CGO (a,b) and GSF-CoCGO (c,d). The blue color represents the CGO or CoCGO phase, whereas the orange the GSF phase.
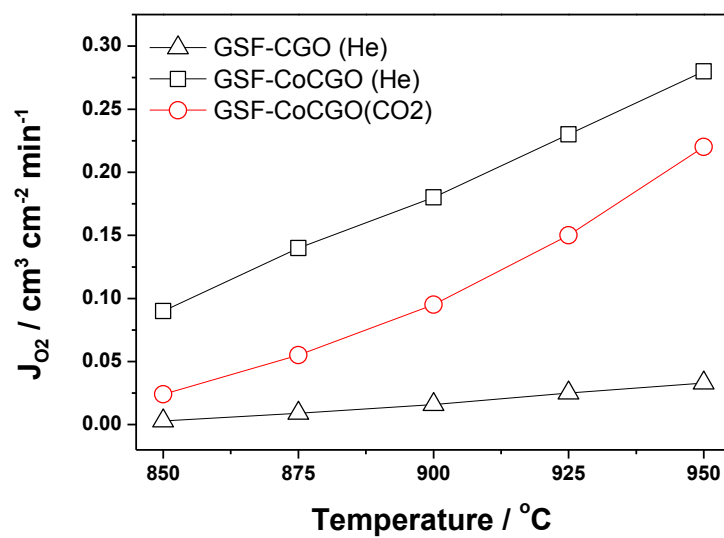
Figure 3. Oxygen permeation fluxes for GSF-CGO and GSF-CoCGO membranes as a function of temperatures using sweep gases. Operation conditions: $F_{air} = 50$ cm^3 min^{-1} as feed gas, $F_{Ne} = 1$ cm^3 min^{-1} and $F_{He} = 29$ cm^3 min^{-1} or $F_{CO2} = 29$ cm^3 min^{-1} as sweep gas. Membrane thickness: 0.7 mm.
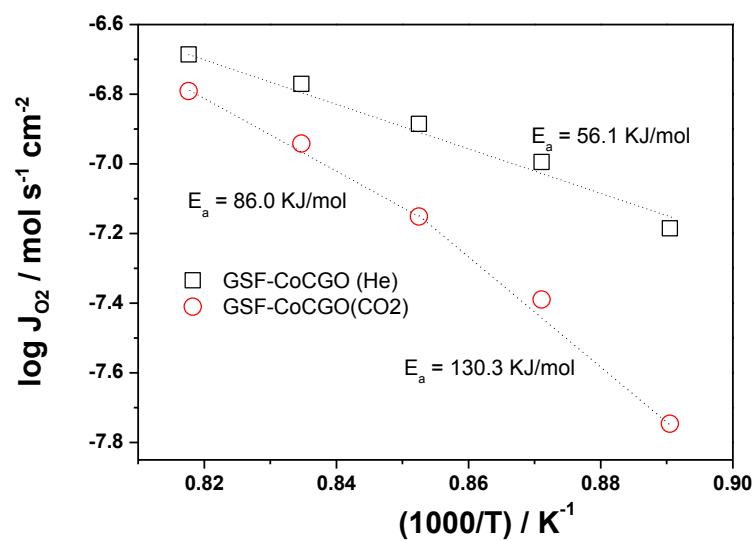
Figure 4. Arrhenius plots of the oxygen permeation fluxes through GSF-CoCGO membrane using different sweep gases. Operation conditions were presented in figure 3.
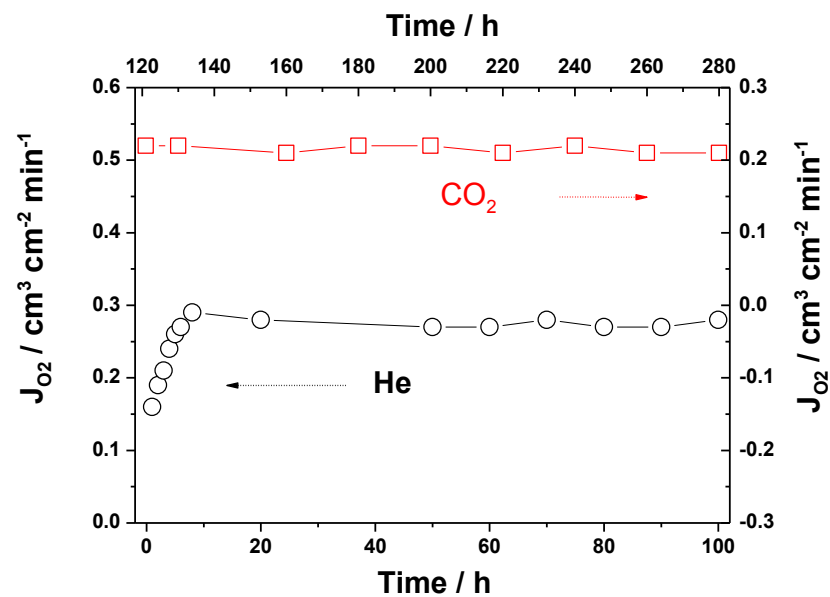
Figure 5. Time dependence of oxygen fluxes of GSF-CoCGO membrane using helium or CO_2 as sweep gas at 950 $^{\circ}$C. Operation conditions were presented in figure 3.
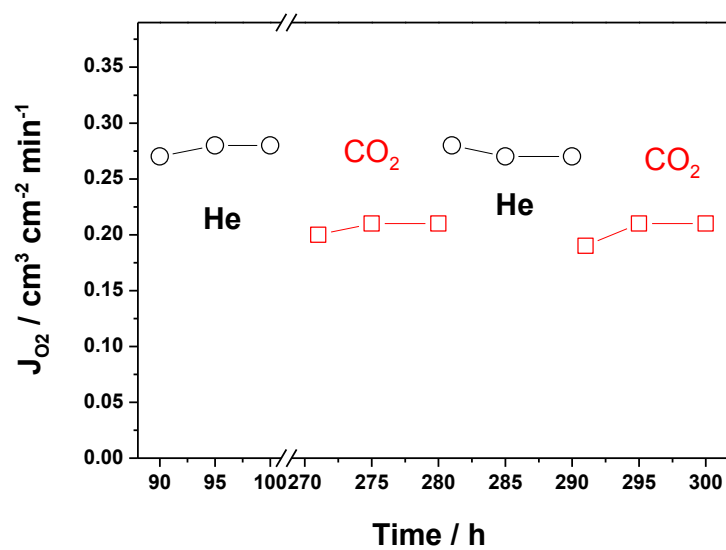
Figure 6. Time dependence of oxygen fluxes of GSF-CoCGO membrane using helium or CO_2 as sweep gas at 950 ^{o}C. Operation conditions were presented in figure 3.
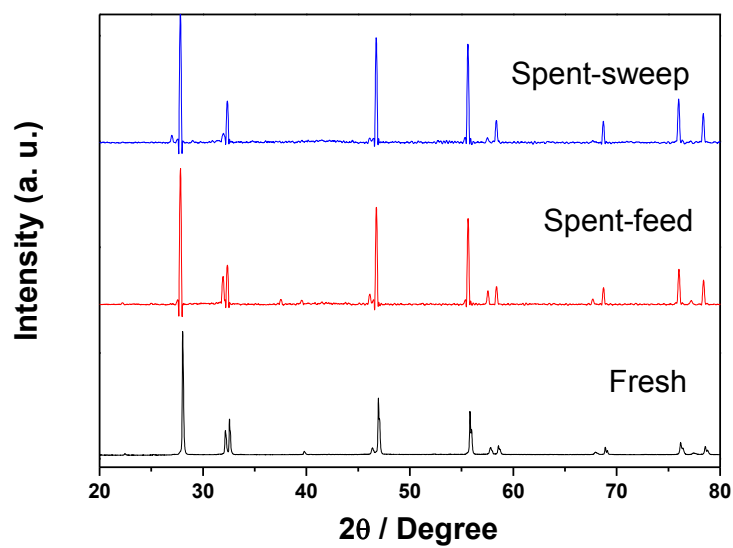
Figure 7. XRD patterns of as-prepared GSF-CoCGO membrane and the membrane applied for the oxygen test, as shown in figure 6.

References

1   Kim, J. & Lin, Y. S. Synthesis and oxygen permeation properties of ceramic-metal dual-phase membranes. *Journal of Membrane Science* **167**, 123-133, doi:10.1016/s0376-7388(99)00273-2 (2000).

2   Zhu, X., Wang, H. & Yang, W. Relationship between homogeneity and oxygen permeability of composite membranes. *Journal of Membrane Science* **309**, 120-127, doi:http://dx.doi.org/10.1016/j.memsci.2007.10.011 (2008).

3   Luo, H. X. *et al.* CO2-Stable and Cobalt-Free Dual-Phase Membrane for Oxygen Separation. *Angew. Chem.-Int. Edit.* **50**, 759-763, doi:10.1002/anie.201003723 (2011).

4   Fagg, D. P., Shaula, A. L., Kharton, V. V. & Frade, J. R. High oxygen permeability in fluorite-type Ce0.8Pr0.2O2−δ via the use of sintering aids. *Journal of Membrane Science* **299**, 1-7, doi:http://dx.doi.org/10.1016/j.memsci.2007.04.020 (2007).

5   Luo, H., Jiang, H., Efimov, K., Caro, J. & Wang, H. Influence of the preparation methods on the microstructure and oxygen permeability of a CO2-stable dual phase membrane. *AIChE Journal* **57**, 2738-2745, doi:10.1002/aic.12488 (2011).

6   Luo, H. X. *et al.* CO(2)-Tolerant Oxygen-Permeable Fe(2)O(3)-Ce(0.9)Gd(0.1)O(2-delta) Dual Phase Membranes. *Industrial & Engineering Chemistry Research* **50**, 13508-13517, doi:10.1021/ie200517t (2011).

7   Kleinlogel, C. & Gauckler, L. J. Sintering of Nanocrystalline CeO2 Ceramics. *Advanced Materials* **13**, 1081-1085, doi:10.1002/1521-4095(200107)13:14<1081::aid-adma1081>3.0.co;2-d (2001).

Chapter 4

Highly efficient catalytic process in membrane reactors

4.1 Summary

The implications of various oxidation processes in membrane reactors based on oxygen transport membranes can be attractive because of the process intensification and the potential of high efficiency. This chapter presents the works on the efficient aromatization of methane and ammonia oxidation on perovskite membrane reactors.

The first work on methane aromatization to liquid fuels and chemicals shows that when the membrane reactor concept was employed, a slower deactivation and an improved selectivity of methane dehydroaromatization can be achieved in comparison with the fixed bed reactor.

The second paper reveals for the ammonia oxidation the benefits of a membrane reactor since the formation of non-selective surface oxygen molecular species can be well suppressed. Under similar operation conditions, the membrane reactor shows a higher catalytic performance towards the oxidation of ammonia to NO, and as a result, 95 % NO selectivity and 81 % NH_3 conversion can be achieved at 850 ^{o}C in the membrane reactor.

4.2 Natural gas to fuels and chemicals: Improved methane aromatization in an oxygen-permeable membrane reactor

Zhengwen Cao [a], Heqing Jiang [b,*], Huixia Luo [a,c], Stefan Baumann [d], Wilhelm A. Meulenberg [d], Jens Assmann [e], Leslaw Mleczko [e], Yi Liu [a] and Jürgen Caro [a,*]

[a] *Institute of Physical Chemistry and Electrochemistry, Leibniz University of Hannover, Callinstr.3A, D-30167 Hannover, Germany*

[b] *Key Laboratory of Biobased Materials, Qingdao Institute of Bioenergy and Bioprocess Technology, Chinese Academy of Sciences. No.189 Songling Road, 266101 Qingdao (China)*

[c] *Department of Chemistry, Princeton University, 08544, Princeton, New Jersey USA*

[d] *Forschungszentrum Jülich GmbH, Institute of Energy and Climate Research, Leo-Brandt-Str., D-52425 Jülich, Germany*

[e] *Bayer Technology Services GmbH, BTS-TD-UP-Chemical Catalysis,D-51368 Leverkusen, Germany*

---

[*] Corresponding authors. Tel.: +49 511 7623175; Fax: +49 511 76219121.

E-mail addresses: jianghq@qibebt.ac.cn (H. Jiang), juergen.caro@pci.uni-hannover.de (J. Caro).

The methane dehydroaromatization (MDA) is attracting considerable interest from both academia and industry because of its potential in the conversion of methane to chemicals and liquid fuels.[1] Compared to the conventional liquid fuels production based on Fischer-Tropsch technology from syngas ($CO + 2 H_2$), the MDA provides a simple, straightforward, and economic pathway from methane to aromatic hydrocarbons without intermediate steps. Intensive efforts have been devoted to the development of suitable catalysts, such as Zn/HZSM-5,[2] Fe/HZSM-5,[3] and Ga/HZSM-5,[4] and encouraging progress has been made especially on Mo/MCM-22,[5] Mo/HMCM-49,[6] and Mo/HZSM-5.[2, 7]

Challenging problems still exist, such as the rapid catalyst deactivation by coke and the limited methane conversion, which hinder the industrialization of the MDA.[8]

To overcome the equilibrium limitation of the reaction (1), it is proposed that the generated hydrogen can be removed by hydrogen-permeable membranes (metal alloys, zeolite or other molecular sieves, proton/electron conducting ceramics). Using a Pd-coated Nb-Ta membrane, the methane conversion could be increased from 3.8 % to 9 % at 600 ℃; however, hydrogen removal is expected to accelerate coking.[9] Thermodynamically favorable is the substitution of the non-oxidative MDA according reaction (1) by the oxidative MDA according to reaction (2).

$$6 CH_4 \leftrightarrows C_6H_6 + 9 H_2 \tag{1}$$

$$6 CH_4 + 9/2 O_2 \rightarrow C_6H_6 + 9 H_2O \tag{2}$$

Additionally, the latter has been demonstrated to be efficient in suppressing the coke formation since the presence of oxygen and steam.[10] However, the presence of stoichiometric oxygen concentrations inhibits the formation of molybdenum carbide, the active catalyst component essential for the aromatics formation.[7a, 11] As a result, side reactions such as the total and/or

partial methane oxidation and the oxidative coupling of methane can become predominant, and the target product selectivity decreases. To manipulate the incompatible reactions mentioned above in the presence of oxygen, various oxygen introduction strategies have been proposed. For example, previous work suggested a mode in which minor amounts of oxygen or soft oxidants were co-fed together with methane.[10, 12] Nevertheless, this concept suffers from a significant decrease of the aromatic productivity starting already for a low oxygen concentration in the fed methane, e.g. < 1 % at 700 ^{o}C. Furthermore, from safety aspect, one should also consider how to avoid the hot spots or even explosions in such co-feeding mode.

To obtain an improved MDA with increased methane conversion with an acceptable aromatics selectivity and better coking-resistance, oxygen has to be finely distributed and continuously fed into the reactor, e.g. by using an oxygen transporting membrane.[13] Recently, we developed a series of membranes for versatile applications, e.g. CO_2 capture integrated in Oxy-fuel power plants,[14] direct decomposition of NO and NO_2[15] and the coupling of two reactions such as water splitting with the partial oxidation of methane/oxidative dehydrogenation of ethane.[16]

Herein we integrate the oxygen generation and the MDA in a membrane reactor system, which is considered to offer a significant advantage for the MDA. As illustrated in Figure 1, in the membrane reactor, oxygen permeates from the air side to the hydrocarbon side, where it is consumed in the MDA. Different to the conventional co-feeding of gaseous O_2 in the fixed bed reactor, here, oxygen is continuously fed into the reaction chamber by the oxygen-permeable membrane; a higher ratio of the oxidative MDA to side reactions without oxidative destruction of the active catalyst component Mo_2C. Furthermore, the presence of oxygen and the production of steam by hydrogen combustion should suppress the coke formation and extend the life time of the catalytic system. The membrane reactor used in this work is based on asymmetric oxygen

transporting $Ba_{0.5}Sr_{0.5}Co_{0.8}Fe_{0.2}O_{3-\delta}$ (BSCF) perovskite membrane consisting of 20 μm thick BSCF dense layer on a porous BSCF support, as shown in Figure S1.[17] As catalyst we used an established bi-functional Mo/HZSM-5 (Si/Al = 27, weight % Mo = 6).

We performed the experiments in both fixed bed reactor (FR) and membrane reactor (MR) in order to observe the direct effect of oxygen supply via membrane on MDA. First, both reactors were purged for 2 h with He, and then methane was supplied. In the case of MR, 1 h after the methane supply the air supply started. That is to say, in the membrane reactor the MDA proceeded without oxygen permeation in the 1st h, and then oxygen was supplied via the membrane. Figure 2 presents the methane conversion obtained in the MR and the FR as a function of time at 750 ^{o}C. The methane conversions in both reactors were comparable in the 1st h. However, immediately after the oxygen permeation started in the MR, the conversion of methane increased and became higher than that in the FR with time on stream. The main reason is that the MDA is thermodynamically more favorable in the presence of oxygen, thus the equilibrium of the reaction is shifted to the product side when the permeated oxygen *in situ* oxidizes the hydrogen liberated from the MDA reaction. Furthermore, the generation of steam reduces coking and extends the life time of the catalyst. As a result, the usual deactivation of the MDA catalytic process proceeds more slowly in the MR.

Figure 3a shows that the aromatics selectivity drops sharply in both reactors with time on stream. However, whereas the aromatics selectivity in the FR continuously dropped with time on stream, in the case of MR it reached a plateau. The rapidly decrease of the aromatics selectivity at the initial stage is attributed to the coke deposition. Whereas the aromatics selectivity in the FR was only 10 % after 1000 min time on stream, the MR still shows aromatics selectivity of about 30 %. Thermodynamically, the partial/total oxidation of methane under oxidative conditions is

more favorable than the oxidative dehydroaromatization of methane. As a result, partial methane was oxidized to CO_x (see Figure 3b), which decreased the aromatics selectivity. Nevertheless, the MR still showed a superior selectivity of aromatics over the FR, indicating that the presence of oxygen has not damaged the catalyst, especially the active compound Mo_2C. With increasing time on stream, the aromatics selectivity in both reactors decreases, however, the MR shows a much higher resistance towards catalyst deactivation due to the presence of oxygen and steam, as discussed below.

The higher methane conversion and higher aromatics selectivity in the MR compared with the in the FR gives higher aromatics yield in the MR (Table 1). After 200 min, the aromatics yield in MR is 30 % higher than in the FR, after 500 min by 200 %. In contrast to the poor aromatics yield (< 1 %) of the FR after ~ 600 min, the aromatics yield is still 3 % in the MR with increasing time on steam. Based on this experimental finding, it can be concluded that the oxygen addition via the perovskite BSCF membrane is an effective way to enhance the performance of MDA.

To qualify the advantage of supplying oxygen via the membrane, we conducted also the oxidative MDA in the FR by co-feeding oxygen and methane. 0.4 cm^3 min^{-1} gaseous O_2 was fed into the fixed bed after the reactor had been conditioned for 1 h with methane to form the active catalyst phase Mo_2C. As shown in Figure 4, the aromatics selectivity decreases dramatically for the FR with gaseous oxygen from 85 % to 5 % after 100 min, but for the MR only from 85 % to 40 %. This finding can be explained by the oxidative destruction of the Mo_2C catalyst in the oxygen co-feed FR. Normally, Mo_2C catalysts tend to deactivate towards MDA when the O_2/CH_4 molar ratio concentration exceeds a critical value for a given temperature because of the oxidation of the active catalyst component Mo_2C of the Mo/HZSM-5 catalyst, which interrupts the production of aromatics immediately. According to Yuan et al., the critical value at 750 ^{o}C is

around 0.02.[10] Therefore, the introduction of 0.4 $cm^3 min^{-1}$ gaseous O_2 (O_2/CH_4 molar ratio = 0.04) results in a rapid deactivation of the catalyst and the aromatics formation stopped immediately in the FR (Figure 4). In the MR, the amount of oxygen calculated based on the CO and CO_2 at outlet is higher than 0.4 $cm^3 min^{-1}$, indicating that the oxygen permeation flux is higher than 0.4 $cm^3 min^{-1}$ and the ratio of O_2/CH_4 is above 0.04. Nevertheless, the aromatization reaction still proceeds and the aromatics yield in the MR is higher than that in the FR, suggesting this critical value was increased at least to 0.04 when the oxygen was supplied in the MR by the BSCF membrane instead of using gaseous oxygen as co-feed in the FR.

The coke selectivities in the MR and the FR (see Figure 3b) in both cases increase with time on stream. However, as expected, the coke selectivity in the MR is much lower than that in the FR. The coke selectivity in the FR is mostly higher than 60 % and increasing with time, but the coke selectivity in the MR was found to be only around 10 % and showing an only slight increase with time. The CS-2000 automatic analyzer which allowing the rapid determination of the carbon content in catalysts was employed to determine the carbon deposition on the spent catalysts from both reactors. It was found that the carbon content in the spent catalyst from FR was around 12 wt% after 40 h, and the catalyst from MR had only a carbon content of 1.2 wt%. These results demonstrate that the coke formation was efficiently suppressed in the MR.

Despite an improved performance in our MR, a slow deactivation of the catalyst was still observed. To elucidate the reason for this deactivation, the spent catalyst (40 h) from the MR was characterized by SEM. As shown in Figure S2, fiber-like particles were dispersed on the spent catalyst surface. EDXS revealed that these fiber-like particles are mainly composed of carbon, indicating that the coke is probably still the reason for the catalyst deactivation in the MR.

In summary, the work presented here demonstrates a new concept to transform natural gas into liquids via improved methane dehydroaromatization using an oxygen-permeable membrane. The addition of oxygen by the membrane improves the methane conversion and the aromatics selectivity, and results in a lower deactivation of the catalyst in the membrane reactor. Therefore, the methane aromatization in the membrane reactor with oxygen dosing gives a better yield of aromatics (benzene, toluene and naphthalene) and a longer durability than in the fixed bed reactor.

Experimental Section

The asymmetric BSCF membrane was prepared by tape casting followed by sintering. More details can be found in previous works.[17a, 18] The effective membrane area was 0.28 cm^2, more detail can be found in the Supporting Information.
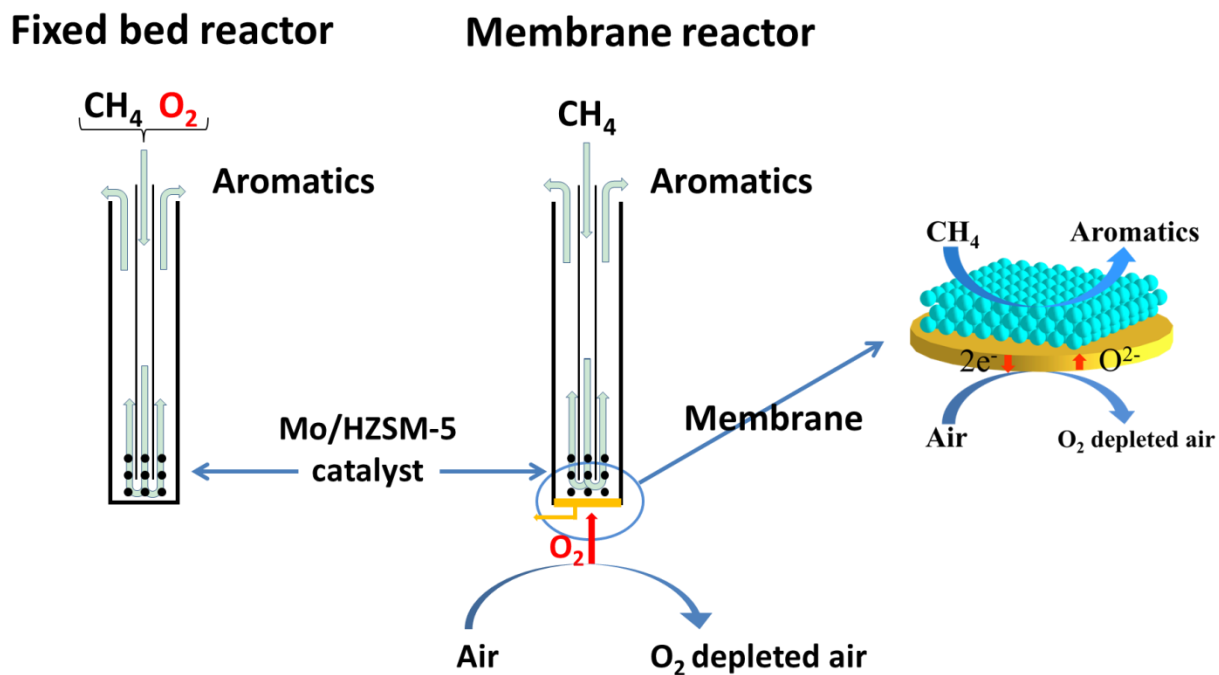
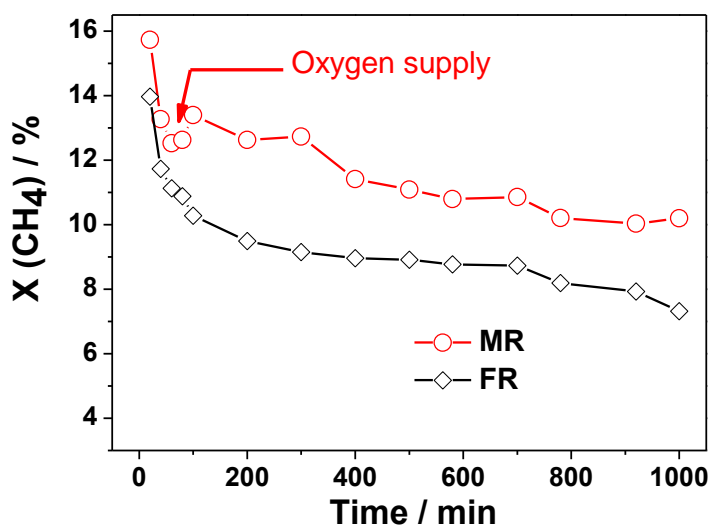**Figure 1**. Scheme of MDA in fixed bed reactor (FR) and membrane reactor (MR).

Figure 2. Methane conversions in membrane reactor (MR) and fixed bed reactor (FR) as a function of time. 0.2 g 6 wt% Mo/HZSM-5 was used in both reactors (FR: $F_{CH4} = 10$ cm^3 min^{-1}, $F_{Ar} = 1$ cm^3 min^{-1} and $F_{He} = 9$ cm^3 min^{-1}; MR: methane side, $F_{CH4} = 10$ cm^3 min^{-1}, $F_{Ar} = 1$ cm^3 min^{-1} and $F_{He} = 9$ cm^3 min^{-1}; air side $F_{Air} = 30$ cm^3 min^{-1}). Oxygen supply (air feed) began in the MR 1 h after starting the MDA reaction with dosing methane.
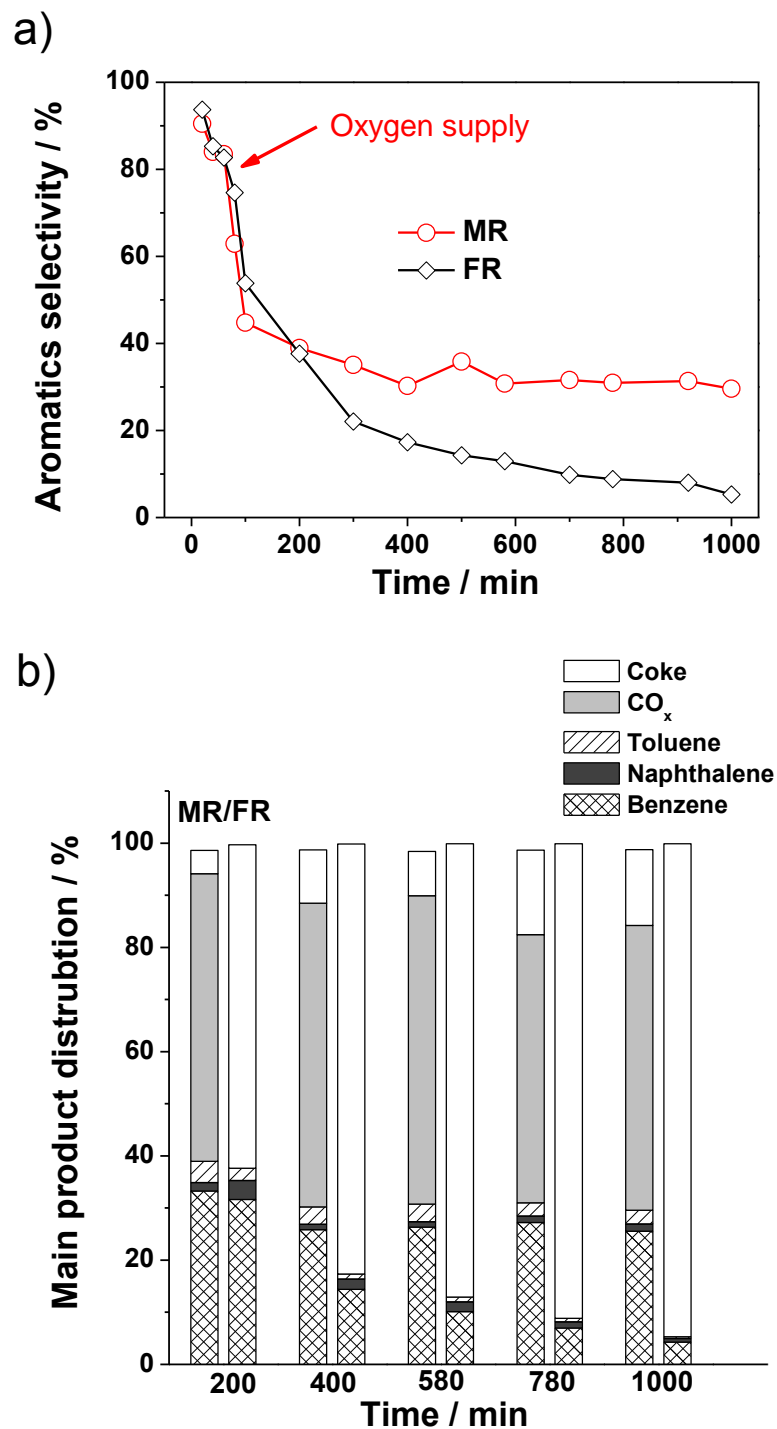
Figure 3. Selectivity of aromatics (a) and the corresponding products distribution (b) based on carbon balance in membrane reactor (MR) and fixed bed reactor (FR) as a function of time. 0.2 g 6 wt% Mo/HZSM-5 was packed in both reactors (FR: $F_{CH4} = 10$ cm^3 min^{-1}, $F_{Ar} = 1$ cm^3 min^{-1} and $F_{He} = 9$ cm^3 min^{-1}; MR: methane side, $F_{CH4} = 10$ cm^3 min^{-1}, $F_{Ar} = 1$ cm^3 min^{-1} and $F_{He} = 9$ cm^3 min^{-1}; air side $F_{Air} = 30$ cm^3 min^{-1})**.** Oxygen supply (air feed) began in MR 1 h after starting the MDA reaction with dosing methane. S(C$_2$) is around 1 % and not presented here.

Table 1. Aromatics (benzene, toluene and naphthalene) yield in membrane reactor (MR) and fixed bed reactor (FR) as a function of reaction time. 0.2 g 6 wt% Mo/HZSM-5 was packed in both reactors (FR: $F_{CH4} = 10$ cm^3 min^{-1}, $F_{Ar} = 1$ cm^3 min^{-1} and $F_{He} = 9$ cm^3 min^{-1}; MR: methane side, $F_{CH4} = 10$ cm^3 min^{-1}, $F_{Ar} = 1$ cm^3 min^{-1} and $F_{He} = 9$ cm^3 min^{-1}; air side $F_{Air} = 30$ cm^3 min^{-1}). Oxygen supply (air feed) began in MR 1 h after starting the MDA reaction with dosing methane.

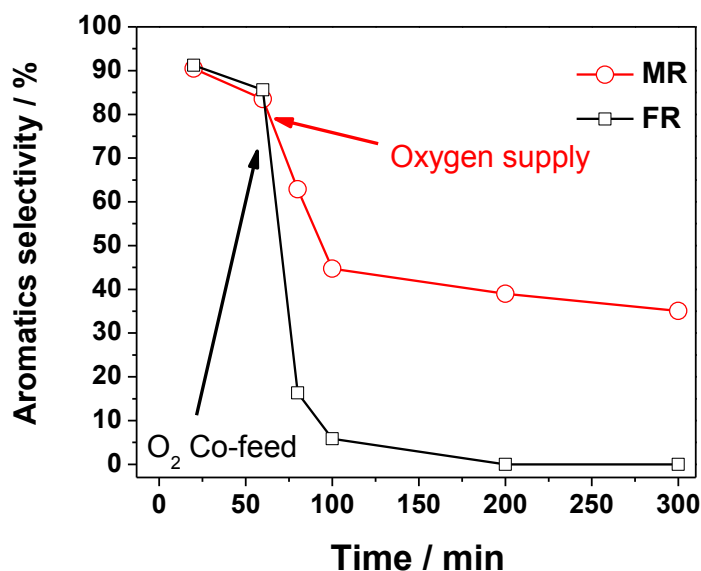| Time / min	Aromatics yield / %	
	Membrane reactor	Fixed bed reactor
100	6.0	5.5
200	4.9	3.6
500	4.0	1.3
580	3.3	1.1
1000	3.0	0.4

Figure 4. Aromatics selectivity as a function of time in the presence of oxygen in the two different reactors: A methane/oxygen was fed into fixed bed reactor (FR: $F_{CH4} = 10$ cm^3 min^{-1}, $F_{O2} = 0.4$ cm^3 min^{-1}, $F_{Ar} = 1$ cm^3 min^{-1} and $F_{He} = 8.6$ cm^3 min^{-1}). In the case of the membrane reactor (MR), oxygen was supplied from air through the BSCF membrane (MR, methane side, $F_{CH4} = 10$ cm^3 min^{-1}, $F_{Ar} = 1$ cm^3 min^{-1} and $F_{He} = 9$ cm^3 min^{-1}; air side $F_{Air} = 30$ cm^3 min^{-1}) 0.2 g 6 wt% Mo/HZSM-5 was used in both reactors. Oxygen supply (air feed) or O_2 feed began 1 h after starting the MDA reaction with dosing methane.

[1]   a) J. H. Lunsford, *Catal. Today* **2000**, *63*, 165-174; b) T. V. Choudhary, E. Aksoylu, D. W. Goodman, *Cat. Rev. - Sci. Eng.* **2003**, *45*, 151-203; c) V. R. Choudhary, A. K. Kinage, T. V. Choudhary, *Science* **1997**, *275*, 1286-1288.

[2]   L. Wang, L. Tao, M. Xie, G. Xu, J. Huang, Y. Xu, *Catal Lett* **1993**, *21*, 35-41.

[3]   B. M. Weckhuysen, D. Wang, M. P. Rosynek, J. H. Lunsford, *J. Catal.* **1998**, *175*, 347-351.

[4]   a) D. Wang, J. H. Lunsford, M. P. Rosynek, *J. Catal.* **1997**, *169*, 347-358; b) Y. J. Li, J. N. Armor, *J. Catal.* **1994**, *145*, 1-9; c) B. S. Kwak, W. M. H. Sachtler, W. O. Haag, *J. Catal.* **1994**, *149*, 465-473.

[5]   N. Chu, J. Wang, Y. Zhang, J. Yang, J. Lu, D. Yin, *Chem. Mater.* **2010**, *22*, 2757-2763.

[6]   D. Y. Wang, Q. B. Kan, N. Xu, P. Wu, T. H. Wu, *Catal. Today* **2004**, *93–95*, 75-80.

[7]   a) Y. Xu, X. Bao, L. Lin, *J. Catal.* **2003**, *216*, 386-395; b) F. Solymosi, J. Cserényi, A. Szöke, T. Bánsági, A. Oszkó, *J. Catal.* **1997**, *165*, 150-161; c) L. Su, L. Liu, J. Zhuang, H. Wang, Y. Li, W. Shen, Y. Xu, X. Bao, *Catal Lett* **2003**, *91*, 155-168; d) H. Jiang, L. Wang, W. Cui, Y. Xu, *Catal Lett* **1999**, *57*, 95-102; e) N. Chu, J. Yang, J. Wang, S. Yu, J. Lu, Y. Zhang, D. Yin, *Catal. Commun.* **2010**, *11*, 513-517; f) J. Yang, S. Yu, H. Hu, Y. Zhang, J. Lu, J. Wang, D. Yin, *Chem. Eng. J.* **2011**, *166*, 1083-1089.

[8]   D. Ma, D. Wang, L. Su, Y. Shu, Y. Xu, X. Bao, *J. Catal.* **2002**, *208*, 260-269.

[9]   a) K. Skutil, M. Taniewski, *Fuel Process. Technol.* **2006**, *87*, 511-521; b) M. C. Iliuta, F. Larachi, B. P. A. Grandjean, I. Iliuta, A. Sayari, *Ind. Eng. Chem. Res.* **2002**, *41*, 2371-2378; c) L. Li, R. W. Borry, E. Iglesia, *Chem. Eng. Sci.* **2002**, *57*, 4595-4604.

[10]   S. Yuan, J. Li, Z. Hao, Z. Feng, Q. Xin, P. Ying, C. Li, *Catal Lett* **1999**, *63*, 73-77.

[11]   H. Zheng, D. Ma, X. Bao, Z. H. Jian, H. K. Ja, Y. Wang, C. H. F. Peden, *J. Am. Chem. Soc.* **2008**, *130*, 3722-3723.

[12]   P. L. Tan, K. W. Wong, C. T. Au, S. Y. Lai, *Appl. Catal. A* **2003**, *253*, 305-316.

[13]   a) C. S. Chen, S. J. Feng, S. Ran, D. C. Zhu, W. Liu, H. J. M. Bouwmeester, *Angew. Chem. Int. Ed.* **2003**, *42*, 5196-5198; b) Y. Liu, X. Zhu, M. Li, H. Liu, Y. Cong, W. Yang, *Angew. Chem. Int. Ed.* **2013**, *52*, 3232-3236; c) X. Dong, W. Jin, N. Xu, K. Li, *Chem. Comm.* **2011**, *47*, 10886-10902; d) P. Zeng, Z. Chen, W. Zhou, H. Gu, Z. Shao, S. Liu, *J. Membr. Sci.* **2007**, *291*, 148-156; e) J. Sunarso, S. Baumann, J. M. Serra, W. A. Meulenberg, S. Liu, Y. S. Lin, J. C. Diniz da Costa, *J. Membr. Sci.* **2008**, *320*, 13-41; f) U. Balachandran, T. H. Lee, S. E. Dorris, *Inter. J. Hydrogen Energy* **2007**, *32*, 451-456; g) H. J. M. Bouwmeester, *Catal. Today* **2003**, *82*, 141-150; h) Z. Shao, W. Yang, Y. Cong, H. Dong, J. Tong, G. Xiong, *J. Membr. Sci.* **2000**, *172*, 177-188.

[14]   a) H. X. Luo, K. Efimov, H. Q. Jiang, A. Feldhoff, H. H. Wang, J. Caro, *Angew. Chem. Int. Ed.* **2011**, *50*, 759-763; b) H. Luo, H. Jiang, T. Klande, Z. Cao, F. Liang, H. Wang, J. Caro, *Chem. Mater.* **2012**, *24*, 2148-2154.

[15]   a) H. Q. Jiang, H. H. Wang, F. Y. Liang, S. Werth, T. Schiestel, J. Caro, *Angew. Chem. Int. Ed.* **2009**, *48*, 2983-2986; b) H. Q. Jiang, L. Xing, O. Czuprat, H. H. Wang, S. Schirrmeister, T. Schiestel, J. Caro, *Chem. Comm.* **2009**, 6738-6740.

[16]   a) H. Q. Jiang, H. H. Wang, S. Werth, T. Schiestel, J. Caro, *Angew. Chem. Int. Ed.* **2008**, *47*, 9341-9344; b) H. Q. Jiang, F. Y. Liang, O. Czuprat, K. Efimov, A. Feldhoff, S. Schirrmeister, T. Schiestel, H. H. Wang, J. Caro, *Chem. Eur. J.* **2010**, *16*, 7898-7903; c) H. Q. Jiang, Z. W. Cao, S. Schirrmeister, T. Schiestel, J. Caro, *Angew. Chem. Int. Ed.* **2010**, *49*, 5656-5660; d) A. M. Champagnie, T. T. Tsotsis, R. G. Minet, E. Wagner, *J. Catal.* **1992**, *134*, 713-730.

[17]   a) S. Baumann, J. M. Serra, M. P. Lobera, S. Escolástico, F. Schulze-Küppers, W. A. Meulenberg, *J. Membr. Sci.* **2011**, *377*, 198-205; b) Z. Cao, H. Jiang, H. Luo, S. Baumann, W. A. Meulenberg, H. Voss, J. Caro, *Catal. Today* **2012**, *193*, 2-7.

[18]   F. Schulze-Küppers, S. Baumann, W. A. Meulenberg, D. Stöver, H. P. Buchkremer, *J. Membr. Sci.* **2013**, *433*, 121-125.
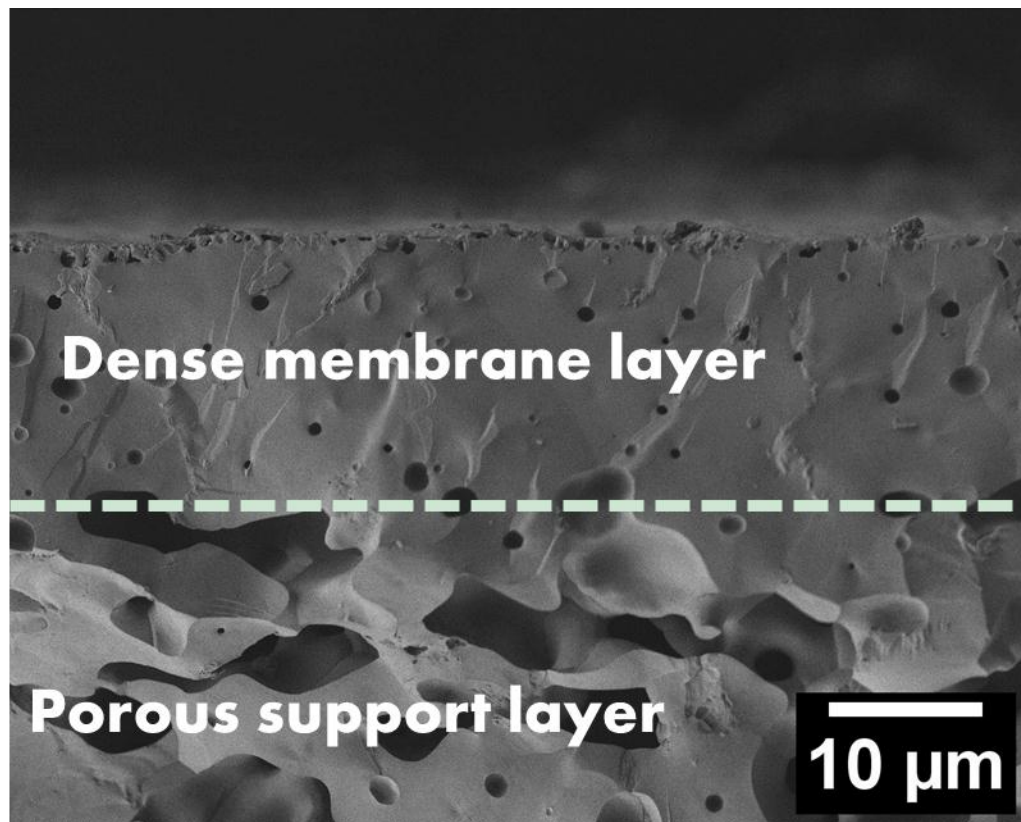
Supporting Information

Figure S1. Cross section of the high-flux $Ba_{0.5}Sr_{0.5}Co_{0.8}Fe_{0.2}O_{3-\delta}$ (BSCF) perovskite membrane. The black spots in the top layer indicate a harmless closed porosity.
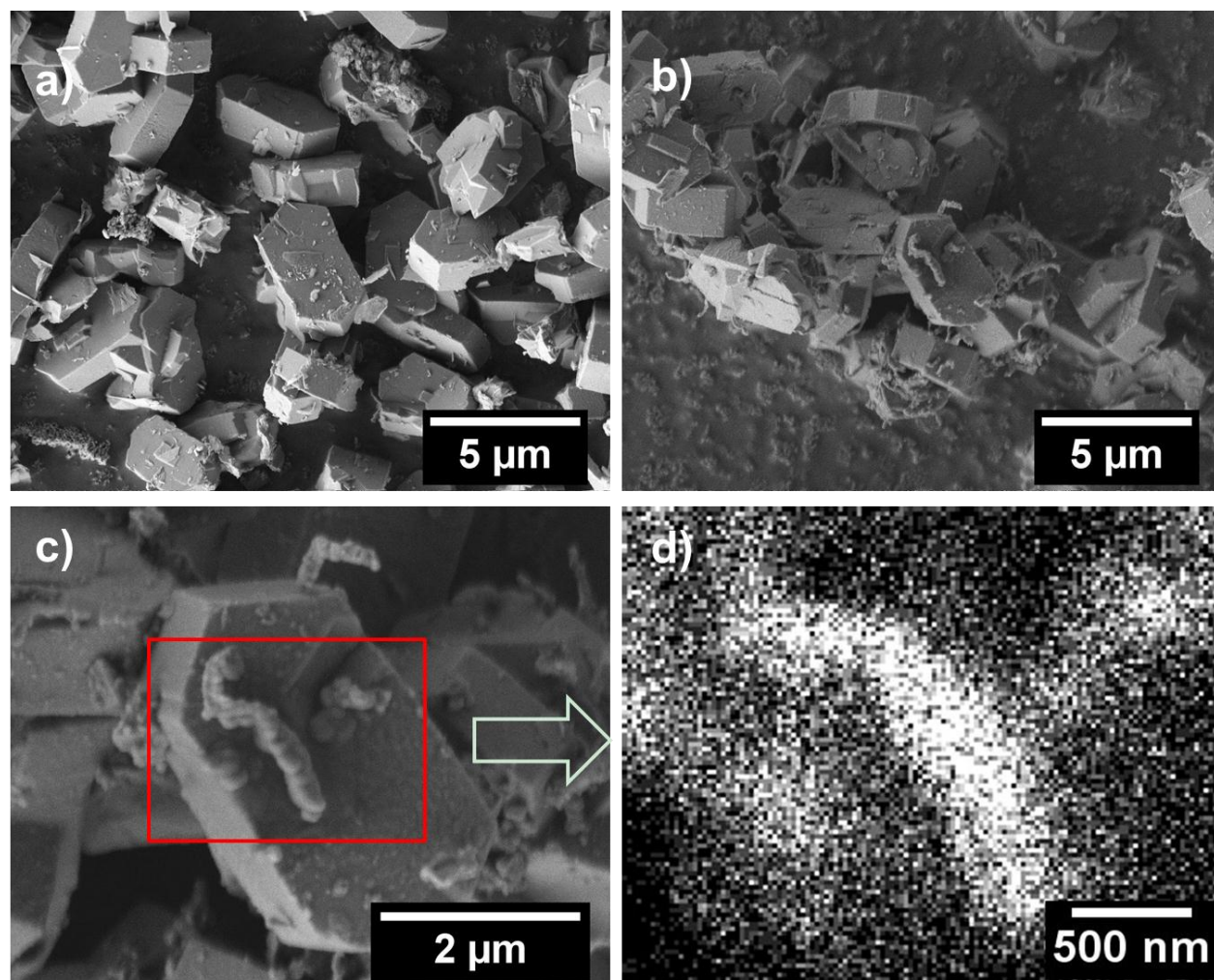
Figure S2. SEM micrographs of fresh (a) and spent catalysts (b,c) and the corresponding carbon distribution (d) image as obtained by EDXS.

Experimental

The thicknesses of the dense layer and the porous layer of the memrbane were 20 μm and 760 μm, respectively. The membrane was sealed onto the alumina tube using ceramic sealant (Huitian, China), the effective membrane area was 0.28 cm². After leakage test under the air/He oxygen partial pressure gradient, 0.2 g 6 wt% Mo/HZSM-5 catalyst (Bayer) was packed on top of the membrane. Methane diluted by He was fed to the one side with the packed Mo/HZSM-5 catalyst and air was fed to the other side, 1 cm³ min⁻¹ Ar was co-fed to the reaction side as internal standard gas. All flow rates were controlled by the gas mass flow controllers (Bronkhorst) and the line connected to the product side was heated to 220 °C. The concentration of the specific gas was monitored by a gas chromatography (GC) (Agilent 7890). The total gas flow rate at outlet (F_{out}) was calculated by using Ar as an internal standard. Therefore, the CH₄ conversion X(CH₄), the aromatics (benzene, toluene and naphthalene) selectivity S(A) and the coke selectivity S(C) were calculated as follows:

$$X(CH_4) = \left(1 - \frac{c_{(CH_4,out)} \times F_{out}}{F_{(CH_4,in)}}\right) \times 100\%$$

$$S(A) = \frac{c_{(aromatics,out)} \times F_{out}}{F_{(CH_4,in)} - c_{(CH_4,out)} \times F_{out}} \times 100\%$$

$$S(C) = \frac{F_{(CH_4,in)} - (c_{(CH_4,out)} + xc_{(aromatics,out)} + 2c_{(C_2,out)} + c_{(CO_x,out)}) \times F_{out}}{F_{(CH_4,in)} - c_{(CH_4,out)} \times F_{out}} \times 100\%$$

Here x is 6 (benzene), 7 (toluene) or 10 (naphthalene), and *F(i)* is the flow rate of species *i* on the reaction side of the disc membrane.

4.3 Ostwald process: An efficient oxygen activation route for improved ammonia oxidation via an oxygen-permeable catalytic membrane

Zhengwen Cao,[1] Prof. Dr. Heqing Jiang, [2, *] Dr. Huixia Luo,[1, 3] Dr. Stefan Baumann,[4] Dr. Wilhelm A. Meulenberg,[4] Dr. Hartwig Voss,[5] Prof. Dr.Jürgen Caro[1, *]

[1]*Institute Physical Chemistry and Electrochemistry, Leibniz University of Hanover, Callinstr.3A, 30167 Hanover, Germany*

[2]*Key Laboratory of Biobased Materials, Qingdao Institute of Bioenergy and Bioprocess Technology, Chinese Academy of Sciences, 189 Songling Road, 266101 Qingdao, China*

[3]*Department of Chemistry, Princeton University Princeton, NJ 08544, USA*

[4]*Institute of Energy Research, Forschungszentrum Jülich GmbH, Leo-Brandt-Str, 52425 Jülich, Germany*

[5]*BASF SE, 67056 Ludwigshaften, Germany*

Key words: Perovskite, oxygen activation, membrane reactor, catalytic membrane and ammonia oxidation
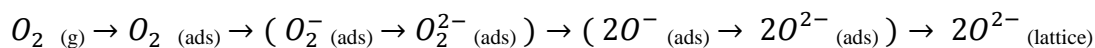
* Corresponding authors. Tel.: +49 511 7623175; Fax: +49 511 76219121.

E-mail addresses: jianghq@qibebt.ac.cn (H. Jiang), juergen.caro@pci.uni-hannover.de (J. Caro).

Extensive research efforts have been devoted to improve the Ostwald process ($4NH_3 + 5O_2 \rightarrow 4NO + 6H_2O$), since this step covers about 90 % of the nitric acid production cost.[76] For many years, nitric acid producer rely on platinum group metal alloy gauzes as catalysts that show a very good activity and 94-96 % NO selectivity with N_2 and N_2O as byproducts. But the utilization of Pt-Rh gauzes is expensive, and linked to N_2O emission and platinum losses in form of volatile oxides. These facts stimulate the research towards the development of new catalysts and new processes for ammonia oxidation. A series of less expensive oxides, especially cobalt oxide (Co_3O_4) and perovskite structure oxides, such as Ca or Sr substituted $LaMnO_3$, $LaCoO_3$ and $LaFeO_3$, have been reported to show promising catalytic performance towards ammonia oxidation.[77] Considering that N_2 from air represents about 70% of the total flow in the current plants, Perez-Ramirez et al. proposed a novel process for ammonia oxidation using a lanthanum ferrite-based oxygen-permeable membrane reactor, in which the oxygen for the ammonia oxidation can be separated from air, and in situ supplied via the membrane, and N_2 in the air flow was completely kept on the other side of the membrane. By using $La_{0.8}Sr_{0.2}FeO_{3-\delta}$ membrane as the reactor for ammonia oxidation, the high NO selectivities (95-98 %) were obtained only when feeding very limited amounts of ammonia (< 0.5 cm^3·min^{-1} NH_3 in a total flow of 130 ml·min^{-1} at 1100 K).[78,79] To obtain a larger oxygen permeation flux, Sun et al. recently employed a $Ba_{0.5}Sr_{0.5}Co_{0.8}Fe_{0.2}O_{3-\delta}$ membrane with high oxygen permeability for the oxidation of ammonia.[80] However, the NO selectivities are relatively low ($< 70\%$). It is, therefore, desirable to study the catalytic process on the membrane surface, thus further improving the membrane-based ammonia oxidation.

During ammonia oxidation on metal oxide catalysts, following the concept of Mars and van Krevelen, the participation of lattice oxygen[81-83] is found to play a very important role in the

formation of NO.[84] The formation of lattice oxygen by re-oxidation of the oxygen-depleted metal

oxides by gaseous oxygen has been suggested as follows:[85]

$$O_2 \;_{(g)} \rightarrow O_2 \;_{(ads)} \rightarrow (\; O_2^- \;_{(ads)} \rightarrow O_2^{2-} \;_{(ads)}\;) \rightarrow (\; 2O^- \;_{(ads)} \rightarrow 2O^{2-} \;_{(ads)}\;) \rightarrow 2O^{2-} \;_{(lattice)}$$

First, oxygen molecules adsorb on the oxides surface, the adsorbed O_2 becomes reduced and is

incorporated into the metal oxide as lattice oxygen O^{2-} as shown in Figure 1 (left). Many efforts

have been taken to identify the role of various oxygen species. It is accepted ammonia can be

directly oxidized by lattice oxygen to NO,[86] and a low NO selectivity is related to high

concentrations of adsorbed molecular oxygen species that react with adsorbed ammonia forming

nitrogen.[87,88] Very recently, Biausque et al. reported that one key route to form N_2 in ammonia

oxidation over perovskite $LaCoO_3$ consists in the reaction of adsorbed ammonia with adsorbed

oxygen species such as peroxide (O_2^{2-}) or superoxide (O_2^-) species.[89] These experimental findings

led us to the assumption that, a high NO selectivity can be achieved if the only oxygen species

involved in the ammonia oxidation is lattice oxygen or atomic surface oxygen species.[90] But this

concept is difficult to implement, since the formation of weakly bound molecular oxygen species

is the first and unavoidable step for the oxygen activation in conventional catalytic packed bed

reactors with an oxygen/ammonia mixture as co-feed.[91-94]

To minimize the formation of surface molecular oxygen species, here we develop the concept

to separate the oxygen activation from the catalytic process through an oxygen-permeable

membrane.[61,95-100] As illustrated in Figure 1 (right), O_2 is reduced to lattice O^{2-} on the air side of

the membrane, which is locally separated from the catalytic ammonia oxidation where oxygen is

consumed. As lattice oxygen, the oxygen ions diffuse through the membrane to the permeate side

where a lower oxygen partial pressure exists. However, since the first oxygen species present on

the ammonia side before oxygen release is lattice oxygen, a proper consumption of the lattice or atomic oxygen species by the ammonia oxidation may effectively suppress the formation of non-selective surface molecular oxygen species. Consequently, a high NO selectivity can be expected.

This work demonstrates that the use of an oxygen-permeable membrane with sufficient surface area can supply catalytically selective lattice oxygen or atomic surface oxygen species and suppress the formation of non-selective molecular oxygen species. A newly developed asymmetric ultrathin perovskite LSCF ($La_{0.6}Sr_{0.4}Co_{0.2}Fe_{0.8}O_{3-\delta}$) membrane was applied.[101] As shown in Figure 2, a thin (25 μm) dense LSCF layer is supported by a mechanically stable approx. 800 μm thick porous LSCF layer. The LSCF material was selected as oxygen-permeable membrane since it combines high permeability with an intrinsic catalytic activity towards ammonia oxidation.[31,77] This, as a rule, an ideal prerequisite for the use in membrane reactors.

To verify our concept, ammonia oxidation in the membrane reactor with oxygen supplied as lattice/atomic oxygen has been compared with the direct feeding of gaseous oxygen (co-feed mode) using the same LSCF membrane as catalyst at 850 $^{\circ}$C, (Support Information, Figure S1). In the co-feed mode, when the oxygen and ammonia are jointly fed to the porous support side of the LSCF membrane, the LSCF membrane acts only as a contactor catalyst providing a large surface. However, in the membrane mode, the oxygen for the ammonia oxidation is separated from air by the LSCF membrane layer. We show the results of this comparison in Figure 3. The highest NO selectivity obtained in the membrane mode after reasonable optimization of the reaction parameters is 95 %, whereas the maximum NO selectivity in the co-feed mode is only 77 %. It has to be noted that the permeated oxygen amounts in membrane reactor mode and co-feed fixed bed reactor mode are the same. Since the operation temperatures for both reactors are also the same, the strengths of the oxygen bonding to the surface are comparable too. The only

difference between the co-feed mode and the membrane mode is the way of oxygen supply: In the co-feed fixed bed reactor, adsorption and reduction of gaseous oxygen and the ammonia oxidation take place in the same compartment. As we can expect from the reduction of oxygen shown in Figure 1 (left), in the fixed bed co-feed reactor, adsorbed molecular oxygen species can react with ammonia and form undesired nitrogen. In contrast, in the membrane mode, the activation of the oxygen is separated from the catalytic reaction and, therefore, the formation of non-selective surface molecular oxygen species can be well suppressed. The NO selectivity as a function of the fed oxygen was also tested in a small range for the co-feed mode, as shown in Figure 3, but the NO selectivity obtained in the membrane reactor is always higher than in the co-feed mode.

In a further experiment, instead of the porous support layer, the dense layer of the LSCF membrane was exposed to the ammonia side. Figure 4 shows the NO selectivity and conversion of the ammonia oxidation plotted versus the ammonia concentration in the feed gas for these two operation modes: Either the dense LSCF or the porous LSCF support layers were facing ammonia. If the ammonia oxidation takes place on the surface of the dense LSCF layer, a low NO selectivity (< 10 %) was found, whereas the selectivity is around 90 % when ammonia oxidation takes place on the porous LSCF support. Although the ammonia conversions were comparable for these two operation modes (Figure 4), the NO yield was much lower compared with the case if the porous LSCF layer is used as large contactor surface for ammonia oxidation. Since the surface morphology - porous contra dense - is the major difference, the surface area appears to be the determining factor for the membrane reactor performance. Compared to a dense surface, as shown in Figure 5a, the porous layer provides a much higher surface area. The permeated oxygen ion can be well distributed through the porous network, and the formation of non-selective surface oxygen species can be sufficiently suppressed.[102] Therefore, there are more lattice oxygen

and atomic surface oxygen species that can be consumed in selective oxidations before molecular oxygen species have been formed. In contrast, when the dense membrane layer is facing the ammonia oxidation side, the permeated oxygen ions with relatively high concentration can combine and form weakly bound oxygen species before desorption as molecular oxygen from the dense LSCF side, as shown in Figure 5b, thus enhancing the formation of the undesired byproduct nitrogen as discussed above. Figure 6 presents the residual oxygen partial pressure at the outlet of the ammonia side measured by gas chromatography for those two different modes. When the dense side is facing ammonia, the oxygen partial pressure is obviously higher, indicating a higher concentration of weakly bound surface molecular oxygen species. This finding further explains the low NO selectivity when the dense side is facing ammonia.

Under the assumption that the good performance of the membrane reactor in the ammonia oxidation benefits from the specific oxygen supply and the surface morphology of the membrane, that is to say in which manner the oxygen is supplied, the two oxygen-permeable pervoskite materials LSCF and $Ba_{0.5}Sr_{0.5}Co_{0.8}Fe_{0.2}O_{3-\delta}$ (BSCF) have been compared using the comparable asymmetric membranes (Figure 7). Since the BSCF membrane shows a higher oxygen transport rate, a higher ammonia conversion can be realized, but LSCF shows a significantly higher NO selectivity. While a NO selectivity of around 90 % is achieved in the LSCF reactor, the best one obtained in the BSCF reactor is around 75 %. This finding can be understood since BSCF exhibits a faster surface exchange rate due to its higher oxygen vacancy mobility than LSCF.[29,103-105] Therefore, a higher concentration of non-selective molecular oxygen species is expected on the membrane surface of BSCF compared with LSCF, since the recombination of the lattice oxygen is easier on BSCF resulting in a higher amount of active peroxide and superoxide ions. This leads to a decreasing NO selectivity on the expense of increasing nitrogen formation.

Evidently, the dominating oxygen species delivered by the membrane plays a big role in the final product distribution.

In conclusion, we present a novel route to activate oxygen for a better catalytic performance in the selective ammonia oxidation to NO by using an oxygen-permeable perovskite membrane, in which the formation of catalytically non-selective molecular oxygen species is suppressed. A large surface provided by a porous perovskite layer can dilute the permeated oxygen ions (lattice oxygen) and suppress the formation of weakly bound molecular surface oxygen species, thus leading to a high selectivity of NO. In the ammonia oxidation, 95 % NO selectivity and 81 % ammonia conversion could be achieved in a catalytic membrane reactor with asymmetric perovskite $La_{0.6}Sr_{0.4}Co_{0.2}Fe_{0.8}O_{3-\delta}$ oxygen-permeable catalytically active membrane at 850 $^{\circ}$C. The oxygen used in the selective ammonia oxidation is taken from the perovskite membrane, and the membrane is re-oxidized on the air side. In the classical Mars and van Krevelen mechanism, this re-oxidation takes place by gaseous oxygen present in the co-feed. This work may open the door for various selective oxidation processes and the detailed analysis of the mechanism of them.
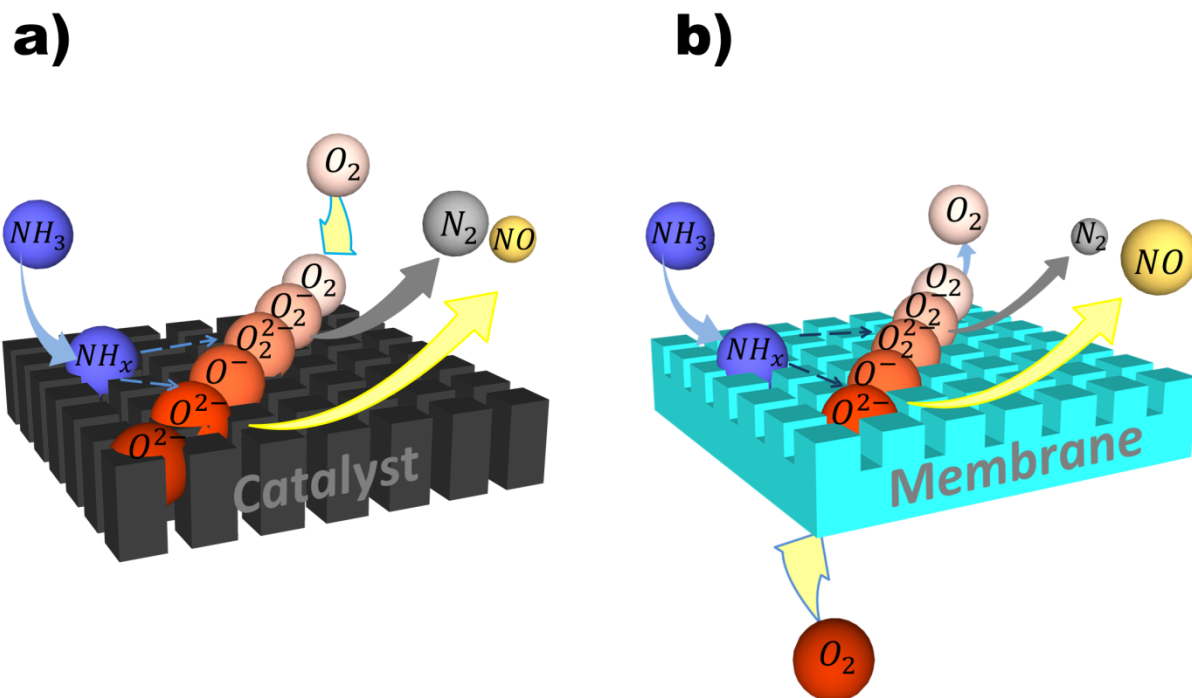
Acknowledgements

Figure 2. Ammonia oxidation over a conventional packed bed perovskite catalyst (a) and a perovskite membrane (b). (a), Oxygen as co-feed becomes incorporated into the oxide catalyst and adsorbed molecular oxygen species are present in the early stage of incorporation. (b), In the case of membrane operation, lattice oxygen species and atomic oxygen species are present in the early stage of oxygen release.
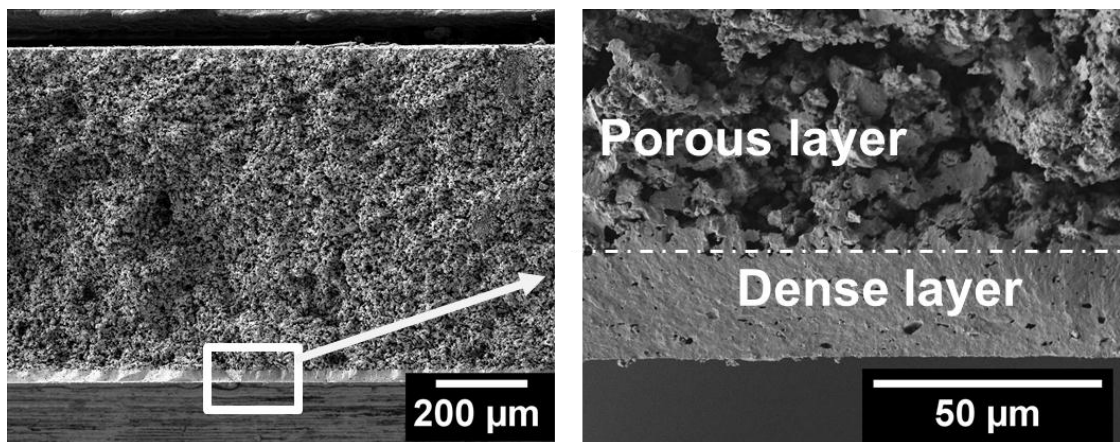
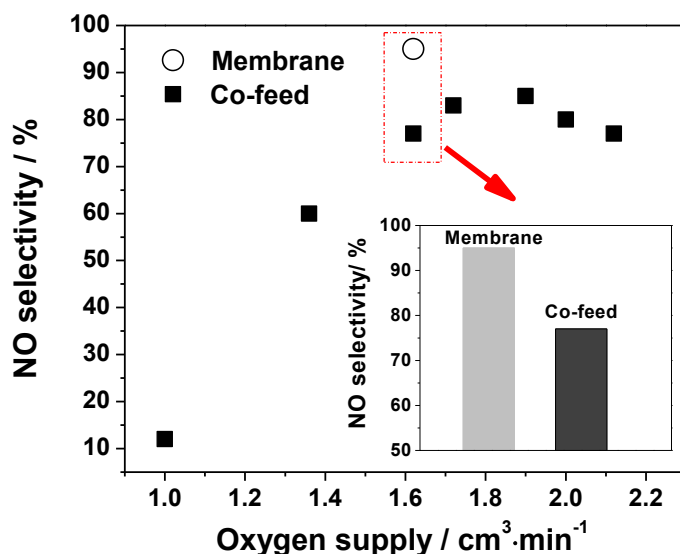**Figure 2.** SEM micrographs of fresh LSCF membrane cross section.

Figure 3. NO selectivity in the ammonia oxidation for two different operation modes at 850 ^{o}C in LSCF membrane reactor. In both modes, the porous support layer of the asymmetric LSCF membrane was facing the (i) NH$_3$/O$_2$ mixture in co-feed mode, or (ii) the pure NH$_3$ in membrane mode (Membrane mode, air side: F$_{air}$ = 100 cm^3·min^{-1}; Ammonia side: F$_{all}$ = 100 cm^3·min^{-1},F$_{NH3}$ = 1.6 cm^3·min^{-1} F$_{Ne}$ = 1 cm^3·min^{-1} and F$_{He}$ = balance. Co-feed mode: F$_{Ne}$ = 1 cm^3·min^{-1}, F$_{NH3}$ = 1.6 cm^3·min^{-1}, F$_{O2}$ + F$_{He}$ = 97.4 cm^3·min^{-1}). The inset shows the NO selectivity for the two different modes when supplying 1.6 cm^3·min^{-1} oxygen.
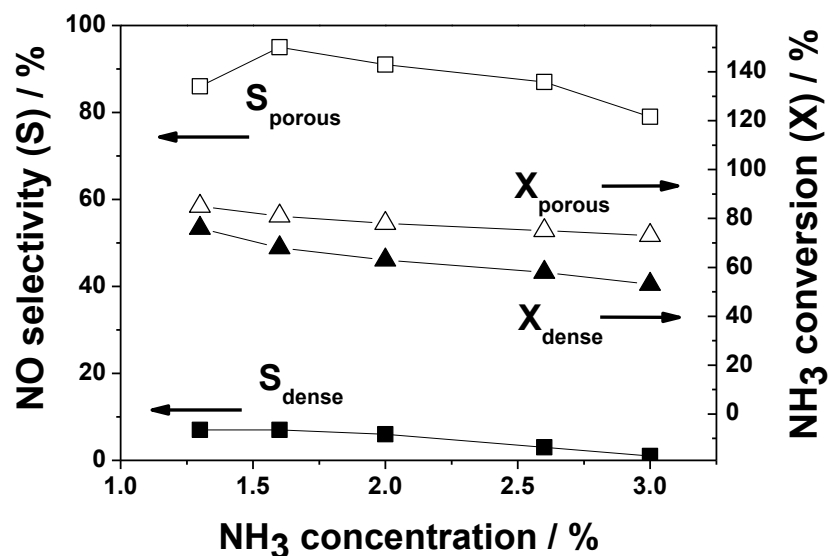
Figure 4. NO selectivity and ammonia conversion in the ammonia oxidation as a function of the ammonia concentration in the feed in two different operation modes of the LSCF membrane reactor at 850 $^{\circ}$C with the porous support layer to ammonia and the dense layer to the ammonia side (Air side: F_{air} = 100 cm^3·min^{-1}; Ammonia side: F_{all} = 100 cm^3·min^{-1} F_{NH3} from 1.3 to 3.0 cm^3·min^{-1}, F_{Ne} = 1 cm^3·min^{-1} and F_{He} = balance).

a)

NH$_3$

NO, H$_2$O

O$_2$

Air

O$_2$ – depleted Air

NO

NH$_x$

NH$_x$

O^{2-}

O^{2-}

NH$_x$

O^{2-}

O^{2-}

b)

NH$_3$

NO, H$_2$O

O$_2$

Air

O$_2$ – depleted Air

N$_2$

NO

NH$_x$

O$_2$

O$_2^{x-}$

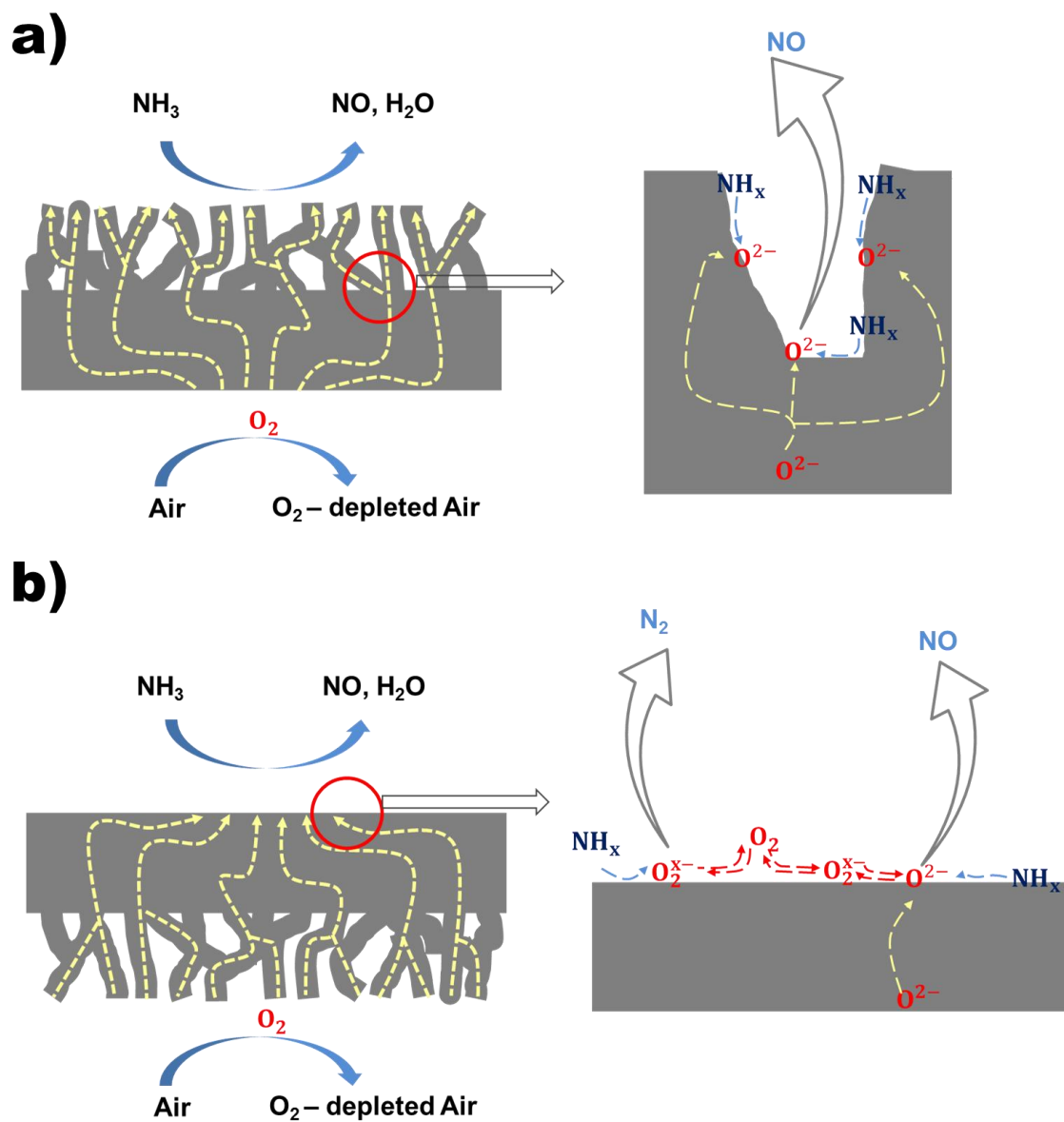O$_2^{x-}$

O^{2-}

NH$_x$

O^{2-}

Figure 5. Asymmetric oxygen-permeable membrane with (i) porous surface, and (ii) smooth surface facing the ammonia side of the membrane reactor.
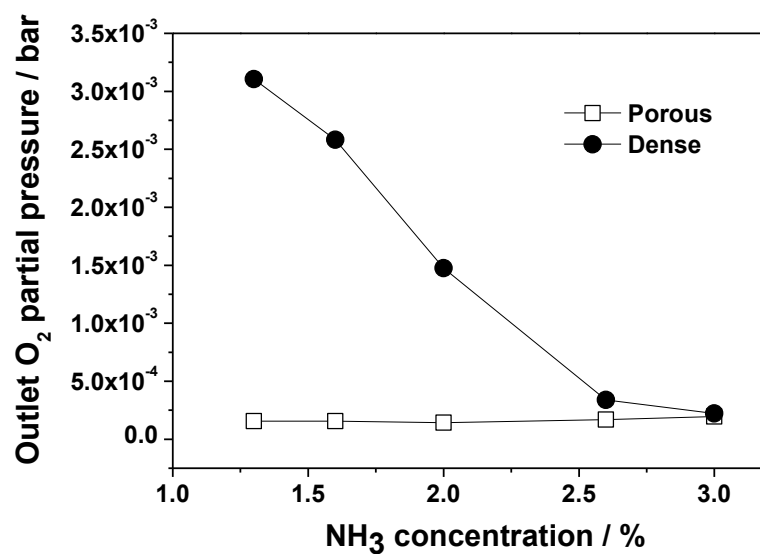
Figure 6. The residual oxygen partial pressure on the ammonia oxidation side as a function of the ammonia concentration in two different operation modes. i.e. porous and dense side, respectively, of the asymmetric membrane at the reaction side.
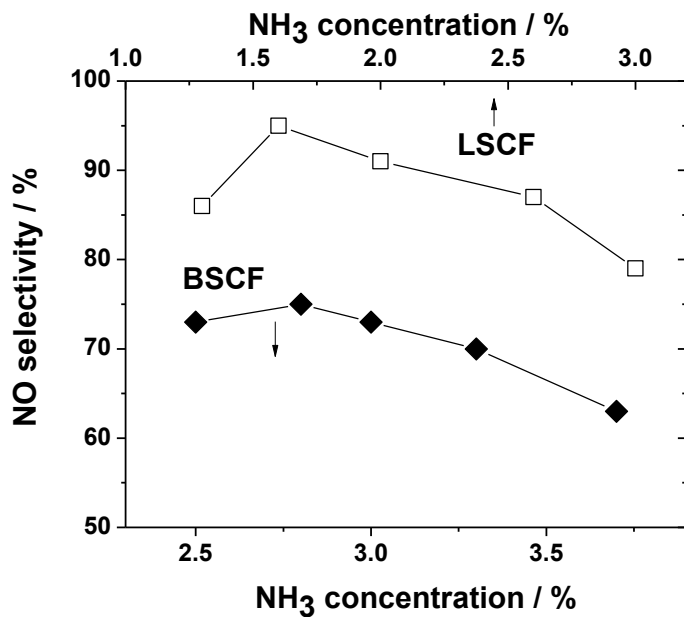
Figure 7. NO selectivity in the ammonia oxidation as a function of the ammonia concentration in the feed gas in membrane reactors with asymmetric BSCF or LSCF membranes. (Porous support side of the asymmetric membranes to the ammonia side, T = 850 ^{o}C; air side: F_{air} = 100 cm^3·min^{-1}; Ammonia side: F_{all} = 100 cm^3·min^{-1}, F_{Ne} = 1 cm^3·min^{-1} and F_{He} = balance.)

References

[1]   V. A. Sadykov, L. A. Isupova, I. A. Zolotarskii, L. N. Bobrova, A. S. Noskov, V. N. Parmon, E. A. Brushtein, T. V. Telyatnikova, V. I. Chernyshev, V. V. Lunin, *Appl. Catal. A-Gen.* **2000**, *204*, 59-87.

[2]   Y. Wu, T. Yu, B.-s. Dou, C.-x. Wang, X.-f. Xie, Z.-l. Yu, S.-r. Fan, Z.-r. Fan, L.-c. Wang, *J. Catal.* **1989**, *120*, 88-107.

[3]   a) J. P. Perez-Ramiriz, B. Vigeland, *Angew. Chem. Int. Edit.* **2005**, *44*, 1112-1115; b) J. Pérez-Ramírez, B. Vigeland, *Catal. Today* **2005**, *105*, 436-442.

[4]   S. Sun, M. Rebeilleau-Dassonneville, X. Zhu, W. Chu, W. Yang, *Catal. Today* **2010**, *149*, 167-171.

[5]   a) H. Over, Y. D. Kim, A. P. Seitsonen, S. Wendt, E. Lundgren, M. Schmid, P. Varga, A. Morgante, G. Ertl, *Science* **2000**, *287*, 1474-1476; b) A. Bueno-López, K. Krishna, M. Makkee, J. A. Moulijn, *J. Catal.* **2005**, *230*, 237-248; c) J. L. Gunjakar, T. W. Kim, H. N. Kim, I. Y. Kim, S. J. Hwang, *J. Am. Chem. Soc.* **2011**, *133*, 14998-15007.

[6]   R. D. a. J. Caro, *in Handbook of Heterogeneous Catalysis (Eds. : G. Ertl, H. Knözinger, F. Schüth, J. Weitkamp), Wiley-VCH, Weinheim* **2008**, 2221.

[7]   A. Bielański, J. Haber, *Catal. Rev.* **1979**, *19*, 1-41.

[8]   Y. Kosaki, A. Miyamoto, Y. Murakami, *Bull. Chem. Soc. Jpn.* **1979**, *52*, 617-618.

[9]   a) B. Bahrami, V. G. Komvokis, M. S. Ziebarth, O. S. Alexeev, M. D. Amiridis, *Appl. Catal. B-Environ.* **2013**, *130–131*, 25-35; b) E. V. Kondratenko, J. Pérez-Ramírez, *Appl. Catal. A-Gen.* **2005**, *289*, 97-103.

[10]   G. Biausque, Y. Schuurman, *J. Catalysis* **2010**, *276*, 306-313.

[11]   Y. Xu, A. V. Ruban, M. Mavrikakis, *J. Am. Chem. Soc.* **2004**, *126*, 4717-4725.

[12]   a) R. Merkle, J. Maier, *Angew. Chem. Int. Edit.* **2008**, *47*, 3874-3894; b) J. Pérez-Ramírez, E. V. Kondratenko, *J. Catalysis* **2007**, *250*, 240-246; c) J. Pérez-Ramírez, F. Kapteijn, K. Schöffel, J. A. Moulijn, *Appl. Catal. B-Environ.* **2003**, *44*, 117-151; d) E. V. Kondratenko, H. Wang, V. A. Kondratenko, J. Caro, *J. Mol. Catal. A: Chem.* **2009**, *297*, 142-149.

[13]   a) C. S. Chen, S. J. Feng, S. Ran, D. C. Zhu, W. Liu, H. J. M. Bouwmeester, *Angew. Chem. Int. Edit.* **2003**, *42*, 5196-5198; b) J. Sunarso, S. Baumann, J. M. Serra, W. A. Meulenberg, S. Liu, Y. S. Lin, J. C. Diniz da Costa, *J. Membr. Sci.* **2008**, *320*, 13-41; c) Z. P. Shao, H. Dong, G. X. Xiong, Y. Gong, W. S. Yang, *J. Membr. Sci.* **2001**, *183*, 181-192; d) H. Q. Jiang, H. H. Wang, S. Werth, T. Schiestel, J. Caro, *Angew. Chem.Int. Edit.* **2008**, *47*, 9341-9344; e) H. Jiang, Z. Cao, S. Schirrmeister, T. Schiestel, J. Caro, *Angew. Chem. Int. Edit.* **2010**, *49*, 5656-5660; f) Y. Liu, X. Zhu, M. Li, H. Liu, Y. Cong, W. Yang, *Angew. Chem. Int. Edit.* **2013**, *52*, 3232-3236; g) H. H. Wang, Y. Cong, W. S. Yang, *Chem. Comm.* **2002**, 1468-1469.

[14]   J. M. Serra, J. Garcia-Fayos, S. Baumann, F. Schulze-Küppers, W. A. Meulenberg, *J. Membr. Sci.* **2013**, *447*, 297-305.

[15]   S. Baumann, J. M. Serra, M. P. Lobera, S. Escolástico, F. Schulze-Küppers, W. A. Meulenberg, *J. Membr. Sci.* **2011**, *377*, 198-205.

[16]   C. Batiot, B. K. Hodnett, *Appl. Catal. A-Gen.* **1996**, *137*, 179-191.

[17]   a) R. M. Lei Wang, Yuri A. Mastrikov, Eugene A. Kotomin and Joachim Maier, *J. Mater. Res.* **2012**, *27*, 2000-2008; b) L. Wang, R. Merkle, J. Maier, *ECS Transactions* **2009**, *25*, 2497-2505; c) F. S. Baumann, J. Fleig, H. U. Habermeier, J. Maier, *Solid State Ionics* **2006**, *177*, 3187-3191; d) H. J. M. Bouwmeester, H. Kruidhof, A. J. Burggraaf, *Solid State Ionics* **1994**, *72*, 185-194.

Support Information

Experimental Section

The asymmetric structure $La_{0.6}Sr_{0.4}Co_{0.2}Fe_{0.8}O_{3-\delta}$ and $Ba_{0.5}Sr_{0.5}Co_{0.8}Fe_{0.2}O_{3-\delta}$ (BSCF) perovskite oxygen transfer membranes both consist of a dense layer and a porous layer. The thicknesses of the dense part of the LSCF and BSCF membrane are about 25 μm and 70 μm, respectively, whereas those of porous part is approx. 800 μm. More information about the membrane preparation can be found elsewhere.[1] A JEOL JSM-6700F field-emission scanning electron microscope was employed to characterize the morphology of the fresh and spent membranes. The oxygen permeation and ammonia oxidation were performed in a self-made high temperature oxygen permeation reactor as described in our group's previous work.[2] The membrane was sealed on the alumina tube with gold paste. After sintering at 950 ^oC, a dense gold layer between membrane and alumina tube was obtained, which ensure the gas tight between different sides of the membrane. Here, the diameter of the uncoated membrane is 1 cm, and the effective membrane area is 0.78 cm^2. Ammonia diluted by helium or air were fed to either dense or porous side of the membrane as required. All gas rates were controlled by gas mass flow controllers (Bronkhorst), and all gas lines were heated to 150 ^oC to ensure no liquid block caused by H_2O. The outlet gas concentrations were measured online by a gas chromatograph (Agilent 6890).

NO selectivity, yield and ammonia conversion were calculated from the total outlet flow rate F_{out} (cm^3 min^{-1}) on ammonia side and NO and NH_3 concentrations, c (NO) and c(NH_3) by using Equation below:

$$X(NH_3) = \left[\frac{F(in, NH_3) - F(out, NH_3)}{F(in, NH_3)} \right] \times 100\%$$

$$S(NO) = \left[\frac{F(out, NO)}{F(in, NH_3) - F(out, NH_3)} \right] \times 100\%$$

$$Y(NO) = X(NH_3) \times S(NO)$$

Where F(i) is the flow rate of specie i calculated by the F(in or out) and the concentration of specie i.
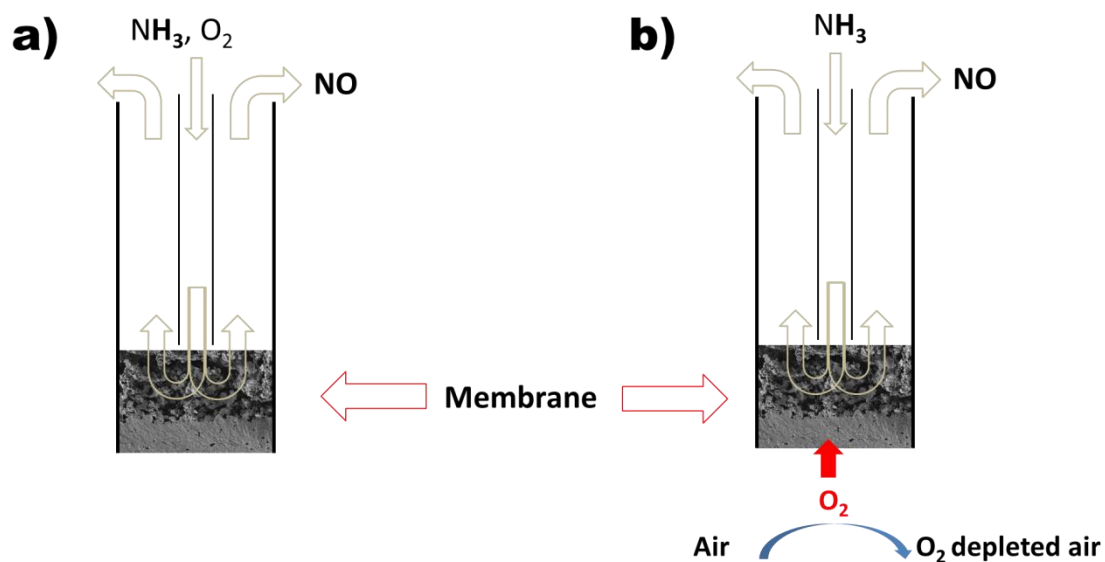
Figure S1. Comparative study of ammonia oxidation in different operation modes: co-feed reactor (Left) and inset membrane reactor (right)

References

[1]   a) J. M. Serra, J. Garcia-Fayos, S. Baumann, F. Schulze-Küppers, W. A. Meulenberg, *J. Membr. Sci.* **2013**, *447*, 297-305; b) S. Baumann, J. M. Serra, M. P. Lobera, S. Escolástico, F. Schulze-Küppers, W. A. Meulenberg, *J. Membr. Sci.* **2011**, *377*, 198-205; c) Z. Cao, H. Jiang, H. Luo, S. Baumann, W. A. Meulenberg, H. Voss, J. Caro, *Catal. Today* **2012**, *193*, 2-7.

[2]   H. H. Wang, C. Tablet, A. Feldhoff, H. Caro, *J. Membr. Sci.* **2005**, *262*, 20-26.

Chapter 5

Conclusions

In this thesis, I explored the feasibility of combining several chemical processes in a membrane reactor with oxygen transporting membrane following the concept of process intensification. I investigated the possibility to improve different catalytic processes in the membrane reactor in comparison with the state of art, i.e. I tried to substitute partial oxidations in fixed bed reactors with a co-feed of oxygen and reactant by the reaction in a catalytic membrane reactor.

In the hydrogen production from water splitting, I coupled the thermal water splitting with the oxidative coupling of methane in the membrane reactor. It is found that the hydrogen production rate is far beyond the equilibrium-limited value of the thermal water splitting. On the other hand, in the oxidative coupling of methane, no oxygen supply or oxygen separation from air is necessary. Through the employment of the oxygen transporting membrane reactor, water can be used as the oxygen supply source.

To develop stable membrane reactors for various applications including the pure oxygen production for the oxy-fuel concept and different catalytic processes, a novel dual-phase oxygen transporting membrane and a novel asymmetric membrane based on $Ce_{0.9}Gd_{0.1}O_{2-\delta}$ were developed and tested. The result of our experiment showed that doping minor amounts of cobalt into the ionically conducting material was prone to improve the performance of the existing dual-phase membrane systems. The resulting membrane shows an improved oxygen permeability in comparison with the un-doped membrane.

I have also demonstrated that the proper utilization of the oxygen transporting membrane reactors could be beneficial for the current heterogeneous catalytic processes. For example, when the oxygen was supplied by the oxygen transporting membrane, a high aromatization selectivity and yield can be achieved; through the proper utilization of the lattice oxygen as oxidant, a highly selective ammonia oxidation to NO can be obtained. It is therefore expected that the membrane reactors may offer in general a high feasibility to improve the performance of catalytic processes. By combining of catalytic processes and high-performance stable membranes, one can develop a membrane reactor with excellent catalytic performance and improved stability.

In summary, my thesis reflects not only the development of the membrane reactors based on several newly-developed oxygen permeation membranes (BSCF, LSCF and CGO-based dual-phase), but also extends its various applications on reactions such as ammonia oxidation, and for the first time such as methane aromatization.

Publications

Publications included in this thesis

1. **<u>Z. Cao</u>**, H. Jiang, H. Luo, S Baumann, W. A. Meulenberg, J. Assmann, L. Mlecko, Y. Liu, J. Caro, Natural gas to fuel and chemicals: Improved methane dehydroaromatization in an oxygen permeable membrane reactor. **Angew. Chem. Int. Ed.** (Accepted DOI: 10.1002/anie. 201307935)**.**

2. **<u>Z. Cao,</u>** H. Jiang, H. Luo, S. Baumann, W. A. Meulenberg, H. Voss and J. Caro, Simultaneous overcome of the equilibrium-limitations in BSCF oxygen-permeable membrane reactors: water splitting and methane coupling, **Catal. Today 193 (2012) 2-7.**

3. **<u>Z. Cao,</u>** H. Jiang, H. Luo, J. Caro, An effective and simple method in the aim of improving the oxygen permeability of the dual-phase membrane based on $Ce_{0.9}Gd_{0.1}O_{2-\delta}$. (In preparation for **J. Membr. Sci.**).

4. **<u>Z. Cao,</u>** H. Jiang, H. Luo, S. Baumann, W. A. Meulenberg, H. Voss and J. Caro, Ostwald process: An efficient oxygen activation route for improved ammonia oxidation via an oxygen-permeable catalytic membrane. (Submitted to **Angew. Chem. Int. Ed.**).

Publications not included in this thesis

5. H. Jiang, **<u>Z. Cao</u>**, S. Schirrmeister, T. Schiestel, J. Caro, A coupling strategy to produce hydrogen and ethylene in a membrane reactor. **Angew. Chem. Int. Ed. 2010**, **49, 5656-5660.**

6. H. Luo, H. Jiang, T. Klande, **Z. Cao,** F. Liang, H. Wang, J. Caro, Novel cobalt-free, noble metal-free oxygen-permeable $40Pr_{0.6}Sr_{0.4}FeO_{3-\delta}–60Ce_{0.9}Pr_{0.1}O_{2-\delta}$ dual-phase membrane, **Chem. Mater. 2012, 24 (11), 2148-2154.**

7. H. Luo, H. Jiang, T. Klande, F. Liang, **Z. Cao,** H. Wang, J. Caro, Rapid glycine-nitrate combustion synthesis of CO_2-stable dual phase membrane $40Mn_{1.5}Co_{1.5}O_{4-\delta}-60Ce_{0.9}Pr_{0.1}O_{2-\delta}$ for CO_2 capture via a oxy-fuel process, **J. Membr. Sci. 2012, 450-458.**

8. H. Luo, **Z. Cao,** T. Klande, F. Liang, H. Wang, J. Caro, Novel CO_2-stable oxygen-permeable dual phase membrane. (In preparation for **J. Membr. Sci.**)

Contributions to Conferences

1. **<u>Z. Cao</u>** and J. Caro, Ammonia oxidation in a catalytic membrane reactor with improved oxygen permeation, 12th International Conference on Inorganic Membranes, University of Twente, Enschede, Netherlands, 9-13th July 2012. **(Talk)**

2. **<u>Z. Cao</u>** and J. Caro, Oxidative coupling of methane in a membrane reactor by employing H_2O as oxygen resource, 10th International Conference on Catalysis in Membrane Reactors, Saint-Petersburg State Institute of Technology, Saint-Petersburg, Russia, 20-24th June 2011. **(Poster)**
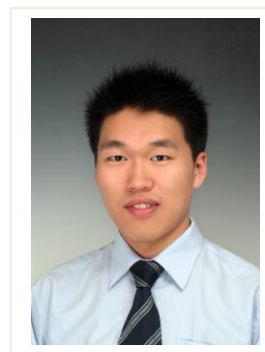
Curriculum Vitae

PERSONAL INFORMATION

Date and of Birth: July 31, 1984

Gender: Male

Nationality: Chinese

Marital Status: Single

EDUCATION

Ph.D Candidate - 11/2010 - now

Master degree study – **10/2008 - 09/2010**: Material and Nanochemistry

Faculty advisor: **Prof. Jürgen Caro** and **Prof. Heqing Jiang**

Bachelor degree study – **09/2002 - 06/2006:** Material Physics

East China University of Science and Technology, Shanghai, China

EMPLOYMENT

Engineer 07/2006– 07/2007

The ZWILLING J.A. HENCKELS Company, Shanghai